Characterization of transcription factor AmtR-DNA interaction

(Charakterisierung der Transkriptionsfaktor AmtR-DNA Interaktion)

Der Naturwissenschaftlichen Fakultät
der Friedrich-Alexander-Universität Erlangen-Nürnberg

zur
Erlangung des Doktorgrades Dr. rer. nat.

vorgelegt von

Christian Schwab

aus Berchtesgaden

Als Dissertation genehmigt

von der Naturwissenschaftlichen Fakultät

der Friedrich-Alexander-Universität Erlangen-Nürnberg

Tag der mündlichen Prüfung: 14.03.2019

Vorsitzender des
Promotionsorgans: Prof. Dr. Georg Kreimer

Gutachter: Prof. Dr. Andreas Burkovski

                                                       Prof. Dr. Heinrich Sticht

Table of contents

1 Zusammenfassung

AmtR ist der Masterregulator der Stickstoffkontrolle in *Corynebacterium glutamicum*. Viele der für den Regulationsmechanismus wichtige DNA Zielsequenzen von AmtR wurden in Interaktionsstudien untersucht, wobei diese Operatoren unterschiedlich stark von AmtR gebunden wurden. Darauf basierend konnte eine Konsensussequenz für AmtR Operatoren mit konservierten Bindehalbseiten und variabler Zwischensequenz abgeleitet werden. Anschließende Transkriptomanalysen des *C. glutamicum* Genoms identifizierten viele DNA Abschnitte, welche dieser Konsensussequenz ähnelten, jedoch nicht von AmtR reguliert wurden. Dies ließ vermuten, dass zusätzliche Faktoren wie die Konformation und Flexibilität des Operators auch einen Einfluss auf die AmtR-DNA Interaktion haben. Da vorherige Studien diesen Aspekt nicht weiter berücksichtigten, wurde in der vorliegenden Arbeit der Einfluss der DNA Form auf die AmtR-DNA Interaktion eingehender untersucht.

Erste Analysen der Interaktionen zwischen gereinigtem AmtR und verschiedenen nativen Operatoren zeigten die stärkste Bindung zwischen AmtR und dem Operator des *amtB* Gens. Basierend auf dieser DNA Sequenz wurden zwei Operatorvarianten erzeugt, welche eine hohe bzw. niedrige Flexibilität in der Zwischensequenz aufwiesen. Die anschließenden DNA Strukturanalysen dieser Operatoren im ungebunden Zustand zeigten eine ähnliche Deformation für den Wildtyp und die deformierbare DNA Variante sowie eine niedrigere Flexibilität für den rigiden Operator. Im AmtR gebundenen Zustand konnten hingegen keine strukturellen Unterschiede zwischen den drei Varianten beobachtet werden. Dies deutete auf eine AmtR induzierte DNA Deformation während der Komplexbildung hin.

Des Weiteren zeigten sowohl Gel-Retardationsanalysen als auch Oberflächen Plasmonen Resonanz Messungen eine stärkere AmtR-Bindung zu den Operatoren mit flexiblen Zwischensequenzen als zum Operator mit rigider Zwischensequenz. Durch zusätzliche kinetische Analysen konnten einheitliche AmtR Assoziationsraten zu allen drei Operatorvarianten gezeigt werden. Im Gegensatz dazu wurden ähnliche AmtR-Dissoziationsraten nur für den Wildtyp und den deformierbaren Operator ermittelt, während für die rigide Variante eine schnellere Dissoziation beobachtet wurde. Darauf basierend konnte ein Interaktionsmodel für AmtR und die *amtB* Operatorvarianten erstellt werden, welches einen eindeutigen Einfluss der DNA Struktur auf die AmtR-DNA Bindung zeigt.

Schließlich wurden, durch Sequenz- und Strukturvergleiche von AmtR mit lokalen und globalen Regulatoren der TetR Familie, bestimmte Aminosäuren an verschiedenen Positionen identifiziert, welche für die Spezifität und Affinität der AmtR-DNA-Bindung von Bedeutung sind.

2 Summary

The regulator AmtR represents an essential function in modulating the transcription of genes of the nitrogen metabolism in *Corynebacterium glutamicum*. Many DNA targets of this regulator were identified in interaction studies, which suggested a differential AmtR binding for these sequences. Based on these operators, a consensus sequence with two conserved half sites and a variable spacer was derived. Transcriptome analyses of the genome of *C. glutamicum* identified many different sequences that matched this consensus sequence but were not AmtR regulated. This suggested that additional properties like the DNA shape or flexibility influence the AmtR-DNA binding. Since previous studies did not address this aspect, the role of the DNA conformation for the AmtR-DNA interaction has been studied in the present work in more detail.

In initial interaction studies, the best binding was shown between purified AmtR and the *amtB* operator. This binding site as well as two artificially generated variants of this operator, one with high deformability and one with reduced deformability in the spacer region, were applied for analysis. Corresponding investigations of their intrinsic DNA conformations in unbound state revealed similar deformations for the wild type and deformable variant and a reduced deformation for the rigid version. Vice versa, in complex with AmtR, identical macroscopic conformations were shown for each operator. This indicated a distinct AmtR-induced DNA deformation during binding.

Additionally, a combination of gel retardation assays and surface plasmon resonance measurements demonstrated a stronger AmtR binding to the operators with rather flexible spacers compared to the operator with reduced deformability in the spacer. Furthermore, the kinetic analyses determined similar AmtR association rates for all operator variants. On the other hand, similar AmtR dissociation rates were determined only for the wild type and deformable operators, while a faster AmtR dissociation was observed for the rigid variant. Based on this, a coherent binding model between AmtR and the *amtB* operator variants was established, that showed a distinct influence of the DNA conformation on the AmtR-DNA binding.

Finally, based on sequence and structure comparisons of AmtR with local and global TetR-type regulators, distinct positions and residues were deduced to be important for the specificity and affinity of AmtR-DNA binding.

3 Introduction

3.1 Corynebacteria

3.1.1 Physiology and taxonomy of corynebacteria

Corynebacteria are non-motile, facultative anaerobe and non-spore forming. The genus belongs to the Gram-positive bacteria with a G-C-rich genome (Liebl *et al.* 1991). The name *Corynebacterium* is derived from its morphology as club shaped rod form (ancient Greek: *coryne*). Corynebacteria are characterized by a mycolic acid layer, the mycomembrane (figure 1A). This layer shelters the entire cell membrane to form a double layer and has similar functions as the outer membrane of Gram-negative bacteria (Burkovski 2013). Therefore, *Corynebacterium* species obtain the required robustness for colonizing diverse milieus (Tauch and Burkovski 2015). Due to the stepwise separation of the resulting double layered cell membrane, a typical V-form is observed by microscopy during cell division, designated as snapping division (figure 1B).
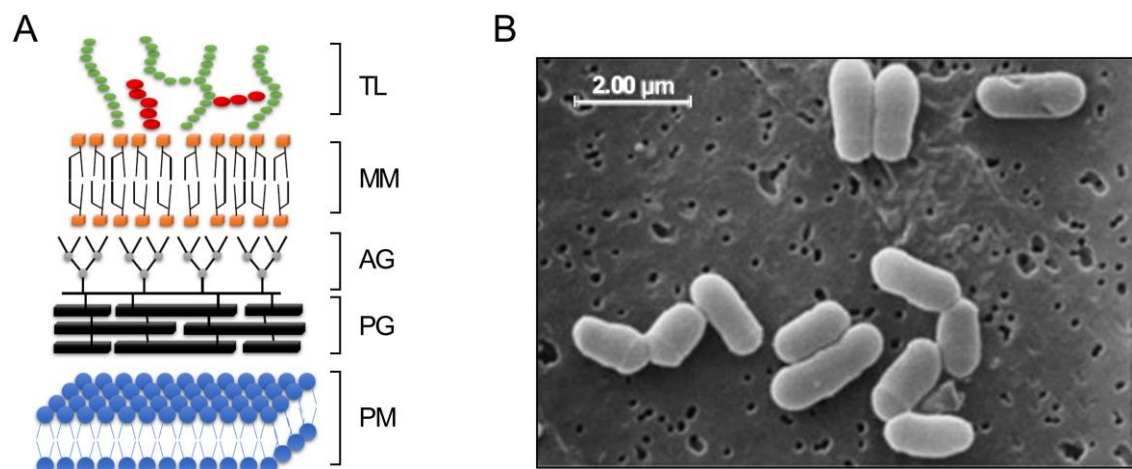
Figure 1 Cell envelope and snapping division of corynebacteria. (A) The cell envelope of *Corynebacterium* species consists of the plasma membrane (PM), the peptidoglycan layer (PG), the arabinogalactan layer (AG), the mycomembrane (MM) and the top layer (TL) (Burkovski 2013; Marrakchi *et al.* 2014). (B) Electron-microscopic capture of *Corynebacterium* cells shows the characteristic snapping division (Handbook of *Corynebacterium glutamicum*; FZ, Jülich).

Corynebacterium was classified as an associate of *Actinobacteria* by a phylogenetic comparison of 16S-rRNAs of various genera (Stackebrandt *et al.* 1997; Ventura *et al.* 2007). Additional chemotaxonomic analyses of the cell wall and lipid constituents demonstrated an

affiliation to the CMNR group of *Corynebacterium*, *Mycobacterium*, *Nocardia* and *Rhodococcus* (Barksdale 1970; Burkovski 2018). Nowadays, 97 distinct species of the genus *Corynebacterium* were discovered in various environments (Tauch and Sandbote 2014; Rückert *et al.* 2015), while more than half of them (52 species) were identified as contagious with only a few inducing severe diseases in humans (Burkovski 2018).

3.1.2 Pathogenic *Corynebacterium* species

Besides species like *Corynebacterium ulcerans*, *Corynebacterium jeikeium* and *Corynebacterium pseudotuberculosis*, the most prominent pathogen of this genus is *Corynebacterium diphtheriae* (Lehmann and Neumann 1896). This type species was identified as causative agent of diphtheria, a respiratory disease in humans with severe symptoms like pseudomembrane formation (Barksdale 1970; Burkovski 2014). Due to the increasing number of infections in the past, extended vaccination programs were investigated resulting nowadays in only 5000 to 6000 new infections per year worldwide (WHO/IVB database 2017). In addition to the pathogenic examples of the *Corynebacterium* genus, several non-pathogenic species like *Corynebacterium glutamicum* were isolated.

3.1.3 *Corynebacterium glutamicum* – The biotechnological workhorse

Non-pathogenic *Corynebacterium* species have been applied in many different areas (Constantinides 1980; Yokota *et al.* 1987; Schröder *et al.* 2011). Due to the production of a large number of biogenic compounds and the subsequent secretion during fermentation (Hoischen and Krämer 1989), *C. glutamicum* was emphasized as one of the most important microorganism in biotechnology besides *Escherichia coli*. It was first isolated in 1957 during screenings for glutamate producing microorganisms in the soil of the Ueno zoo in Tokyo (Kinoshita *et al.* 1957). In the following decades, many fast growing and high productive strains of *C. glutamicum* have been employed harvesting a wide range of compounds at industrial quantities (Sahm *et al.* 1996; Ohnishi *et al.* 2002). Besides several vitamins and nucleotides (Hermann 2003), distinct strains of *C. glutamicum* accumulate high amounts of amino acids like L-glutamate (3.3 million tons per year) or L-lysine (2.2 million tons per year) for the food or feed industry during fermentation processes (Sanchez *et al.* 2018). According to Sanchez and coworkers, additional amino acids of the feed industry such as L-lysine, D/L-methionine, L-threonine, and L- tryptophan represent the largest part of the total amino acid market with 2.4 million tons per year, which was estimated at approx. 6 billion $US. Today, the worldwide total amino acid market is about 8 billion $US, while it is forecasted to reach 20.4 billion $US by the year 2020 (Sanchez *et al.* 2018). These trends promote the

development of enhanced bioprocesses in *C. glutamicum*. Therefore, the characterization of metabolomes, the biosynthesis of important amino acids and regulatory networks within this species is mandatory (Ikeda and Nakagawa 2003; Kalinowski *et al.* 2003). This may also provide a better understanding of the regulatory mechanisms of corynebacteria in response to changing environmental conditions.

3.2 Bacterial gene regulation

Prokaryotes can monitor and adapt to ecological changes like altering nutrition supplies, pH fluctuations or heavy metal pollution (Giller *et al.* 1998). This is crucial for survival in changing environments like the soil, which is the natural habitat of *C. glutamicum* (Kinoshita *et al.* 1957). In response to such stress situations, microorganisms employ distinct regulatory mechanisms and alternative metabolic pathways mainly by varying gene expression. The regulation of such modulation of bacterial gene expression usually proceeds at the level of transcription (Browning and Busby 2004).

3.2.1 Transcription in bacteria

In prokaryotic cells, the transcription reaction starts with the RNA polymerase (RNAP) association to the DNA. The RNAP consists of the following subunits (Burgess 1969): the two α-subunits, the two β-subunits and the ω-subunit. This polymerase core enzyme complex binds to the DNA non-specifically and diffuses along the DNA strand. For the specific transcription initiation, the RNA polymerase holoenzyme complex is formed with an additional σ-factor, which is bound to the -10 and -35 regions of the promoter (DeHaseth *et al. 1998)*. Subsequently, the double-stranded DNA (closed complex) is melted to form two single-stranded DNA fragments (open complex) for the transcription initiation. After multiple short transcripts, an elongation complex with a significantly lower affinity to the σ-factor is established (Hsu 2010). Therefore, the σ-factor is cleaved off, the promoter is released, and the transcription starts. This process is regulated to control the gene expression in bacteria.

3.2.2 Transcription regulation

The transcription initiation is the most common and strongest regulated step of bacterial gene expression (Browning and Busby 2004). It can be either activated by transcription activators like the cAMP response protein (Kolb *et al.* 1993) or repressed by transcription repressors like *lac* repressor LacI (Lewis 2005). The majority of transcription factors consists of two domains, namely the effector domain to interact with regulator molecules

and the DNA-binding domain to interact with the DNA. Besides zinc finger, leucine zipper and helix-loop-helix formations, the predominant orientation of DNA-binding domains in prokaryotes is the helix-turn-helix (HTH) motif with about 95 % (Perez-Rueda and Collado-Vides 2000; Perez-Rueda and Collado-Vides 2001). Most of the amino acids of DNA-binding domains are positively charged to non-specifically interact with the negatively charged phosphate-groups of the DNA backbone (Cherstvy 2009; Coulocheri *et al.* 2007). For specific protein-DNA binding, functional groups of the DNA bases are recognized by distinct amino acids of the DNA-binding domain (for review, Harteis and Schneider 2014). For this purpose, a sequence-specific binding site upstream of the target gene is crucial. However, a simple recognition code between the base pairs and amino acids does not exist. In many cases, a sequence-based recognition is not enough for specific protein-DNA interaction. Therefore, the specific recognition of base pairs must be extended by additional features like the readout of the DNA shape (Rohs *et al.* 2010).

This transcription regulation allows to differentially modulate the gene expression pattern of bacteria. Consequently, such microorganisms like *C. glutamicum* can modify cellular properties and adjust various metabolisms like the pathways for carbon, oxygen and nitrogen.

3.3 Nitrogen metabolism in *C. glutamicum*

Besides oxygen and carbon, nitrogen is one of the most essential elements for the biosynthesis of proteins, nucleic acids and distinct messenger substances like hormones. However, molecular nitrogen (78.1 % of the terrestrial atmosphere) cannot be directly assimilated by most organisms due to its inertness. Only some prokaryotes, specifically diazotrophic microorganisms, allow to reduce atmospheric nitrogen to ammonia (NH_3) (Shin *et al.* 2016). Ammonia is in equilibrium with its charged form, ammonium, which is one of the main nitrogen sources for many organisms to produce other nitrogen-containing compounds. In addition to ammonium, many microorganisms can use alternative nitrogen sources like urea, creatinine and L-glutamine (Beckers *et al.* 2004; Bendt *et al.* 2004; Rehm *et al.* 2010). For this purpose, a wide range of mechanisms for uptake and assimilation of these nitrogen sources are active in prokaryotes.

3.3.1 Nitrogen uptake and assimilation

The nitrogen metabolism of *C. glutamicum* was thoroughly investigated in terms of absorption and assimilation (Jakoby *et al.* 2000; Burkovski 2003a, 2003b, 2007). The preferred nutrient source in the nitrogen metabolism is the positively charged ammonium,

which is in equilibrium with the uncharged ammonia. At excess, uncharged ammonia can be absorbed by *C. glutamicum* without energy costs by passive diffusion. At these conditions, oxidative amination of intracellular 2-oxoglutaric acid and ammonium to L-glutamate is catalyzed with an additional NADPH by the low affine glutamate dehydrogenase (GDH, K_M of approx. 1 mM) (Beckers *et al.* 2001).
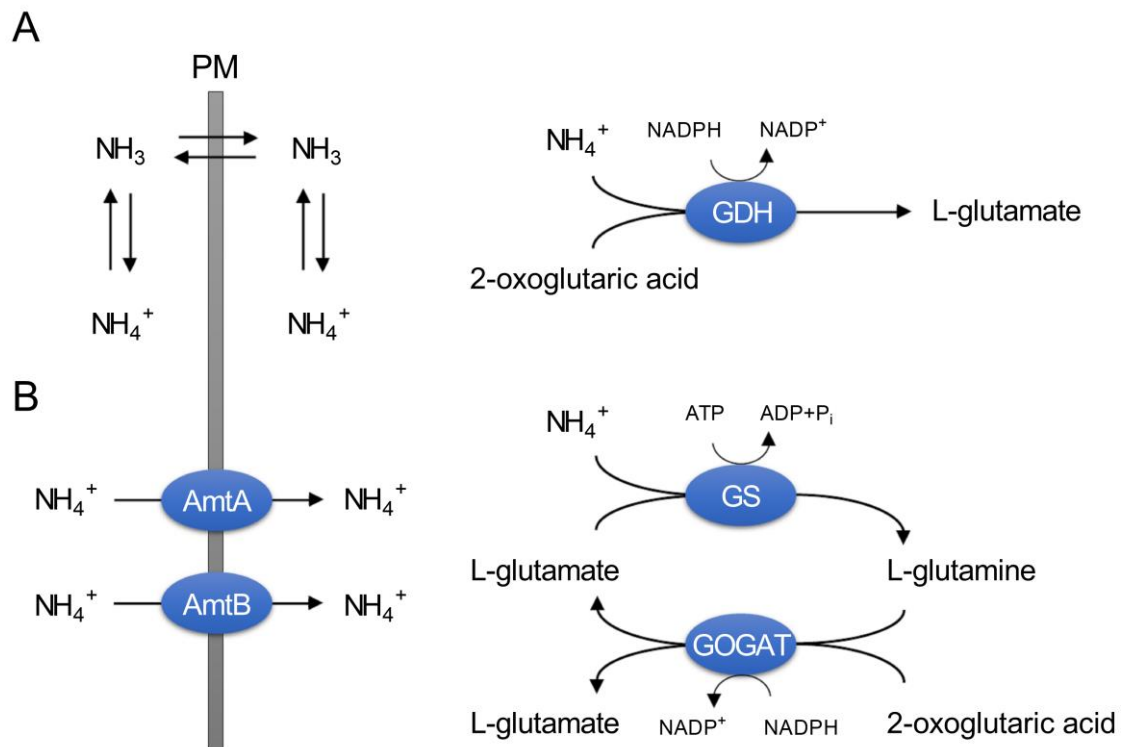
Figure 2 Ammonium uptake and assimilation in *C. glutamicum*. (A) Nitrogen metabolism in *C. glutamicum* at surplus: Due to the equilibrium between ammonium and ammonia, passive diffusion of ammonia through the plasma membrane (PM) can be observed. Under these conditions, intracellular ammonium and 2-oxoglutaric acid are assimilated by GDH to form L-glutamate. (B) Nitrogen metabolism in *C. glutamicum* at deprivation: without ammonia diffusion, ammonium uptake is only achieved by the ammonium transporters AmtA and AmtB. Furthermore, the alternative nitrogen assimilation pathway is activated. The reaction of intracellular ammonium and L-glutamate into L-glutamine is catalyzed by GS. Subsequently, L-glutamine and 2-oxoglutaric acid is transformed to two L-glutamate molecules by GOGAT.

At ammonium concentrations under 1 mM, passive diffusion through the membrane and ammonium assimilation by GDH is insufficient. To counteract the reduced nitrogen absorption, the two ammonium transporters AmtA and AmtB are employed in *C. glutamicum* (Walter *et al.* 2008). Due to its high substrate affinity, AmtA represents the major uptake

system, while the low affinity of AmtB indicates a supportive secondary role in ammonium transportation. For the ammonium assimilation under nitrogen limitation, an alternative anabolic pathway via glutamine synthetase (GS) and glutamate synthase (GOGAT) is activated. The high substrate affinity of GS to ammonium allows to assimilate ammonium under limited nitrogen supply. In contrast to the GDH pathway, an additional ATP is used for the transformation of ammonium and L-glutamate to L-glutamine by GS. Subsequently, the reaction of L-glutamine, 2-oxoglutaric acid and an additional NADPH to two L-glutamate molecules is catalyzed by GOGAT (Tesch *et al.* 1999). Due to the higher energy consumption, the ammonium assimilation by GS and GOGAT is strictly regulated at both, activity and transcription levels (Burkovski 2003b).

3.3.2   Nitrogen regulation

The uptake and assimilation of different nitrogen sources are regulated in response to the current supply. This regulatory mechanism is designated as nitrogen control (Burkovski 2003a, 2003b, 2007). Furthermore, studies of Fischer in 1999 suggested different mechanisms to regulate the nitrogen metabolism in prokaryotes (Fisher 1999).

First analyses of *E. coli* provided a detailed insight in the nitrogen control of enterobacteria (for review, Merrick and Edwards 1995). Like in *C. glutamicum*, GDH is activated under nitrogen surplus, while GS and GOGAT are active under nitrogen limitation in *E. coli*. These enzymes are controlled by four crucial regulator proteins namely the uridylyl transferase GlnD, the trimeric P_{II} signal transduction proteins GlnB, the adenylyl transferase GlnE and the 2-component system NtrB/NtrC. In nitrogen excess, GS is inhibited by adenylation, while NtrB, NtrC and GlnB are inhibited by demodification. During nitrogen limitation, a GlnB-GlnD complex is formed resulting in an uridylyl residue transfer by the UTase to each of the three subunits of GlnB. The modification of GlnB promotes the deadenylation of GS and the adenylation of NtrB. Finally, the transcription activator of nitrogen regulated genes, NtrC, is activated by the adenylated kinase NtrB.

Analysis of *Bacillus subtilis* revealed a different nitrogen metabolism and regulation (Fisher 1999). GDH, for example, is not involved in the ammonium assimilation but L-glutamate degradation in *B. subtilis* (Kane *et al.* 1981). This suggests an exclusive amino acid anabolism by GS and GOGAT. GS is not regulated by modification but rather by feedback inhibition. In contrast to NtrB/NtrC of *E. coli*, three different regulatory proteins are involved in the transcription regulation in *B. subtilis*, specifically GlnR, TnrA and CodY. GlnR and TnrA regulate the transcription of genes under different nitrogen supply, while CodY controls the transcription of genes depending on the growth rate.

In *C. glutamicum*, the AmtR regulon represents the regulatory network of the transcription of nitrogen dependent genes and consists of three main components: the nucleotide transferase GlnD, the P_{II} signal transduction protein GlnK and the transcription repressor AmtR (Burkovski 2003a, 2003b, 2007; Amon *et al.* 2010). Here, GlnD is an adenylyl transferase (ATase), which is responsible for the adenylation and deadenylation of GlnK. Therefore, GlnD is bi-functionally active with an N-terminal modification activity and a C-terminal demodification activity (Strösser *et al.* 2004). The activity of GlnD is adjusted by a still unexplained direct or indirect sensing of the intracellular nitrogen concentration (Nolden *et al.* 2001b). At good nitrogen supply, GlnK is inactivated by deadenylation, while it is activated by adenylation under nitrogen starvation. In contrast to other proteobacteria, GlnK is the only P_{II}-type signal transduction protein in *C. glutamicum* (Jakoby *et al.* 1999). Its corresponding gene *glnK* is organized in an operon with *glnD* (coding for the adenylyl transferase) and *amtB* (coding for the secondary ammonium transporter), which is regulated by AmtR (Jakoby *et al.* 1999; Nolden *et al.* 2001b). The structure of GlnK comprises three uniform subunits of a molecular weight of about 13 kDa. In response to nitrogen deprivation, GlnK is expressed and activated by adenylation at the tyrosine residue 51 of each subunit (Ninfa and Atkinson 2000). Thus, activation of GlnK promotes the formation of the AmtR-GlnK complex resulting in the AmtR dissociation off the DNA (Strösser *et al.* 2004). Consequently, AmtR regulated genes can be transcribed by RNA-polymerase. At increasing nitrogen concentrations, GlnK is deadenylated by GlnD resulting in the segregation of the AmtR-GlnK complex. After separation, deadenylated GlnK is bound to the membrane protein AmtB, but not to the primary transport system AmtA. Strösser and coworkers demonstrated that the localization change is crucial for a specific proteolytic degradation of GlnK (Strösser *et al.* 2004). Furthermore, they suggested that the ClpP protease, the ClpXP protease complex and the membrane-linked protease FtsH are involved in the specific proteolysis of GlnK.

In addition, bioinformatics and molecular biology approaches identified AmtR as the main regulatory protein for the nitrogen control in *C. glutamicum* (Jakoby *et al.* 2000). Based on the AmtR binding sites within the promoters of the first identified genes *amtA* and *amtB*, an initial genome wide screening for alternative AmtR target sequences was accomplished. In the following decades, new genes have been found and analyzed by gene mutation and interaction analyses. Therefore, about 42 directly or indirectly AmtR regulated genes are known today (Buchinger *et al.* 2009). According to their functions, most of these genes can be assigned to the main groups of catalytic enzymes, transporters and signal transduction proteins.
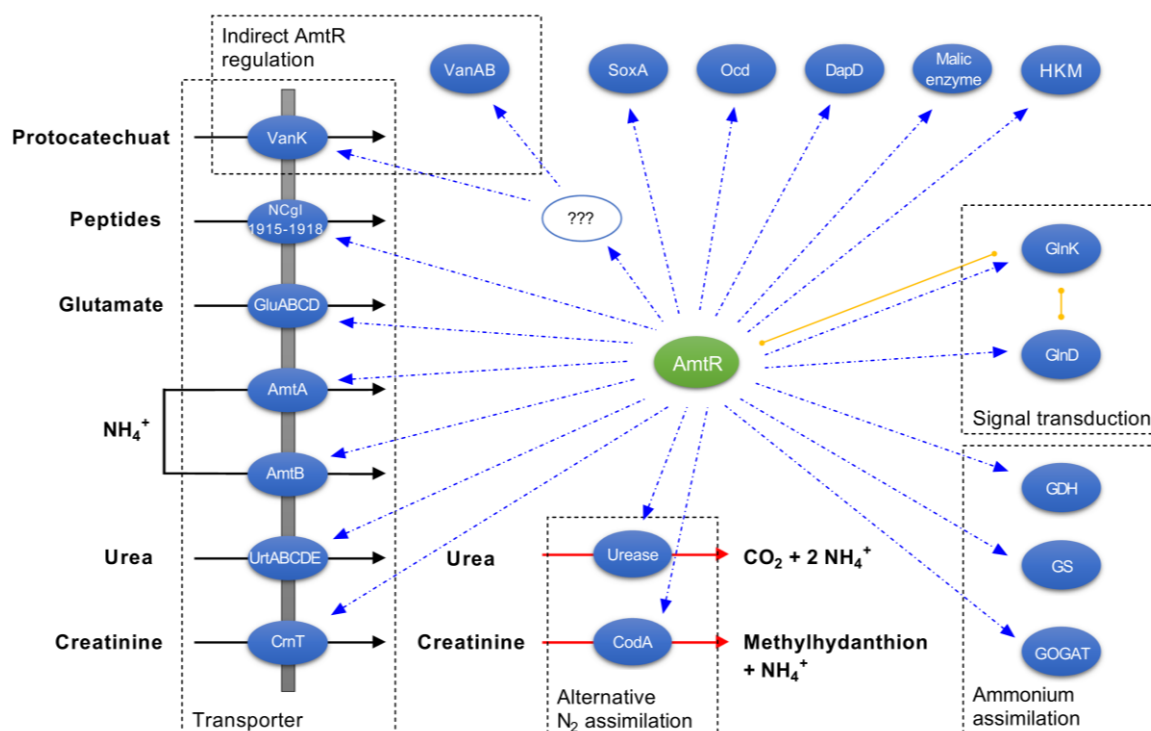
Figure 3 Model of the AmtR regulon in *C. glutamicum*. AmtR (green) regulated genes can be divided into the different groups of transportation, nitrogen assimilation, signal transduction and putative biosynthesis. In addition to directly controlled genes, an indirect modulation of the vanillate pathway by AmtR is suggested for *C. glutamicum* (Silberbach 2004; Beckers *et al.* 2005; Merkens *et al.* 2005; Buchinger *et al.* 2009). (Black arrows: uptake by membrane-linked transporters; red arrows: catalytic reactions by assimilatory enzymes; blue dotted arrows: transcriptional repression by AmtR; yellow lines: signal transduction by protein-protein interaction).

The largest group comprises genes coding for proteins of biosynthesis and assimilation. For example, genes of the ammonium assimilation apparatus like *gdh* encoding the glutamate dehydrogenase (Beckers *et al.* 2005), *glnA*, which codes for the glutamine synthetase (Nolden *et al.* 2001a) and the operon *gltBD* coding for the glutamate synthase (Beckers *et al.* 2001) are part of this group. Genes coding for alternative nitrogen assimilation enzymes are also associated to this group of AmtR target genes: *ureABCEFGD* coding for the urease (Nolden *et al.* 2000; Beckers *et al.* 2004) and *codA* encoding a creatinine deaminase (Bendt *et al.* 2004). Additionally, genes for a putative ornithine cyclodeaminase protein (*ocd*), a sarcosine oxidase (*soxA*), a sensor histidine kinase of a 2-component system (*hkm*), a malic enzyme (*malE*) and a tetrahydrodipicolinate succinylase (*dapD*) seem to be AmtR regulated, as well (Beckers *et al.* 2005; Schulz *et al.* 2001; Buchinger *et al.* 2009; Krause *et al.* 2012; Wehrmann *et al.* 1998). Transporters represent the second-largest group of AmtR-regulated genes. This includes more than a dozen genes

like *amtA* and *amtB* encoding the ammonium transporters (Jakoby *et al.* 2000), the *gluABCD* operon coding for the glutamate transporter (Kronemeyer *et al.* 1995), the gene cluster *urtABCDE*, which encodes the urea transporter (Beckers et al. 2004), the creatinine permease gene *crnT* (Bendt *et al.* 2004) and genes for a putative ABC type oligopeptide uptake system (NCgl1915-1918) (Beckers *et al.* 2005; Hasselt *et al.* 2011). Additionally, the AmtR regulon comprises the genes *glnD* and *glnK* of signal transduction proteins in *C. glutamicum* (Jakoby *et al.* 1999; Nolden *et al.* 2001b). Moreover, Merkens and coworkers suggested an additional indirect regulation mechanism by AmtR for the operon *vanABK*, which contains the genes *vanAB* encoding a vanillate-o-demethylase and *vanK* coding for a putative protocatechuate uptake system (Merkens *et al.* 2005).

In addition to the large set of target genes, a high diversity in the transcription repression was demonstrated for AmtR regulated genes. Based on previous studies, this was attributed to the different binding affinities between the diverse operator sequences and the TetR-type transcription regulator AmtR (Beckers *et al.* 2005; Muhl *et al.* 2009; Nolden *et al.* 2001a).

3.4 Transcription factors in *C. glutamicum*

For the transcription modulation of the 3058 identified genes in *C. glutamicum*, over 159 regulators are known nowadays. These regulatory proteins are organized in 7 σ-factors, 13 response regulators (2-component system) and more than 128 transcription factors. This represents an expanded regulatory network compared to other *Corynebacterium* species like *C. diphtheriae*, *C. efficiens* or *C. jeikeium* (Brinkrolf *et al.* 2007). Based on their amino acid sequence similarity, transcription factors can be grouped into different evolutionary regulator protein families (Perez-Rueda and Collado-Vides 2000). The classification of transcription regulators in *C. glutamicum* revealed at least 24 different protein families, which are conserved in all corynebacteria (Brune *et al.* 2005). Despite many regulatory protein families with only 1 to 3 assigned members, the TetR family was identified as the largest family including 16 regulators.

3.4.1 The TetR family of transcription regulators

Regulators from the TetR family consist of two different domains namely the effector (ED) and the DNA-binding domain (DBD). In particular, the DNA-binding domain with its common helix-turn-helix (HTH) orientation shows a high conservation among TetR-type transcription factors (Ramos *et al.* 2005; Cuthbertson and Nodwell 2013). In the effector domain, proteins of the TetR family vary significantly in their protein structure because of the numerous signals, which are recognized by these repressors. Typically, these signals comprise a wide

range of low-molecular-weight effector molecules such as antibiotics, nucleotides and single amino acids (Ramos *et al.* 2005; Cuthbertson and Nodwell 2013). Unlike common TetR-type regulatory proteins, one distinct regulator does not interact with small metabolites but with macromolecules like GlnK (Beckers *et al.* 2005; Strösser *et al.* 2004). This regulatory protein was identified as the master regulator of the nitrogen metabolism, designated as AmtR.

3.4.2 The TetR-type repressor AmtR

AmtR is the master regulator of the nitrogen control in *C. glutamicum*. Its corresponding gene was named after the first identified function of AmtR as **am**monium **t**ransport **r**epressor (Jakoby *et al.* 2000). Target DNA sequences are bound by dimeric AmtR, whereas each monomer of approx. 24.4 kDa contains 222 amino acids. Furthermore, each monomer consists of one DNA-binding and one effector-binding domain, respectively (Sevvana *et al.* 2017). For the effector-binding domain of AmtR, Palanca and coworker recently published distinct structural properties, which are involved in the modulation of the DNA-binding affinity of AmtR by GlnK (Palanca and Rubio 2016). They identified an additional C-terminal α-helix and an extended loop between helices 8 and 9 of 16 amino acids. Crystal structure analysis additionally revealed a large open cavity on the intersubunit boundary, which shapeshifts upon AmtR-DNA binding. The N-terminal DNA-binding domain of AmtR is similar to other TetR-type regulator domains because of its three α-helices oriented in an HTH motif. Helix 2 and 3 are involved in the direct and indirect base pair readout of the respective target sequences, while analysis of helix 1 showed structural characteristics (Muhl *et al.* 2009). Additionally, the first 19 amino acids at the N-terminus seem to be responsible for unspecific protein-DNA interaction to the minor groove of the DNA (Palanca and Rubio 2016).

AmtR regulates genes by binding to specific DNA sequences within the promoter region. These sequences contain the two conserved half sites "CTAT" and "ATAG", which are separated by six nucleotides (Muhl *et al.* 2009), flanked by A-T-rich sequences (Palanca and Rubio 2016) and can be found on the sense- and antisense strand. Initial interaction studies suggested various binding affinities of AmtR for these sequences, while transcription patterns of AmtR regulated genes after induction suggested different kinetics for the AmtR-DNA interaction (Jakoby *et al.* 2000; Nolden *et al.* 2001a; Beckers *et al.* 2005). Based on the identified DNA motifs, a consensus sequence for AmtR operators was established (figure 4; Beckers *et al.* 2005). Nevertheless, additional transcriptome analyses of the genome of *C. glutamicum* identified many different sequences that match this consensus sequence but are not AmtR-regulated (Beckers *et al.* 2005; Silberbach and

Burkovski 2006). Therefore, additional properties like the shape or flexibility of the operators were suggested to influence the AmtR-DNA binding. Even though the structure of AmtR as well as the AmtR binding to DNA was intensively characterized in the last decades, the role of the DNA conformation for the AmtR-DNA interaction has not been investigated so far.
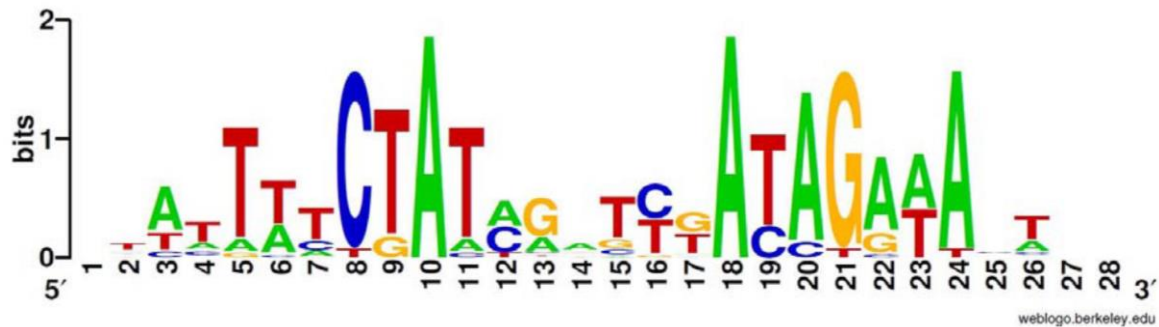
Figure 4 DNA binding box of the transcription regulator AmtR of *C. glutamicum*. Based on DNA targets predicted by bioinformatic analyses, this consensus sequence was derived. The size of the depicted letters represents the conservation of nucleotides in AmtR binding sites, respectively (Beckers *et al.* 2005).

3.5 Scope of the thesis

Studies of the AmtR interaction with operators from different AmtR-regulated genes revealed specific AmtR binding to these operators with diverse binding affinities. Since additional screenings of the genome of *C. glutamicum* identified many putative AmtR binding sites in promoter regions of not AmtR-regulated genes, additional properties like the shape or flexibility of the operators were suggested to influence the AmtR-DNA binding. Therefore, investigations will be carried out in this study, to assess, if operators of several AmtR controlled genes, which comprise conserved half sites and variations in the spacer sequence with different structural properties, provoke distinct regulation patterns. For this purpose, gel retardation assays in combination with surface plasmon resonance experiments will be performed with the wild type *amtB* operator and two designed operator variants with altered deformation properties. The results of these analyses may derive a dynamic model for the AmtR-DNA interaction.

4   Materials and methods

4.1   Bacterial strains and plasmids

4.1.1   Bacterial strains

Table 3.1: *C. glutamicum* **and** *E. coli* **strains used in this work.**

Strain	Genotype, phenotype	Reference
E. coli		
BL21	B F$^-$ *ompT gal dcm lon hsdS$_B$*($r_B^-$$m_B^-$)	(Studier *et al.* 1990)
DH5α MCR	F$^-$ *endA1 supE44 thi-1 λ$^-$ recA1 gyrA96 relA1 deoR Δ(lacZYA-argF) U169 Φ80ΔlacZ ΔM15mcrA Δ(mrr hsdRMS mcrBC)*	(Grant *et al.* 1990)

4.1.2   Plasmids

Table 3.2: Plasmids used in this work.

Plasmid	Description	Reference
pMal-c2x	*ptac*, Ap^R, pBR322 *ori*, M13 *ori*, *malE*, *lac^q*, *lacZα*, *E. coli* vector for protein purification	(di Guana *et al.* 1988; Maina *et al.* 1988)
pMal-c2*amtR*	pMal-c2 containing *amtR* gene for overexpression of AmtR with N-terminal fused maltose-binding protein	(Jakoby *et al.* 2000)
pBR322	*pP1*, *pP2*, *pP3*, Ap^R, Tc^R, pMB1 ori, *rop*, cloning vector with matching multiple cloning site	(Bolivar *et al.* 1977)
pQE30	*pT5*, Ap^R, ColE1 *ori*, cloning vector with matching multiple cloning site	Qiagen GmbH (Hilden)

pCSC0	Cloning vector pQE30 with integrated multiple cloning site of pBR322, integrated AmtR binding site and HindIII replaced by PstI restriction site	This thesis
pCSC1	Cloning vector pCSC0 with additionally integrated EagI restriction site	This thesis
pCSC2	Cloning vector pCSC1 with additionally integrated BsaI restriction site	This thesis
pCSC4	Cloning vector pCSC2 with EcoRV replaced by EcoRI restriction site	This thesis
pCSC5 WT	Cloning vector pCSC4 with double insertion, wild type AmtR binding site	This thesis
pCSC5 DE	Cloning vector pCSC4 with double insertion, deformable AmtR binding site	This thesis
pCSC5 RI	Cloning vector pCSC4 with double insertion, rigid AmtR binding site	This thesis

4.2 Oligonucleotides

Table 3.3: Oligonucleotides used in this work. (Producer MWG Biotech AG)

Primer	DNA-sequence	Description
amtR amplification in pMal-c2*amtR*		
amtRw/oATG-BamHI	GGTCGGATCCGCAGGAGCAGTGGG	without ATG, integrated BamHI site
amtR-PstI-rev	GGCGCCTGCAGTTATTTCGCGTCAGCCTGC	Integrated PstI site

AmtR binding sequences for interaction analysis

glnA_fw	AAAAGTTTTGATAGATCGACAGGTAATGCA	Wild type *glnA* operator
glnA_rev	TGCATTACCTGTCGATCTATCAAAACTTTT	Wild type *glnA* operator
amtB_fw	TAAATTACCTGTTAAACTATAGAAAATATC	Wild type *amtB* operator
amtB_rev	GATATTTTCTATAGTTTAACAGGTAATTTA	Wild type *amtB* operator
gltB_fw	CCGTTTTCCTATAGGTTGATCGAAAGTAAC	Wild type *gltB* operator
gltB_rev	GTTACTTTCGATCAACCTATAGGAAAACGG	Wild type *gltB* operator
codA_fw	TATCTATTCTATTGCTTGACAGGTATTAGT	Wild type *codA* operator
codA_rev	ACTAATACCTGTCAAGCAATAGAATAGATA	Wild type *codA* operator
urtA_fw	ACAACTACCTATAGGCTGACAGAAACTCTA	Wild type *urtA* operator
urtA_rev	TAGAGTTTCTGTCAGCCTATAGGTAGTTGT	Wild type *urtA* operator
crnT_fw	CATACTTTCTATAGATTGATAGAAATGTGG	Wild type *crnT* operator
crnT_rev	CCACATTTCTATCAATCTATAGAAAGTATG	Wild type *crnT* operator
amtB RI_fw	TAAATTACCTGTGGGGGGATAGAAAATATC	Rigid *amtB* operator
amtB RI_re	GATATTTTCTATCCCCCCACAGGTAATTTA	Rigid *amtB* operator
amtB DE_fw	TAAATTACCTGTCGCGCGATAGAAAATATC	Deformable *amtB* operator

amtB DE_rev	GATATTTTCTATCGCGCGACAGGTAATTTA	Deformable *amtB* operator
DNA unspec_fw	CGCGATAATCTTTGCTAACCCTTTTGAGTT	unspec. DNA fragment
DNA unspec_rev	AACTCAAAAGGGTTAGCAAAGATTATCGCG	unspec. DNA fragment

Cloning for DNA permutations

fw prime AmtR-sBS HindIII	CGATAAGCTTTAATGCGG	Forward primer with HindIII site
re /wo HindIII pQE30neu	CCAAGCTCAGCTAATTACGATTGGCTGCAGG	Reverse primer without HindIII site
rev CP AmtR-sBS PstI	CGATTGGCTGCAGGTCGACCC	Reverse primer with PstI site
Mutagenesis primer BsaI	CGCTACTTGGTCTCTATCGACTACGC	Integration of BsaI restriction site
Mutagenesis primer EagI	CTACGCGATCACGGCCGCCACACCCGTCC	Integration of EagI restriction site
rev muta EcoRI CP new	GCTGTCGGAATGGACGAATTCCCGCAAGAGG	Replacement of EcoRV by EcoRI
re AmtR sBS AgeI /wo PstI	ATTGGACCGGTGTCGACCCGG	Integration of AgeI site, reverse primer
fw PrimerAmtR-sBS AgeI	GCGACCGGTGCTTTAATGCGG	Integration of AgeI site, forward primer
fw AmtR WT KpnI, XmaI	CTAAATTACCTGTTAAACTATAGAAAATATCGGAACC	Insertion of wild type AmtR binding site
re AmtR WT KpnI, XmaI	CCGGGGTTCCGATATTTTCTATAGTTTAACAGGTAATTTAGGTAC	Insertion of wild type AmtR binding site
fw AmtR RI KpnI, XmaI	CTAAATTACCTGTGGGGGGATAGAAAATATCGGAACC	Insertion of rigid AmtR binding site
re AmtR RI KpnI, XmaI	CCGGGGTTCCGATATTTTCTATCCCCCCACAGGTAATTTAGGTAC	Insertion of rigid AmtR binding site
fw AmtR DE KpnI, XmaI	CTAAATTACCTGTCGCGCGATAGAAAATATCGGAACC	Insertion of deformable AmtR binding site

17

re AmtR DE KpnI, Xmal	CCGGGGGTTCCGATATTTTCTATCGCG CGACAGGTAATTTAGGTAC	Insertion of deformable AmtR binding site

4.3 Enzymes and markers

Table 3.4: Enzymes and markers used in this work.

Product	Producer
DNA-ladder 100 bp	PeqLab
DNase I	Roche
Dual color prestained protein ladder	Bio-Rad
Factor Xa protease	New England Biolabs
Lysozyme	Roth
PeqGold unstained protein ladder	PeqLab
Phusion® High-Fidelity DNA polymerase	New England Biolabs
Rapid alkaline phosphatase	New England Biolabs
Restriction endonucleases	New England Biolabs
T4-DNA ligase	New England Biolabs
T4-polynucleotide kinase	New England Biolabs
Taq DNA polymerase	New England Biolabs
Terminal transferase	Roche

4.4 Kits

Table 3.5: Kits used in this work.

Product	Producer
DIG Gel Shift Kit, 2nd generation	Roche
NucleoBond® PC 10000 EF kit	Macherey-Nagel
NucleoSpin® Gel and PCR Clean-up	Macherey-Nagel
NucleoSpin® Plasmid	Macherey-Nagel

4.5 Software

Table 3.6: Software used in this work.

Programm	Purpose	Version	Reference
BiaEvaluation	Evaluation of SPR measuerments	4.0	GE Healthcare
CloneManager	Primer designing, in silico cloning	5.0	Scientific & Education Software
Excel	Spreadsheet	2013	Microsoft Corp.
Genome Compiler	Primer designing, in silico cloning		Genome Compiler Corporation
GraphPad Prism	Preparation and editing of graphics	7.04	GraphPad Software Inc.
ImageLab	Western blot quantificiation	5.0	Bio-Rad
Mendeley Desktop	Reference manager	1.17.13	Mendeley
Nanodrop 2000	Nanodrop measurements	1.4.2	PeqLab
PowerPoint	Evaluation of SPR and Äkta data	2013	Microsoft Corp.
PrimeView	Evaluation of protein purification	5.0	GE Healthcare
SeqMan	Sequencing evaluation	4.0	DNASTAR
SnapGene	Primer designing, in silico cloning	4.1	GSL Biotech LLC
Swiss PdbViewer	Crystal structure analysis	4.1	ExPASy
Word	Word processing	2013	Microsoft Corp.

4.6 Media and additives

4.6.1 Media

Media were autoclaved before using.

LB (Luria-Bertani, (Sambrook *et al.* 1989))

Sodium chloride	1 % (w v^{-1})
Tryptone	1 % (w v^{-1})
Yeast extract	0.5 % (w v^{-1})

SOB (Hanahan 1983)

Magnesium chloride	10 mM
Magnesium sulfate	10 mM
Potassium chloride	2.5 mM
Sodium chloride	10 mM
Tryptone	2 % (w v^{-1})
Yeast extract	0.5 % (w v^{-1})

TB buffer (Inoue *et al.* 1990)

Pipes	10 mM
Calcium chloride	20 mM
Potassium chloride	250 mM
pH 6,7	

After adjusting the pH to 6.7, 22.5 mM of manganese chloride was added to the solution. Subsequently, the buffer was sterile filtrated.

4.6.2   Additives

Agar

For solid media	1.5 % (w v^{-1})

Antibiotics

Antibiotics were prepared as sterile stock solution by filtration. Antibiotics were added to the media after autoclaving and cooling down.

Table 3.7

Antibiotics	Abbreviation	Solvent	Stock [mg/ml]	*C. glutamicum* [µg/ml]	*E. coli* [µg/ml]	Storage
Ampicillin	Amp	H2O$_{bidest.}$	100	-	100	-20 °C

Glucose

In LB medium	2 % (w v^{-1})

4.7 Buffers

All buffers were prepared in deionized water and autoclaved, if necessary.

4.7.1 Agarose gel electrophoresis

Agarose

Solved in TAE buffer (1x)	0.6 to 1.5 % (w v^{-1})

Purple gel loading dye (1x)

EDTA	10 mM
Ficoll®-400	2.5 % (w v^{-1})
Dye 1	0.02 %
Dye 2	0.001%
SDS	0.08% (w v^{-1})
Tris-HCl	3.3 mM
pH 8	

TAE buffer (50x)

EDTA	50 mM
Sodium acetate	500 mM
Tris	2 M
pH 7.8 (acetic acid)	

4.7.2 Polyacrylamide gel electrophoresis

4.7.2.1 Native PAGE

6 % native polyacrylamide gel

Tris-HCl pH 8.8	45.4 mM
Acrylamide/bisacrylamide	6 % (v v^{-1})
APS	0.1 % (w v^{-1})
Glycerol	10 % (v v^{-1})
TEMED	0.1 % (v v^{-1})

Native PAGE running buffer (Evans 2017)

Glycine	192 mM
Tris	25 mM

Native loading buffer (5x)

Glycerol	50 % (v v^{-1})
Serva blue G-250	1 % (w v^{-1})
Tris	300 mM
pH 6.8 (NaOH)	

4.7.2.2 SDS-PAGE

10% separating polyacrylamide gel

Tris-Borat pH 8.8	99.8 mM
Tris-HCl pH 8.8	86.5 mM
Acrylamide/bisacrylamide	10 % (v v^{-1})
APS	0.1 % (w v^{-1})
SDS	1 % (w v^{-1})
TEMED	0.01 % (v v^{-1})

Stacking polyacrylamide gel

Tris-HCl pH 6.8	86.5 mM
Acrylamide/bisacrylamide	10 % (v v^{-1})
APS	0.5 % (w v^{-1})
SDS	0.1 % (w v^{-1})
TEMED	0.1 % (v v^{-1})

SDS-PAGE running buffer

Glycine	1.25 M
SDS	2 % (w v^{-1})
Tris	0.125 M

SDS loading buffer (5x)

2-mercaptoethanol	10 % (v v^{-1})
Glycerol	60 % (v v^{-1})
Serva brilliant blue G-250	0.1 % (w v^{-1})
SDS	20 % (w v^{-1})
Tris	250 mM
pH 6.8 (HCl)	

Coomassie staining buffer

Methanol	45 % (v v^{-1})
Acetic acid	10 % (v v^{-1})
Coomassie Brilliant Blue G-250	0.2 % (w v^{-1})
H$_2$O$_{bidest}$	44.8 %

4.7.2.3 TBE-PAGE

8 to 12 % TBE gel

5x TBE running buffer	20 % (v v^{-1})
Acrylamide/bisacrylamide	8 to 12 % (v v^{-1})
APS	0.1 % (w v^{-1})
Glycerol	10 % (v v^{-1})
TEMED	0.01 % (v v^{-1})

5x TBE running buffer (Evans 2017)

Boric acid	890 mM
EDTA	20 mM
Tris	890 mM
pH 8.0 (boric acid)	

4.7.3   Protein purification

All buffer used for the Äkta prime system were filtrated with 0.2 µm filters.

4.7.3.1 MBP-Trap chromatography

MBP washing buffer

EDTA	1 mM
Sodium chloride	200 mM
Tris	20 mM
pH 7.4 (HCl)	

MBP elution buffer

EDTA	1 mM
Maltose	20 mM
Sodium chloride	200 mM
Tris	20 mM

pH 7.4 (HCl)

Factor Xa protease buffer

Calcium chloride	2 mM
Sodium chloride	100 mM
Tris	20 mM

pH 7.4 (HCl)

4.7.3.2 Size exclusion chromatography

HBS-EP buffer

EDTA	3 mM
HEPES	10 mM
Sodium chloride	150 mM

pH 7.4 (HCl)

4.7.4 Surface plasmon resonance spectroscopy (SPR)

HBS-EP buffer (GE healthcare, Uppsala)

EDTA	3 mM
HEPES	10 mM
Sodium chloride	150 mM
Surfactant p20	0.005 % (v v^{-1})

pH 7.4

4.7.5 DIG-Gelshift detection

Maleic acid buffer

Maleic acid	100 mM
Sodium chloride	150 mM

pH 7.5 (NaOH)

Washing buffer

Maleic acid	100 mM
Sodium chloride	150 mM
Tween 20	0.3 % (v v^{-1})
pH 7.5 (NaOH)	

10x blocking solution

Blocking reagent (Roche Diagnostics, Mannheim) in maleic acid buffer	10 % (w v^{-1})

Detection buffer

Magnesium chloride	50 mM
Sodium chloride	100 mM
Tris	100 mM
pH 9.5 (HCl)	

CSPD solution

CSPD reagent (Roche Diagnostics, Mannheim) in detection buffer	1 % (v v^{-1})

4.8 Cultivation of bacteria

4.8.1 Growth conditions for *E. coli*

For plasmid DNA isolation from *E. coli* (see section 4.10.1) as well as cultivation of chemical competent bacteria (see section 4.11.1), cells were inoculated in 4 ml LB medium. Subsequently, the cell suspension was incubated with antibiotics overnight at 37 °C and 180 rpm.

For overexpression studies using pMal-c2*amtR, E. coli* strains were grown at 37 °C. To ensure enough agitation during growth, baffled flasks were used and the frequency of the rotary shaker (Innova 2350, New Brunswick Scientific) was set to 180 rpm, respectively. The following standardized inoculation scheme was applied for cultivation of *E. coli* obtaining highly reproducible conditions. 20 ml LB medium was inoculated and incubated overnight. On the next day, this culture was used for the inoculation of about 800 ml LB medium with 2 % glucose to an optical density of 0.05 at a wavelength of 600 nm (oD$_{600}$). The culture was incubated at 37 °C for about 2 hours to 3 hours to an oD$_{600}$ of 0.5. At this oD$_{600}$, 0.3 mM IPTG was used for induction of the gene expression for additional 4 hours.

For long-term storage, the cells were harvested by centrifugation for 15 min at 4000 xg and stored at minus 20 °C.

4.8.2 Long-term conservation of bacteria

Prior permanent storage of bacteria, cells were inoculated in 4 ml to 20 ml of the respective medium and incubated overnight according to the protocol of *E. coli* (see section 4.8.1). On the next day, 0.5 ml of the overnight culture with an oD_{600} of at least 2 was added to cryo vials (Roti®-Store Cryoröhrchen) containing a small number of beats. The cell suspension was inverted and incubated at 4 °C for 5 min. Finally, the supernatant was discarded, and the vial was stored permanently at minus 80 °C.

4.9 Working with proteins

4.9.1 Preparation of *E. coli* cell extract

The obtained cell pellet from cultivation was resuspended in 30 ml MBP washing buffer (described in section 4.7.3.1). Additionally, the protease inhibitor Complete (Roche Diagnostics, Mannheim) and lysozyme (Merck, Darmstadt) was added to the suspension. Cell disruption was carried out by sonification (SonoPlus UW2070 Bandelin, Berlin) for 3x 30 s with 60 % power at 4 °C. Afterwards, the suspension was centrifuged for 60 min at 50,000 xg and 4 °C. The supernatant was digested with DNaseI for 15 min at 4 °C and filtered for chromatography. The suspension was stored at 4 °C for further experiments.

4.9.2 Protein purification

Based on previous studies, the preparative purification of recombinant AmtR was carried out (Hasselt *et al.* 2009; Sevvana *et al.* 2017). AmtR was overexpressed as maltose-binding protein (MBP) fusion in *Escherichia coli* BL21 in large scale of 1.5 l cultures (see section 4.8.1). Before the disruption of the cells, the cell pellet was resuspended in MBP washing buffer (see section 4.7.3.1).

4.9.2.1 MBP-Trap affinity chromatography

The cell extract (section 4.9.1) was loaded onto a 5 ml MBP-Trap Dextrin HP column (GE healthcare, Uppsala), which was equilibrated with 10 to 15 column volumes of MBP washing buffer. The fusion protein was loaded onto the column following a washing step of 10 volumes. Afterwards, the fusion protein was cleaved by protease digestion (see section 4.9.2.2). The protein of interest was isolated by washing the column with MBP washing

buffer. The remaining MBP was washed out by using MBP elution buffer (see section 4.7.3.1). The flow rate was 2.5 ml min^{-1}. After purification, the 5 ml MBP-Trap column was regenerated with 10 volumes H$_2$O$_{bidest}$ and 10 volumes 0.5 M NaOH. The sample fractions were stored at 4 °C.

4.9.2.2 Factor Xa protease digestion

The cleavage site of factor Xa (Ile-(Glu or Asp)-Gly-Arg) is located between MBP and AmtR. For cleaving off the MBP-tag, an on-column cleavage was performed for about 4.5 hours at 4 °C. For this purpose, the serine protease factor Xa (NEB, Frankfurt) was applied in a concentration of 5 µg ml^{-1} in factor Xa protease buffer (see section 4.7.3.1). The protease suspension was loaded on the column by the 5 ml loop of the ÄKTA prime system (GE healthcare, Uppsala).

4.9.2.3 Superdex200 size exclusion chromatography

For isolating native AmtR, the protein suspension was loaded onto a size exclusion column (Superdex200 16/60, bed volume 120 ml, GE healthcare) by the 5 ml loop of the ÄKTA prime system (GE Healthcare, Uppsala). Before sample injection, the column was equilibrated with 200 ml HBS-EP buffer. After a 7 ml injection, the column was washed with additional 150 ml HBS-EP buffer. The flow rate was 0.5 ml min^{-1}. After the purification, the size exclusion column was regenerated with 150 ml H$_2$O$_{bidest}$ and 150 ml 0.5 M NaOH. The sample fractions were stored at 4 °C.

4.9.3 Photometric determination of the protein concentration

To measure the protein concentration of purified AmtR, the Nanodrop ND-1000 photospectrometer (Nanodrop Technologies, Delaware USA) was used. The molecular extinction coefficient ε of 16.960 M^{-1} cm^{-1} and the molecular weight of 24.4 kDa of one AmtR monomer were determined by the website http://web.expasy.org/protparam/ (SIB, Swiss Institute of Bioinformatics).

4.9.4 Native polyacrylamide gel electrophoresis (Native PAGE)

After purification, AmtR preparations were analyzed with 6 % non-denaturing polyacrylamide gels (Sambrook *et al.* 1989). Protein samples were mixed with native loading buffer and loaded on the gel at 4 °C. Native running buffer was used as buffer (see section 4.7.2.1). The gel electrophoresis was performed in a mini-PROTEAN tetra cell

apparatus (Bio-Rad) at 4 °C and 100 V for about 2 hours. Proteins characterized by native PAGE and SDS-PAGE (see section 4.9.5) were stained by Coomassie staining buffer for 5 min to 10 min after gel electrophoresis (see section 4.7.2.2). Finally, gels were destained by 10 % acetic acid overnight.

4.9.5 SDS polyacrylamide gel electrophoresis (SDS-PAGE)

Proteins were electrophoretically separated on 10 % denaturing polyacrylamide gels (Sambrook *et al.* 1989). Protein samples were mixed with SDS loading buffer, incubated for 5 minutes at 85 °C, and loaded on the gel with an additional protein marker (PeqGold protein marker II, PeqLab Biotechnologie GmbH, Erlangen). SDS running buffer was used as buffer (see section 4.7.2.2). Gel electrophoresis was performed using a mini-PROTEAN tetra cell apparatus (Bio-Rad) at 120 V for 1 to 2 hours. Gels with proteins were stained and destained by Coomassie staining buffer and 10 % acetic acid (see section 4.7.2.2).

4.9.6 Surface plasmon resonance measurements (SPR)

Determination of kinetic rates and equilibrium constants of protein-DNA interactions were performed using the Biacore X100 system (GE healthcare, Uppsala) at 25 °C. For SPR studies of AmtR-DNA interaction, 3`end biotinylated operator variants and non-specific DNA were used. Approx. 25 response units (RU) of unspecific DNA was immobilized in flow cell 1, while 25 RU of operator variants were immobilized in flow cell 2 on the surface of a streptavidin attached (SA) sensor chip (GE healthcare, Uppsala). For this purpose, the respective DNA was diluted in HBS-EP buffer to a concentration of approx. 5 nM and injected into the SPR device. The DNA immobilization was controlled by a template, which was previously programmed with the BiaEvaluation 4.0 software (LG healthcare, Uppsala). Subsequently, the sensor surface was washed with HBS-EP buffer (GE Healthcare) at least for 2 hours getting a consistent baseline with no background noise. During association, 150 µl AmtR of different concentrations (diluted in HBS-EP buffer, GE healthcare, Uppsala) were injected with a flow rate of 50 µl min^{-1}. For the AmtR dissociation off the sensor chip surface, 100 µl HBS-EP buffer were injected with the same flow rate. The regeneration of the chip surface was performed by using 25 µl of 1.5 M NaCl diluted in HBS-EP buffer (GE healthcare, Uppsala). The data evaluation was carried out by BiaEvaluation 4.0.

To provide a high performance of the Biacore X100 device, the maintenance was performed once a week by washing the system with 0.5 % SDS and 50 mM glycine-NaOH (pH 9.5). For additional sterilization, the system was washed with sodium hypochlorite (GE healthcare, Uppsala) once a month.

4.10 Working with DNA

4.10.1 Plasmid isolation of *E. coli*

For the plasmid preparation of *E. coli*, cells were incubated and harvested, respectively (see section 4.8.1). Plasmid DNA was obtained by using the NucleoSpin Plasmid Kit (Macherey-Nagel, Düren), according to the protocol of the manufacturers.

In addition, significantly higher concentrations of purified DNA were obtained by the NucleoBond® PC 10000 EF kit (Macherey-Nagel, Düren). Prior to the purification, 800 ml to 1000 ml LB medium was inoculated with *E. coli* preculture. The suspension was incubated at 37 °C and 180 rpm overnight. On the next day, the cells were harvested by the Avanti J-25 centrifuge (Beckmann). The plasmid was purified according to the protocol of the manufactures.

4.10.2 Gel electrophoretic separation of DNA

The analysis of the size of nucleic acids was carried out by agarose gel electrophoresis (Sambrook *et al.* 1989). The DNA samples were mixed with purple gel loading dye (see section 4.7.1). Additionally, DNA ladder for 100 bp (New England Biolabs) was loaded on the gel. The samples were separated at 120 V for about 1 hour. Afterwards, the gels were stained in ethidium bromide staining solution for 10 min to 15 min following a washing step in H_2O_{bidest}. The resulting fluorescence emission was detected by the ChemiDoc XRS+ (Bio-Rad).

4.10.3 Purification and gel extraction of DNA

For the purification of plasmid DNA and PCR products, the NucleoSpin® Gel and PCR Clean-up kit (Macherey-Nagel) was used. Furthermore, DNA extraction from agarose gels was also performed by this kit according to the protocol of the manufacture.

4.10.4 Modification of nucleic acids

DNA restriction cleavage was performed with specific endonucleases. All enzymes, used in this work, were purchased by New England Biolabs (Schwalbach). The DNA cleavage reaction was carried out according to the protocol of the manufacture. For hydrolysis, the DNA was incubated with H_2O_{bidest}, the restriction enzyme and the respective restriction buffer at 37 °C for 20 min to 60 min. After restriction digestion of plasmids, an incubation with rAPid alkaline phosphatase at 37 °C was carried out for 30 min. Therefore, religation of cleaved vectors was avoided. Endonucleases and restriction buffers were removed by

agarose gel electrophoresis and gel extraction or directly by the PCR clean up kit (see section 4.10.3).

4.10.5 Phosphorylation of nucleic acids

To add phosphate at the 5`-ending of hybridized DNA and PCR products, approx. 300 pmol of nucleic acids were mixed with 1 µl T4-polynucleotidekinase (PNK), 5 µl 10x T4-DNA ligase buffer (T4-PNK exhibits 100 % activity in this buffer) and H_2O_{bides} in a final reaction volume of 50 µl. The suspension was incubated at 37 °C for 30 min following a heat inactivation at 65 °C for 20 min.

4.10.6 Ligation of DNA

Hydrolyzed and purified plasmid DNA was ligated with DNA fragments containing complimentary endings. 25 ng to 30 ng of plasmid DNA were mixed with the fivefold amount of DNA fragments. Additionally, the respective amount of 2x quick ligase buffer, 1 µl of T4 DNA ligase (New England Biolabs) and H_2O_{bidest} were added to a final reaction volume of 20 µl. The reaction was carried out at room temperature for 20 min.

Under certain circumstances, the ligation was performed overnight at 4 °C. For this purpose, the 2x quick ligase buffer was substituted by 10x T4-DNA ligase buffer. After ligation, the mixture was transformed in *E. coli* cells (see section 4.11.2).

4.10.7 Sequencing analysis

The company GATC Biotech (European Genome and Diagnostic Centre, Konstanz) analyzed the nucleotide sequences of PCR products and plasmid DNA. DNA was purified (see section 4.10.3) and diluted in water to a final concentration of 30 ng µl^{-1} to 80 ng µl^{-1}. 20 µl of sample DNA and 20 µl of the respective forward and reverse primer (10 µM) were used for analyses. Data were evaluated by CloneManager 5.0 (Scientific & Education Software), Seqman 4.0 (DNASTAR) and Genome Compiler (Genome Compiler Corporation).

4.10.8 Polymerase chain reaction (PCR)

The amplification of DNA fragments with a specific length and sequence was carried out in *vitro* by polymerase chain reaction (Mullis *et al.* 1986). The PCR was performed with the respective reaction mixture containing reaction buffer, DMSO, dNTPs, forward and reverse primers, template DNA, the respective polymerase and H_2O_{bidest} (see section 4.10.8.2)

The reaction was achieved by repeating one PCR cycle for 30 to 35 times. Each cycle contained different denaturation, annealing and elongation settings depending on fragment length, polymerase and primers (see section 4.10.8.2)

Because of its proof-reading activity, the Phusion® DNA polymerase (NEB) was used for synthesis of new DNA fragments and plasmids. In addition, colony PCRs were carried out by the Taq DNA polymerase (NEB) and ThermoPol reaction buffer (NEB).

4.10.8.1 Site directed mutagenesis and overlap extension PCR

The introduction of point mutations at specific positions as well as the extension of DNA sequences were carried out via site directed mutagenesis and overlap extension PCR. Two successive PCRs using different primer pairs were performed. Besides the standard primer (forward or reverse), a specific mutagenesis primer containing the point mutation, or the overlapping region was applied in the first PCR. After purification, the resulting DNA fragment of the first PCR was used as primer for the second PCR (see section 4.10.8.2). Due to the increased length of this DNA fragment, the annealing temperature was increased for optimal PCR conditions.

4.10.8.2 PCR reaction mixtures and programs

PCR reaction mixture for Phusion® polymerase

5x Phusion GC buffer	10 µl
DMSO	1.5 µl
dNPTs (10 mM)	1 µl
Forward primer (10 µM)	2.5 µl
Reverse primer (10 µM)	2.5 µl
Template DNA	<250 ng
Phusion® DNA polymerase	0.5 µl
H_2O_{bidest}	to 50 µl

For site directed mutagenesis and overlap extension PCR, one of the primers contained the respective nucleotide exchange or the extended DNA sequence.

Second PCR mixture for site directed mutagenesis and overlap extension PCR

5x Phusion GC buffer	10 µl
DMSO	1.5 µl
dNPTs (10 mM)	1 µl
Forward/reverse primer (10 µM)	2.5 µl
First PCR product	10 µl
Template DNA	<250 ng
Phusion® DNA polymerase	0.5 µl
H_2O_{bidest}	to 50 µl

Purifying the first PCR product resulted in DNA fragments, which were used as primer for the second PCR reaction of the site directed mutagenesis or overlap extension PCR. Template DNA for colony PCR was obtained by resuspending one single colony in the PCR mixture. These cells were lysed during the initial denaturation step.

Colony PCR reaction mixture for Taq polymerase

10x ThermoPol reaction buffer	2.5 µl
dNPTs (10 mM)	0.5 µl
Forward primer (10 µM)	0.5 µl
Reverse primer (10 µM)	0.5 µl
Template DNA	<250 ng
Taq DNA polymerase	0.125 µl
H_2O_{bidest}	to 25 µl

PCR program for the Phusion polymerase

Cycles	Temperature	Time	Step
1	98 °C	30 s	Initial denaturation
	98 °C	10 s	Denaturation
30 to 35	45 to 72 °C (*)	15 s	Annealing
	72 °C	15 s (**)	Elongation
1	72 °C	5 min	Final elongation
	4 °C	∞	Storage

(*)   depending on the melting temperature of the used primers

(**)   depending on the fragment length and the reaction speed of the polymerase

PCR program for the Taq polymerase

Cycles	Temperature	Time	Step
1	96 °C	2 min	Initial denaturation
30 to 35	96 °C	10 s	Denaturation
	45-68 °C (*)	15 s	Annealing
	68 °C	30 s (**)	Elongation
1	68 °C	5 min	Final elongation
	4 °C	∞	Storage

(*)   depending on the melting temperature of the used primers

(**)   depending on the fragment length and the reaction speed of the polymerase

4.10.9   Tris-borate-EDTA polyacrylamide gel electrophoresis (TBE-PAGE)

Hybridization of nucleic acids and protein-DNA interaction were analyzed by 8 % to 12 % non-denaturing TBE polyacrylamide gels without stacking gel (section 4.7.2.3). Protein samples were mixed with native TBE loading buffer (Roche diagnostics, Mannheim) and loaded on the gel. The gel electrophoresis was carried out with native 0.5x TBE running buffer at 4 °C and 100 V for 2 hours (Sambrook *et al.* 1989).

4.10.10 Hybridization of AmtR binding sites

For protein-DNA interaction analysis as well as vector cloning, complementary single stranded oligonucleotides (MWG Biotech AG, Martinsried) of 30 bp to 45 bp were hybridized. DNA fragments used for SPR measurements were biotinylated at the 3´-end. The primer concentration was set to 100 µM. Forward and reverse primers (section 4.2) were mixed in the same ratio and hybridized by using the thermocycler Primus 96 (PeqLab Biotechnologie GmbH, Erlangen). At the beginning, the oligonucleotides were denatured for 30 s at 98 °C. Subsequently, the temperature was decreased in 5 °C steps of 30 s from 70 °C to 55 °C. This cycle was repeated 30 times.

4.10.11 Construction of equal-sized DNA fragments with altered operator positions

DNA fragments of the same size were generated containing either amtB$_{wt}$, amtB$_{ri}$ or amtB$_{de}$ at varying positions. Therefore, the multiple cloning site (MCS) of pBR322 and pQE30 were fused by restriction digestion with the endonuclease HindIII. Subsequently, one of the flanking HindIII restriction site of the resulting DNA fragment (approx. 400 bp) of pQE30

was replaced by PstI using an overlap extension PCR. Additionally, the restriction sites EagI, BsaI and EcoRI were integrated at position 59 bp, 77 bp and 192 bp with respect to the distance of the operator center between restriction site KpnI and XmaI. In parallel, wild type, rigid and deformable operators were generated by hybridization of respective primer pairs (see section 4.2) containing the restriction sites KpnI (upstream) and XmaI (downstream). The resulting operators with flanking restriction sites were integrated in the vector to generate the plasmids pCSC4 WT (with wild type operator), pCSC4 RI (with rigid operator) and pCSC4 DE (with deformable operator). Thus, the 418 bp spanning fragment was isolated by the restriction endonuclease HindIII and PstI. Subsequently, the restriction site AgeI was added by overlap extension PCR in one fragment at the 3´-ending and in the other fragment at the 5`-ending, respectively. Afterwards, a double insertion was generated by ligation of these two fragments. Via subsequent restriction digestion with HindIII and PstI, the double insertion was integrated in HindIII and PstI digested pCSC4 resulting in the plasmids pCSC5 WT, pCSC5 RI and pCSC5 DE (see appendix figure 24). Each of the two repeats contained one of the operator variants and one of every applied restriction site. Finally, by restriction digestion with the enzymes AfeI, BamHI, BsaI, EagI, EcoRI, SacI or SphI, fragments were obtained of exactly 418 bp with either $amtB_{wt}$, $amtB_{ri}$ or $amtB_{de}$ at different positions with respect to the fragment ending.

4.10.12 Electro mobility shift assay (EMSA)

EMSA experiments were carried out for qualitative interaction studies of high concentrated AmtR protein and operator sequences containing one single AmtR binding site. DNA fragments at a final concentration of 0.3 µM to 1 µM and native AmtR protein at different concentrations were diluted in HBS-EP buffer (see section 4.7.3.2). Protein-DNA interaction assays were performed by mixing AmtR protein and promoter fragments to a final volume of 10 µl. The mixture was incubated for 15 min at room temperature. Before loading on 8 % to 12 % non-denaturing TBE polyacrylamide gel, the samples were mixed with 2 µl native TBE loading buffer (see section 4.10.9). The gel electrophoresis was performed with native 0.5x TBE running buffer at 4 °C for 2 hours (Evans 2017). To detect the DNA signals, gels were stained with ethidium bromide.

For qualitative interaction of AmtR and operator variants at low nanomolar DNA concentration ranges, EMSAs were performed with digoxigenin (DIG)-labeled promoter sequences. The labeling reaction was carried out by incubating 38.5 pmol DNA with cobalt dichloride, DIG-labeling buffer, DIG-ddUTP solution and terminal transferase for 15 min at 37 °C as mentioned in the DIG gel shift kit, 2nd generation (Roche Diagnostics). The reaction

was stopped by adding 16 mM EDTA. Labeled DNA fragments were diluted in HBS-EP buffer to a final concentration of 1.5 nM, while different protein concentrations of AmtR were applied. The samples were prepared, preincubated and electrophoresed as described above, respectively. Before DNA blotting, the positively charged nylon membrane (Roche Diagnostics) was activated in H_2O_{bidest} and equilibrated in 0.5x TBE running buffer. Blotting was performed by stacking four filter paper sheets (Whatman International Ltd., England), the equilibrated nylon membrane, the native TBE polyacrylamide gel and again four filter papers within the blotting system (semi-dry transfer unit TE77, Amersham Biosciences). Filter papers were equilibrated in 0.5x TBE running buffer. The blotting was carried out for one hour at 150 mA and 15 V. For covalent coupling between DNA and membrane, autocrosslink (120,000 µJ) was performed by the UV-stratalinker® 1800 (Stratagene). The membrane was incubated in 1x blocking solution (see section 4.7.3) for 30 min. Afterwards, anti-DIG alkaline phosphatase (Roche Diagnostics, Mannheim) was diluted to 1:10,000 in this blocking solution and incubated for additional 30 min. After two washing steps with washing buffer (see section 4.7.3) for about 15 min each, the membrane was equilibrated in detection buffer (see section 4.7.3). The membrane was incubated in CSPD solution for 15 min at 37 °C and chemiluminescence was determined (ChemiDoc XRS+, Bio-Rad).

4.11 Manipulation of bacteria cells

4.11.1   Production of manganese chloride competent *E. coli* cells

For producing chemical competent *E. coli* DH5α MCR cells, the protocol of previous studies was adapted (Inoue *et al.* 1990). After inoculating 4 ml LB medium with the respective cells, the suspension was incubated at 37 °C for 7 hours to 8 hours. To ensure enough agitation during growth, baffled flasks were used and the frequency of the rotary shaker (innova 2350, New Brunswick Scientific) was set to 180 rpm, respectively. After incubation, 0.5 ml of the preculture was used to inoculate 50 ml of SOB medium (see section 4.6.1). The resulting cell suspension was grown at 37 °C and 180 rpm overnight. On the next day, this culture was used for the inoculation of 250 ml SOB medium to an oD_{600} of 0.1 following an incubation step. After reaching an oD_{600} of approx. 0.4 to 0.5, the cells were harvested. The resulting cell pellet was washed two times with 40 ml cold TB buffer (see section 4.6.1). Subsequently, the remaining cells were resuspended in 6.4 ml cold TB buffer. After adding 400 µl of sterile DMSO, the suspension was aliquoted to 200 µl portions. For long-term storage, cells were frozen to minus 80 °C.

4.11.2 Transformation of chemical competent *E. coli* cells

100 µl of competent cells were added either to the complete ligation mixture (see section 4.10.6) or to approx. 500 ng plasmid DNA (see section 4.10.1). The resulting cell-DNA suspension was incubated on ice for 1 hour following a heat shock at 42 °C for 2 min. After directly adding 1 ml LB medium, the cells were incubated at 37 °C for 45 min. Finally, the cells were harvested and plated at LB agar plates containing antibiotics for selection. Plates were incubated at 37 °C overnight.

5 Results

The TetR-type regulator AmtR is the most important transcription regulator of the nitrogen metabolism in *C. glutamicum* (Burkovski 2003a, 2003b, 2007). For the regulation, AmtR binding to specific DNA sequences within the promoter region is necessary. Initial interaction studies suggested various binding affinities of AmtR for these sequences (Jakoby *et al.* 2000; Nolden *et al.* 2001a; Beckers *et al.* 2005). Thus, the identified DNA motifs allowed to derive a consensus sequence for AmtR operators with the two conserved half sites "CTAT" and "ATAG", that are palindromic and separated by six nucleotides (Muhl *et al.* 2009; Hasselt *et al.* 2011). In addition to the specific AmtR binding sites, further DNA targets were identified that match this consensus sequence but showed no AmtR dependent regulation in transcriptome studies (personal communication by E. Socher and H. Sticht; Beckers *et al.* 2005; Silberbach and Burkovski 2006). Apparently, additional properties like the 3D-structure or flexibility of the operators seems to affect AmtR-DNA binding. This idea was further supported by previous studies on DNA deformations, which can significantly influence the binding affinity (Kim *et al.* 2000; Lindemose *et al.* 2014; Harteis and Schneider 2014).

In addition to the regulatory mechanism, recent works revealed several properties of the AmtR-DNA structure (Palanca and Rubio 2016) and of DNA-binding by AmtR (Beckers *et al.* 2005; Hasselt *et al.* 2011). However, these studies did not address the role of DNA shape for the AmtR-DNA binding. Therefore, interaction analyses were carried out in this work to investigate the influence of the DNA shape on the AmtR-DNA interaction.

5.1 Preparation of AmtR

For the characterization of the protein-DNA interaction, recombinant AmtR protein was fused to the maltose-binding protein (MBP) and heterologously overexpressed in *E. coli* (Muhl *et al.* 2009; Hasselt *et al.* 2011). Prior to structural and functional tests, the MBP-tag was cleaved off by the serine protease factor Xa. Based on previous proteolysis assays (Dian *et al.* 2002; Jenny *et al.* 2003), an on-column cleavage at 4 °C for 4.5 h was optimal for purification of AmtR. Subsequently, noncleaved MBP-AmtR and cleaved MBP were separated from AmtR by size exclusion chromatography.

After purification, the purity and homogeneity of AmtR was tested by SDS-PAGE. For every AmtR preparation only one band at 24.4 kDa and no impurities were detected in the respective SDS-PAGEs. Additionally, the stability of AmtR was investigated by non-denaturing PAGEs every 24 hours for a minimum of 6 days to assess the stability of AmtR

for a typical period of an SPR analysis. In contrast to SDS-PAGEs, native PAGEs revealed differences in the protein signals of AmtR preparations. In these approaches, protein signals as one distinct band over a period of 6 days indicated a stable AmtR preparation with only one conformation, which would be ideal for subsequent interaction studies (figure 5A). On the other hand, additional bands in native PAGEs already after 24 h suggested additional AmtR conformations and, therefore, instability for these AmtR preparations (figure 5B).
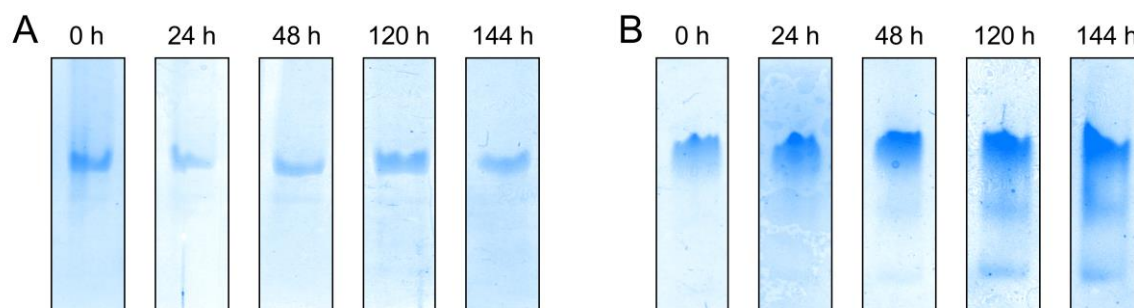
Figure 5 Protein stability examinations of different AmtR preparations. Different protein preparations (A and B) were analyzed using 6 % non-denaturing polyacrylamide gels at the indicated time points after purification. 1 µg of the different AmtR preparations in a concentration of 10 µM (diluted in HBS-EP buffer) were loaded onto gels.

To verify if the protein stability was influenced by a mutation, the pMalc2*amtR* vectors of the overexpression cultures were sequenced. The stable preparation contained a plasmid with a spontaneous deletion of 15 bp at the linker between the sequences coding for the protease cleavage site and the *amtR* gene. This mutation resulted in 3 nucleotides encoding a threonine residue between the factor Xa cleavage site and AmtR. The resulting protein after cleavage carried an additional threonine at the N-terminus, designated as $AmtR_T$. Because of the high protein stability, this AmtR variant was chosen and prepared for analyses.

To assess, whether the additional threonine at the N-terminus of $AmtR_T$ affects the binding affinity, the same native operators as in previous studies were investigated (Beckers *et al.* 2005). Furthermore, the best operator for analysis was identified by these interaction assays.

5.2 Interaction studies of AmtR$_T$ and native operators

The interaction of AmtR$_T$ with native binding sites were analyzed by EMSAs. For that purpose, the wild type operators of AmtR controlled genes coding for ammonium assimilation (*glnA* and *gltB*), ammonium and urea transport (*amtB* and *urtA*) and creatinine metabolism (*codA* and *crnT*) were applied. These sequences of 30 bp contained the binding half sites, spacer sequences and flanking regions. 1 µM of these DNA fragments were titrated with 0.01 µM to 10 µM AmtR$_T$ (figure 6).
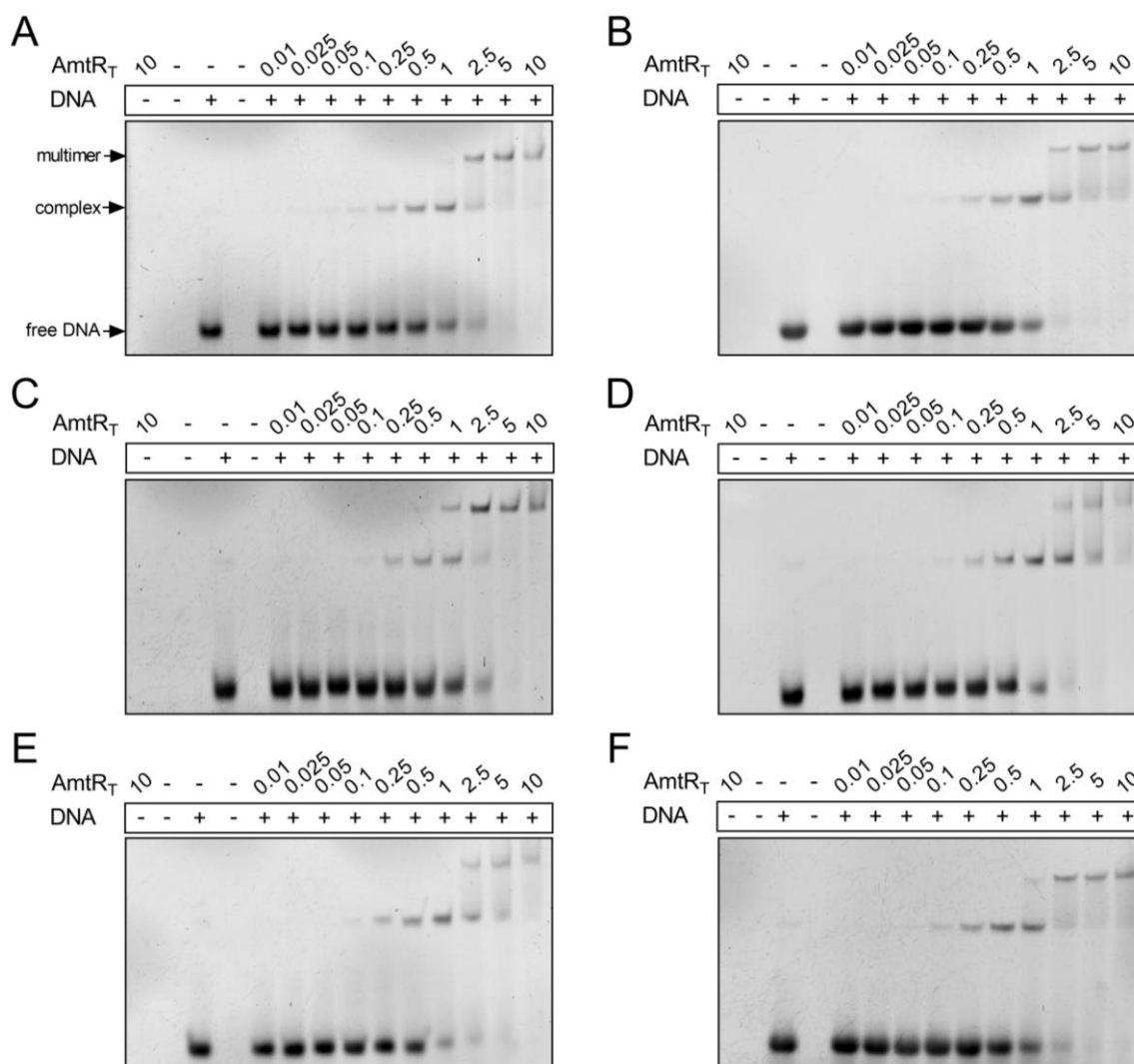
Figure 6 Interaction analyses of AmtR$_T$ with different native operators. 30 bp fragments of the wild type operator sequences of the genes *glnA* (A), *amtB* (B), *gltB* (C), *codA* (D), *urtA* (E) and *crnT* (F) were used as target DNAs. 1 µM of DNA and different concentrations of purified AmtR$_T$ (indicated concentrations were depicted in µM) were applied for the interaction studies. 10 µM AmtR$_T$ without DNA (lane 1) and target DNA without protein (lane 3) were loaded onto the gels as controls, respectively. Arrows, depicted in A, indicated the running front of free operator DNAs, AmtR$_T$-DNA complexes or putative AmtR$_T$ multimers bound to DNA.

DNA fragments with different migration speed were detected in the EMSAs of every analyzed operator. Unbound DNA was shown at the bottom of gels (free DNA), while DNA binding by $AmtR_T$ resulted in a clear shift (complex, multimer). At concentrations less than 1 µM $AmtR_T$, only distinct DNA bands either for unbound or complexed state and no smear were observed. At $AmtR_T$ concentrations of 1 µM and above, additional DNA signals, migrating at higher position than the apparent $AmtR_T$-DNA complexes, were detected. This observation suggested additional binding events of $AmtR_T$ to the DNA fragments, compared to the 1 to 1 interaction between $AmtR_T$ and DNA. Furthermore, the EMSAs showed small but significant differences in the $AmtR_T$ binding to the applied operator sequences. The weakest binding was shown for the interaction between $AmtR_T$ and the operators of *glnA* and *gltB*, while moderate binding was observed for the *codA*, *crnT* and *urtA* operators. The highest affinity was suggested between $AmtR_T$ and the *amtB* operator. Therefore, this *amtB* operator, further designated as $amtB_{wt}$, was used as basis for the construction of artificial operator variants with different deformations.

5.3 Designing artificial operators with different structural features

The central six base pairs between the palindromic half sites of the consensus sequence of AmtR operators are not conserved (Muhl *et al.* 2009). Recent crystal structure analysis of the AmtR-DNA complex revealed no direct interaction between AmtR and these central bases (personal communication, F. Grau and Y.A. Muller; Palanca and Rubio 2016). To address, whether the shape of this spacer region affected the AmtR-DNA binding, two artificial operator variants were designed based on $amtB_{wt}$. Even though, the binding half sites "CT$\underline{G}$T"-"ATAG" of $amtB_{wt}$ differed from the consensus sequence of AmtR operators in one base pair (underlined letter), strong AmtR binding to this operator was shown in this study and previous analyses (Beckers *et al.* 2005; Hasselt *et al.* 2011). The artificial DNAs of 30 bp contained the binding half sites and flanks of $amtB_{wt}$ but differed in their spacer sequences (figure 7). Based on previous studies, spacer variants with diverse base pair steps were designed resulting in different structural properties (Yakovchuk *et al.* 2006; Harteis and Schneider 2014). The first operator with CGCGCG as spacer sequence contained three successive pyrimidine-purine base steps. This sequence was designated as $amtB_{de}$, due to its rather deformable properties. The second operator with a GGGGGG spacer contained only purine-purine base steps. Because of its reduced deformability, that sequence was termed 'rigid' ($amtB_{ri}$). Prior to qualitative and quantitative binding analyses, the sequence-dependent shape of $amtB_{wt}$, $amtB_{de}$ and $amtB_{ri}$ were characterized.
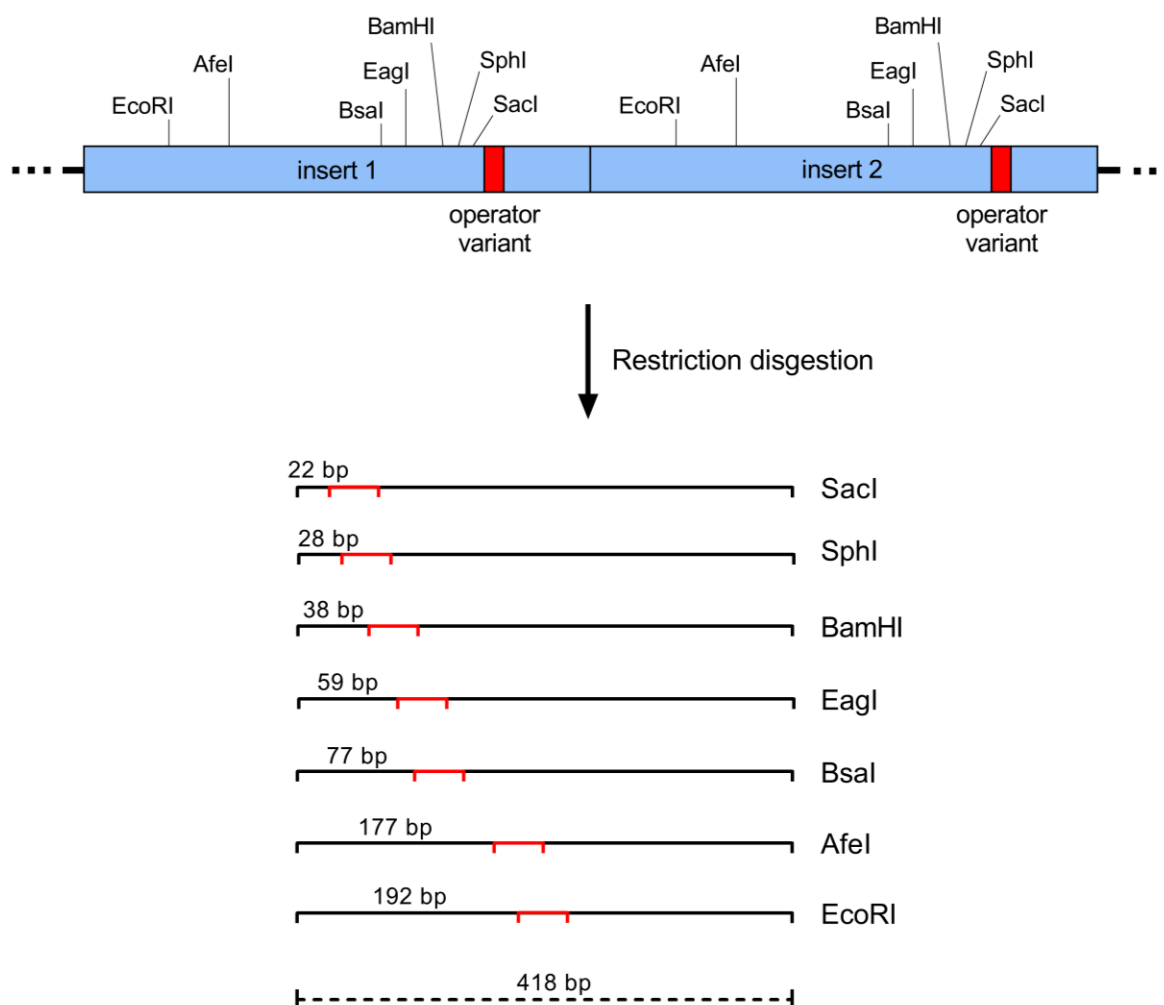
Figure 7 Designed operator variants with different spacer sequences. Based on the first AmtR binding site within the *amtB* promoter (amtB$_{wt}$), two additional operator variants were generated. The 30 bp DNA fragments contained the AmtR binding half sites (bold), the different spacer sequences (red) and 7 flanking nucleotides up- and downstream. The artificial DNA sequences were termed amtB$_{ri}$ (spacer: GGGGGG) and amtB$_{de}$ (spacer: CGCGCG).

5.4 Characterization of the shape of the *amtB* operator variants

Equal-sized DNA fragments with different structural properties were demonstrated to migrate at different positions in polyacrylamide gels (Thompson and Landy 1988; Niederweis and Hillen 1993; Tovar and Hillen 1989). Additionally, in previous studies it was suggested that a higher level of distortion results in a lower diffusion speed and vice versa (Thompson and Landy 1988). Furthermore, the deformation locus within a DNA fragment affects gel migration, since DNA with the distortion at the end of the fragment shows the highest gel mobility and DNA with the deformation at the center reveals the lowest mobility (Wu and Crothers 1984). Such DNA distortion can be caused by DNA sequence-dependent deformations or by protein-DNA binding.

Therefore, the relative shape of amtB$_{wt}$, amtB$_{ri}$ or amtB$_{de}$ in unbound state and the effect of AmtR-binding on the DNA conformation of theses operator variants were studied by EMSA in the same way as in previous publications (Wu and Crothers 1984; Thompson and Landy 1988; Niederweis and Hillen 1993; Tovar and Hillen 1989). For this purpose, three sets of DNA fragments were generated by duplicating a DNA sequence (insert 1 and 2) each containing either amtB$_{wt}$, amtB$_{ri}$ or amtB$_{de}$ and different restriction sites at varying distances to the operator variants (see section 4.10.11). Subsequent cleavage with restriction enzymes that cut once in each insert generated equal-sized fragments. Every DNA sequence contained the operator variants at different distances to the ends of the fragment (figure 8). Only operator positions on one side of the DNA fragment between the end (SacI) and the center (EcoRI) were applied, because fragments with operators positioned on the opposite side would have identical distances between the operator and the fragment end.

Figure 8 Construction of DNA fragments with operator variants at different positions. Plasmids were constructed with double insertion (insert 1 and 2) each containing one of the operator variants and different restriction sites at varying distances to the operator. Respective restriction enzymes that cut once in each insert were used to generate equal-sized fragments of 418 bp with the operator variants at different positions. Position of the operator variants were depicted as red lines.

In non-denaturing PAGEs, the migration properties of these seven different fragments with either $amtB_{wt}$, $amtB_{de}$ or $amtB_{ri}$ were analyzed in both, the presence and absence of $AmtR_T$. Therefore, an $AmtR_T$ to DNA concentration ratio of 1:2 was applied to obtain free and complexed DNA. For a valid intrinsic comparison of the mobilities of the different DNA fragments, all possible combinations of fragments were analyzed on TBE gels (figure 9).
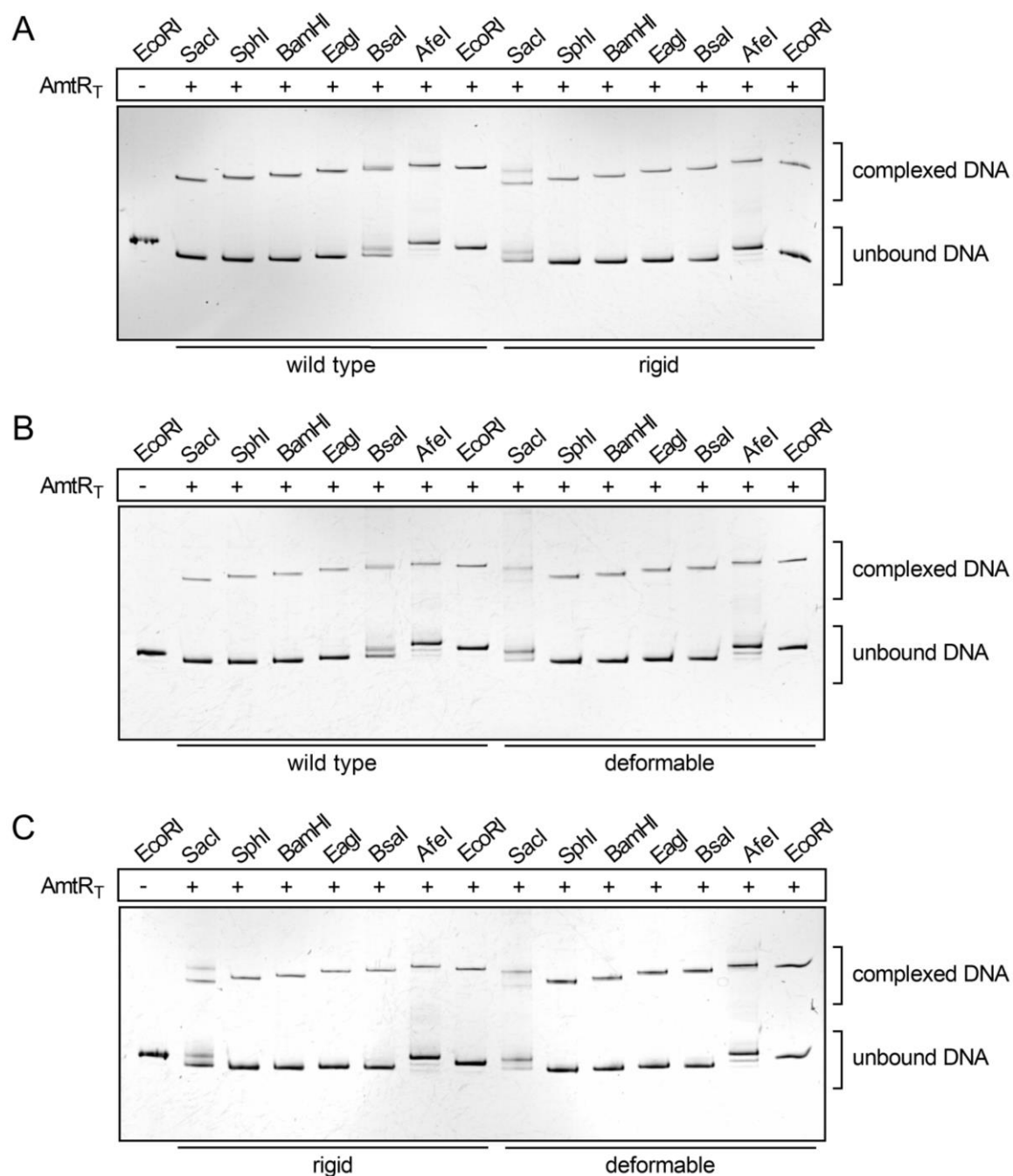
Figure 9 EMSAs of DNA fragments with operator variants at different positions. DNA fragments were generated by using different restriction enzymes (indicated at the top). The resulting equal-sized DNA sequences (418 bp) contained the operator variants at different positions (see figure 8), due to the varying distance between operator and different restriction sites. 20 nM of DNA fragments with either (A) wild type and rigid operator, (B) wild type and deformable operator or (C) rigid and deformable operator were analyzed with 10 nM AmtR$_T$ on a 12 % TBE PAGE. Additionally, 20 nM of EcoRI digested DNA fragment containing amtB$_{wt}$ were applied without AmtR$_T$ as negative control.

The EMSAs of the DNA fragments revealed distinct bands for free DNA and clearly shifted DNA bands for the $AmtR_T$-bound state. Furthermore, the different equal-sized DNA fragments, which were obtained by cleavage with the respective restriction enzymes, showed distinct alterations in gel migration. For both, unbound and complexed DNAs, the highest gel mobility occurred when the operator variants were located at the end of the fragment, while the lowest mobility was observed for DNA fragments with the binding sites at the center. These observations showed that the DNA fragments were deformed in $AmtR_T$-bound and in unbound state at each operator position. Moreover, these EMSAs showed additional DNA bands for the fragments digested with SacI and AfeI. Such additional signals were also detected in previous studies of TetR using the identical approach (Tovar and Hillen 1989). Tovar and coworker suggested that these signals were caused by protruding ends from restriction digestion or small internal curvatures in the DNA. Therefore, the additional bands, detected in EMSAs of this study, were not considered in the following analyses.

Furthermore, the location and level of deformation in the equal-sized DNA fragments (figure 8) were analyzed in more detail for unbound and complexed state. For this purpose, the running fronts of complexed (m_c) and free (m_{dna}) DNA fragments in the EMSAs were determined (figure 9), while the maximum running front (m_{max}) was defined as a global reference point. Subsequently, the mobility ratios of m_{max} over m_{dna} or m_{max} over m_c were established. As reference point, m_{max} was set to 1, while m_{dna} and m_c was determined below 1. Consequently, low mobility ratios corresponded with high mobilities and, therefore, less DNA deformation. Vice versa, high ratios corresponded with slow DNA migration and high DNA distortion.

The position as well as the level of the deformation in unbound DNA fragments were investigated by plotting the mobility ratios of m_{max} over m_{dna} versus the distance between the operator center and the different restriction sites (figure 10). The plotted mobility ratios of free DNA, obtained from the EMSAs (figure 9), showed the highest ratios for the equal-sized fragments with the operator in the center, whereas the lowest ratios were detected for the fragments with the AmtR binding site at the end. The linear regressions of the ratios revealed a DNA deformation directly at the position of all three operator variants. Furthermore, the slope of the regressions resembled and, therefore, suggested similar DNA conformations only for the DNA fragments with $amtB_{wt}$ and $amtB_{de}$. In contrast, the plotted mobility ratios of free DNA fragments containing $amtB_{ri}$ showed a decrease in the slope of the regression indicating a reduced DNA deformation at the operator locus.
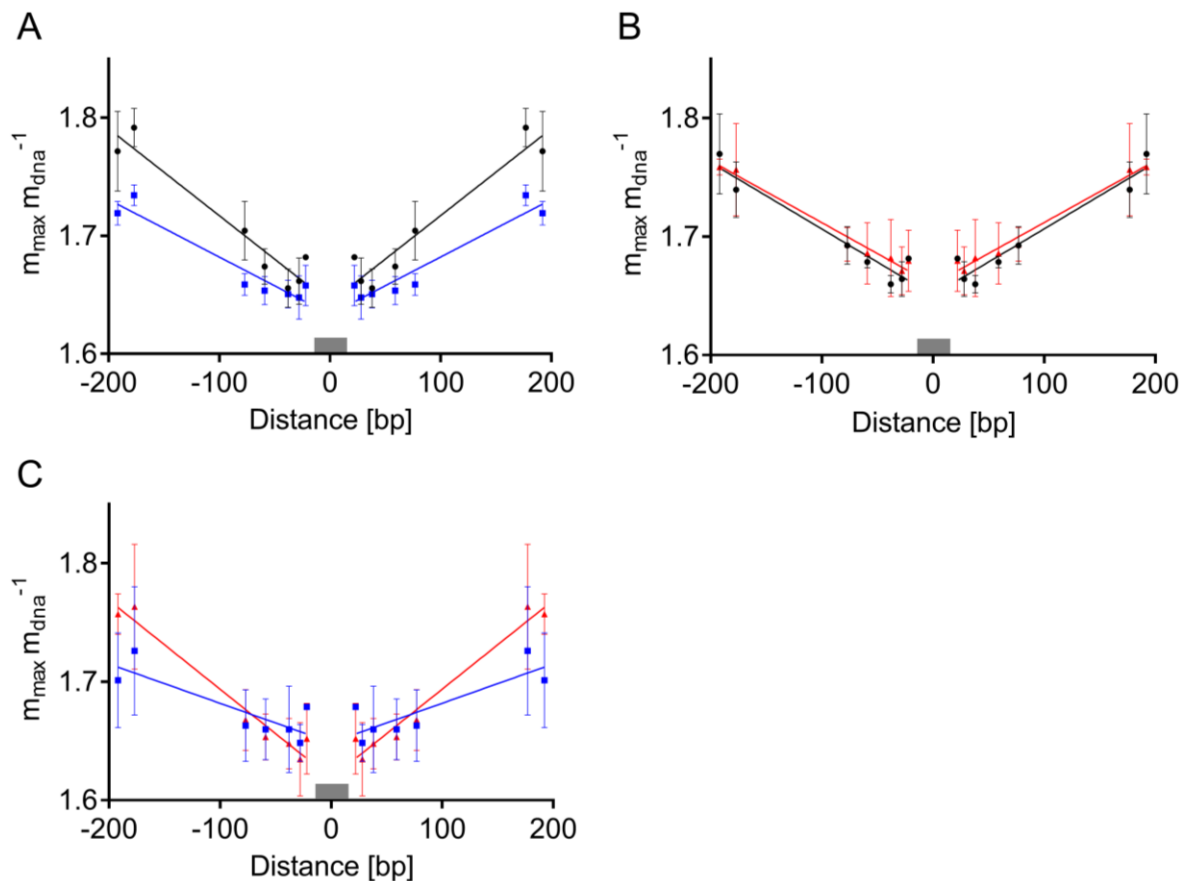
Figure 10 Mobility ratios of free DNA fragments versus the distance between operators and restriction sites. Each fragment of the same length (418 bp) contained one operator at different distances to the end of the fragment (see figure 8): $amtB_{wt}$ (black lines), $amtB_{ri}$ (blue lines) or $amtB_{de}$ (red lines). The respective running fronts of unbound DNA fragments (m_{dna}) and the maximum running front (m_{max}) were determined on a 12 % TBE gels. Ratios of m_{max} over m_{dna} were plotted versus the distance between operator center and fragment ending. The operators were depicted as grey boxes (-15 bp to 15bp). Original data points were reflected to the opposite site of the operator center (0 bp) to show how strong DNA is deformed. Ratios of unbound DNA fragments with either $amtB_{wt}$ and $amtB_{ri}$ (A), $amtB_{wt}$ and $amtB_{de}$ (B) or $amtB_{ri}$ and $amtB_{de}$ (C) were analyzed.

In addition to the investigations of unbound DNA fragments, the shapes of $AmtR_T$-bound DNA fragments were analyzed. For this purpose, mobility ratios of the reference (m_{max}) over the running front of complexed DNA (m_c) were plotted versus the distance between the operator center and the end of the different fragments (figure 11). The respective running fronts were obtained from the EMSAs (figure 9).
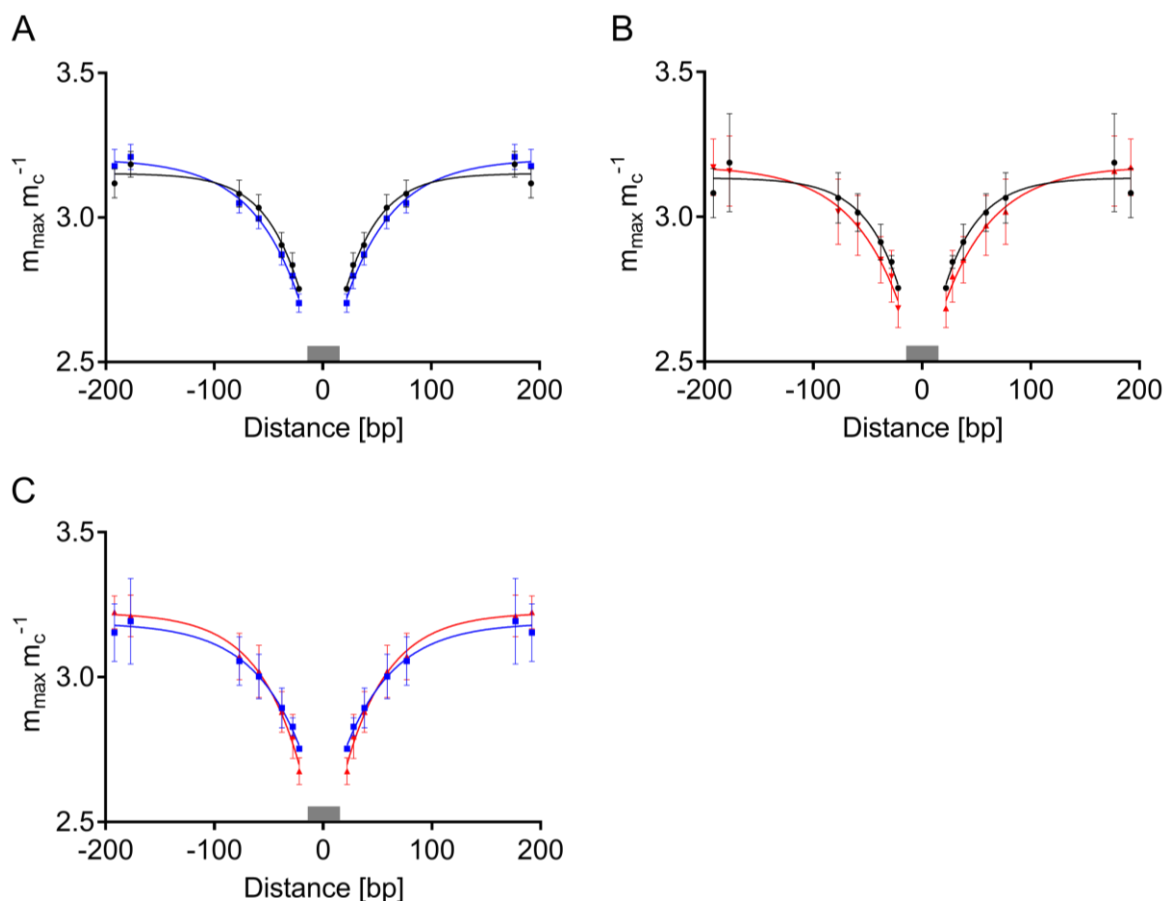
Figure 11 Mobility ratios of complexed DNA fragments versus the distance between operators and restriction sites. Each fragment of the same length (418 bp) contained one operator at different distances to the end of the fragment (see figure 8): $amtB_{wt}$ (black lines), $amtB_{ri}$ (blue lines) or $amtB_{de}$ (red lines). The respective running fronts of complexed DNA fragments (m_c) and the maximum running front (m_{max}) were determined on a 12 % TBE gels. Ratios of m_{max} over m_c were plotted versus the distance between operator center and fragment ending. The operators were depicted as grey boxes (-15 bp to 15bp). Original data points were reflected to the opposite site of the operator center (0 bp) to show how strong DNA is deformed. Mobility ratios of $AmtR_T$ bound DNA fragments with either $amtB_{wt}$ and $amtB_{ri}$ (A), $amtB_{wt}$ and $amtB_{de}$ (B) or $amtB_{ri}$ and $amtB_{de}$ (C) were analyzed.

Like the ratios of free DNA fragments, analyses of $AmtR_T$-DNA complexes showed the highest mobility ratios for equal-sized fragments with the operator in the center, while the lowest ratios were observed for the fragments with the AmtR binding site at the end. The approximation of the plotted ratios of the three sets of complexed DNA fragments demonstrated a DNA deformation exactly at the operator position. Additionally, at distances between operators and fragment ends of 100 bp and above, mobility ratios remained unchanged resulting in a steady-state-like approximation. Apparently, there is no effect of long DNA fragments in complex with proteins on the gel mobility in polyacrylamide gels.

Based on previous studies (Tovar and Hillen 1989; Diekmann 1989), the reason for this may be the higher distance between restriction sites and DNA deformation compared to one persistence length of the DNA. Furthermore, the approximations of the plotted mobility ratios of complexed DNA fragments showed no differences between wild type, deformable and rigid operators. These observations suggested a distinct conformational change of the DNA during AmtR$_T$ binding, which resulted in uniform macroscopic states of the complex with each operator. As a consequence, different levels of DNA deformation occurred during AmtR-DNA complex formation depending on the DNA spacer sequence. To address, whether these differences affect the affinity of the protein-DNA interaction, the AmtR$_T$ binding to the three operator variants were analyzed in EMSAs.

5.5 Analyses of the AmtR$_T$ binding to the operator variants

To study the influence of the conformation of operators on the AmtR-DNA binding, the interaction between AmtR$_T$ and the operator variants was analyzed by EMSAs. For this purpose, only the wild type and designed operator sequences of 30 bp were applied as target DNAs.

5.5.1 Qualitative analysis of the interaction between AmtR$_T$ and the operator variants

The interaction studies between AmtR$_T$ and native operators at AmtR$_T$ concentrations above 1 µM showed additional bands with decreased electrophoretic mobility than the AmtR$_T$-DNA complex (figure 6). These signals suggested additional binding events or non-specific binding. Furthermore, the operator concentration of 1 µM resulted in diffuse signals of free DNA. These observations indicated that the concentrations of DNA and AmtR$_T$ were too high to observe distinct differences in the AmtR$_T$ binding to the operator variants. Therefore, the operator concentration was decreased to 0.3 µM, while AmtR$_T$ was used at a concentration of 0.6 µM (figure 12). In addition to the three operator variants, a sequence of 30 bp of the *amtR* gene was applied. Since this DNA fragment contained no AmtR$_T$ regulated operator sequence, specific AmtR$_T$ binding to this DNA was ruled out. For EMSAs, this DNA fragment was used as negative control and designated as unspecific DNA. Based on previous studies, unspecific DNA was also used to determine the unspecific background signals in the SPR measurements (Muhl *et al.* 2009; Hasselt *et al.* 2011).
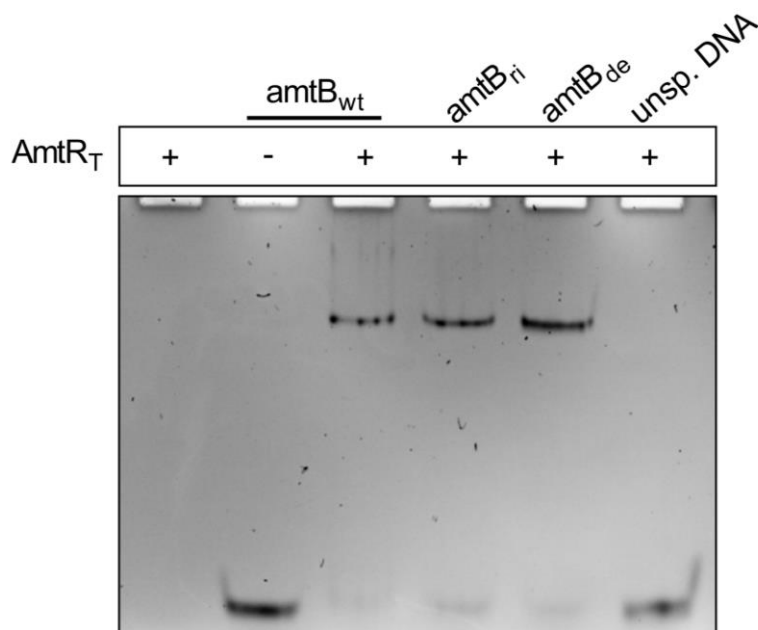
Figure 12 Qualitative analysis of the interaction between AmtR$_T$ and different target DNAs. AmtR$_T$ in a concentration of 0.6 µM was tested with the wild type (amtB$_{wt}$), the rigid (amtB$_{ri}$) and deformable (amtB$_{de}$) operator variants as well as unspecific DNA (used for SPR measurements) in a concentration of 0.3 µM. In addition, AmtR$_T$ without DNA (lane 1) and amtB$_{wt}$ without AmtR$_T$ (lane 2) was loaded onto an 8 % native TBE gel as controls. DNA signals were detected by ethidium bromide staining.

The EMSA revealed no complex formation between unspecific DNA and AmtR$_T$ (figure 12, lane 6), which suggested no AmtR$_T$ binding to the unspecific DNA. The analyses of the AmtR$_T$ binding to the operator variants (lane 3 to 5) showed similar DNA retardation patterns for each interaction with faint signals for unbound DNA and strong signals for AmtR$_T$-DNA complexes.

These results indicated that distinct differences of the AmtR$_T$ binding to the operator variants cannot be distinguished by this setup. To assess, whether this also occurred at low concentrations of protein and DNA, the concentration of AmtR$_T$ and amtB$_{wt}$ was decreased to a low nanomolar concentration range. Because of the concentration limits of EtBr to detect DNA, digoxigenin (DIG)-labeled DNA was used for the subsequent EMSAs.

5.5.2 Adaptation of analyses of the AmtR$_T$ interaction with operator variants

Based on previous studies, the concentration of the DNA fragments was decreased to 1.5 nM (Muhl *et al.* 2009; Hasselt *et al.* 2011). Due to this low nanomolar DNA concentration, ethidium bromide staining of EMSAs resulted in insufficient signal intensity

for detection. Therefore, applied DNA fragments were DIG-labeled at the 3`-ending and detected by anti-DIG antibody. This allowed analyzing AmtR$_T$-DNA interactions in EMSAs with up to 200-fold lower DNA concentrations. Prior to analyses of all operator variants, the optimal AmtR$_T$ concentration for investigation was determined. For this purpose, 1.5 nM of amtB$_{wt}$ was titrated with 1.5 nM to 1000 nM AmtR$_T$ (figure 13).
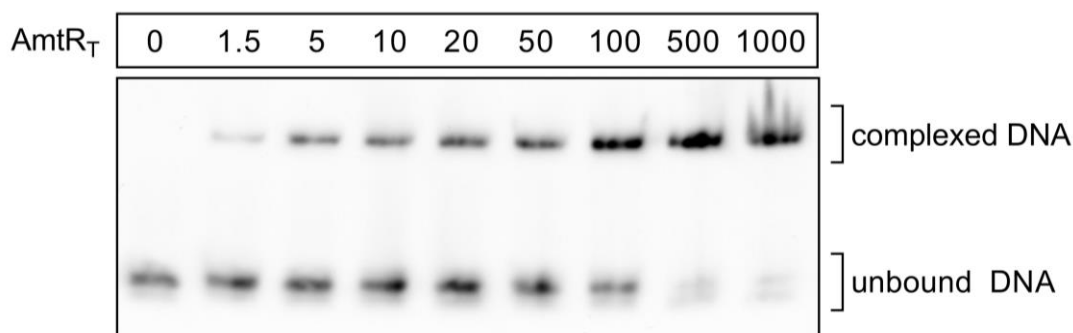

Figure 13 EMSA of an AmtR$_T$ titration with amtB$_{wt}$ operator DNA. To estimate optimal AmtR$_T$ concentrations for EMSAs, 1.5 nM amtB$_{wt}$ was investigated with AmtR$_T$ titrated from 1.5 nM to 1000 nM on an 8 % native TBE gel. The DNA fragments were DIG-labeled and detected by anti-DIG antibody.

The EMSA showed only signals for unbound and complexed DNA and no additional bands indicated non-specific AmtR$_T$-DNA binding. Complex formation between AmtR$_T$ and amtB$_{wt}$ already occurred at concentrations of 1.5 nM AmtR$_T$, which indicated strong binding of AmtR$_T$ to amtB$_{wt}$. With increasing AmtR$_T$ concentrations, the signal intensity of complexed DNA increased, and unbound DNA bands declined. At 500 nM AmtR$_T$, the EMSA revealed only weak signals for unbound DNA and a distinct strong band for the AmtR$_T$-amtB$_{wt}$ complex. At the highest concentration of 1000 nM AmtR$_T$, an additional smear above the AmtR$_T$-DNA complex was shown. This observation suggested additional binding events of AmtR$_T$ to the DNA fragment. To prevent the additional non-specific binding of AmtR$_T$ to DNA fragments, a concentration of 500 nM AmtR$_T$ was used for the subsequent EMSA.

5.5.3   Quantitative analysis of AmtR$_T$ binding to the operator variants

For analysis, 1.5 nM amtB$_{wt}$, amtB$_{ri}$, amtB$_{de}$ and unspecific DNA were tested by EMSAs with 500 nM AmtR$_T$ (figure 14A). To determine relative AmtR$_T$ binding to the different operator variants, signal intensities of bound and unbound DNA fragments were quantified with the ImageLab software (figure 14B).
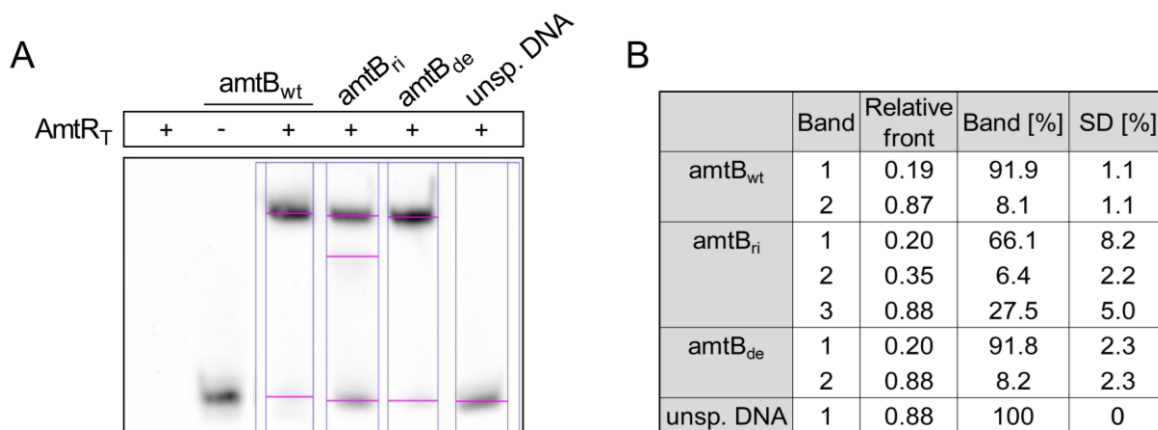
Figure 14 EMSA of AmtR$_T$ binding to different operator variants and quantification of signal intensities. (A) DIG-labeled wild type (amtB$_{wt}$), rigid (amtB$_{ri}$) and deformable (amtB$_{de}$) operator variants as well as unspecific DNA were used. 1.5 nM of DNA fragments were tested with 500 nM AmtR$_T$. In addition, AmtR$_T$ without DNA (lane 1) and amtB$_{wt}$ without AmtR$_T$ (lane 2) were analyzed on an 8 % native TBE gel as controls. The DNA fragments were DIG-labeled and detected by anti-DIG antibody. (B) Relative signal intensities (Band) as well as corresponding standard deviations (SD) were determined with the ImageLab software.

The EMSAs showed no complex formation between the unspecific DNA variant and AmtR$_T$, while different signals of unbound and complexed DNA were obtained for the interactions between AmtR$_T$ and the specific operator variants. The analyses of AmtR$_T$ binding to amtB$_{wt}$ and amtB$_{de}$ revealed similar bands of unbound and complexed DNA, while increased signals for unbound and not fully shifted DNA were shown for the AmtR$_T$-amtB$_{ri}$ interaction. By quantifying the obtained signals for unbound, not fully shifted and complexed DNA of every interaction study, significant differences for the AmtR$_T$ binding to the different operator variants were observed. While the signals for unbound and complexed amtB$_{wt}$ and amtB$_{de}$ DNA were almost identical, the analyses of AmtR$_T$ with amtB$_{ri}$ showed approx. 4.1-fold increased signals for unbound and not fully shifted DNA. Therefore, similar binding affinities for AmtR$_T$-amtB$_{wt}$ and AmtR$_T$-amtB$_{de}$ complexes as well as a 4.1-fold lower binding affinity for the AmtR$_T$-amtB$_{ri}$ interaction were suggested, respectively. Furthermore, these observations indicated that the AmtR$_T$-DNA binding is influenced by the structural properties of the operators, like the high deformation of amtB$_{wt}$ and amtB$_{de}$ and the reduced deformation of amtB$_{ri}$.

To examine the correlation between the operator conformation and the binding affinity of the AmtR$_T$-DNA interaction in more detail, SPR measurements were carried out. This allowed determining kinetic rates and binding constants of the AmtR$_T$-DNA interaction with respect to the DNA deformation of the operator variants.

5.6 Determination of dynamic properties of the AmtR-DNA interaction

To analyze the influence of DNA flexibility on $AmtR_T$-operator binding in more detail, the kinetic rates as well as dissociation equilibrium constants of the $AmtR_T$ interaction with $amtB_{wt}$, $amtB_{de}$ and $amtB_{ri}$ were determined by SPR measurements. In initial experiments, the appropriate sensor chip, amount of coupled DNA and flow rate were established for SPR analysis.

Non-specific binding of $AmtR_T$ to the sensor surface matrix of the applied streptavidin-coated SA chip was tested. For this purpose, $AmtR_T$ was injected onto the chip surface without captured DNA. Since there was no signal, non-specific binding of $AmtR_T$ to the SA chip matrix was ruled out. Therefore, SA chips were suitable for the subsequent analyses. Furthermore, the experimental system was optimized for kinetic measurements by reducing the mass transport limitation. In the case of mass transport limitation, the association of free analyte ($AmtR_T$) to immobilized ligand (operator DNA) is restricted by the diffusion of the analyte to the chip surface (Majka and Speck 2007). This phenomenon can be minimized by decreasing the amount of immobilized DNA and increasing the flow rate. In each subsequent response difference sensorgram, the time was plotted versus the response difference in resonance units (RU). The RU resulted from the signal difference between flow cell 1 (unspecific DNA variant) and flow cell 2 (operator variants). For kinetic analyses, an amount of ligand should be coupled that results in a maximum response difference signal below 100 RU after analyte injection (Majka and Speck 2007). Based on this, 25 RU of ligands (unspecific DNA and operator variants) were coupled at the SA sensor chip in this study, which corresponded to a maximal response difference signal of about 60 RU after injection of $AmtR_T$. To additionally reduce mass transport limitation, the optimal flow rate for SPR measurements were determined in this work. For this purpose, the $AmtR_T$-$amtB_{wt}$ interaction was investigated with a constant $AmtR_T$ concentration of 2 nM at different flow rates in the range of 5 µl min^{-1} to 50 µl min^{-1} (figure 15).

During dissociation, the obtained response difference signals were constant for each flow rate. During association (0 s to 120 s), the sensorgrams showed a higher curvature and a higher slope with an increasing flow rate. Above 20 µl min^{-1}, the association curves approximated the response signals obtained from investigations at flow rates of 40 µl min^{-1} to 50 µl min^{-1}. Apparently, flow rates above 40 µl min^{-1} were sufficient to avoid mass transport for $AmtR_T$-DNA binding. Therefore, pre-conditions for mass transport-free measurements in the subsequent SPR investigations were given for 25 RU of immobilized DNA and a flow rate of 50 µl min^{-1}.
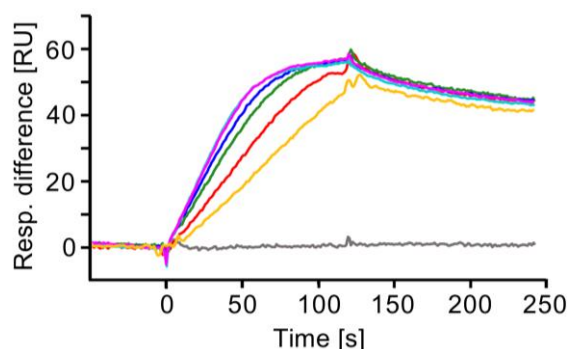
Figure 15 SPR measurements of AmtR$_T$-amtB$_{wt}$ interaction with different flow rates. 25 RU of unspecific DNA in flow cell 1 (fc 1) and amtB$_{wt}$ in flow cell 2 (fc 2) were immobilized at the SA sensor chip. For analysis, the association (0 s to 120 s) and dissociation (120 s to 250 s) of 2 nM AmtR$_T$ were investigated, respectively. Flow rates of 5 µl min^{-1} (yellow), 10 µl min^{-1} (red), 20 µl min^{-1} (green), 30 µl min^{-1} (blue), 40 µl min^{-1} (turquoise) and 50 µl min^{-1} (pink) were investigated**.**

5.6.1 Characterization of the AmtR$_T$-DNA interaction at different protein concentrations

To determine the optimal AmtR$_T$ concentration range for dynamic analyses, DNA-binding properties of AmtR$_T$ at different AmtR$_T$ concentrations were analyzed. In initial analyses, 25 RU of the coupled DNA fragments, unspecific DNA (fc 1) and amtB$_{wt}$ (fc 2), were titrated with 1 nM to 1000 nM AmtR$_T$ in SPR analysis (figure 16).
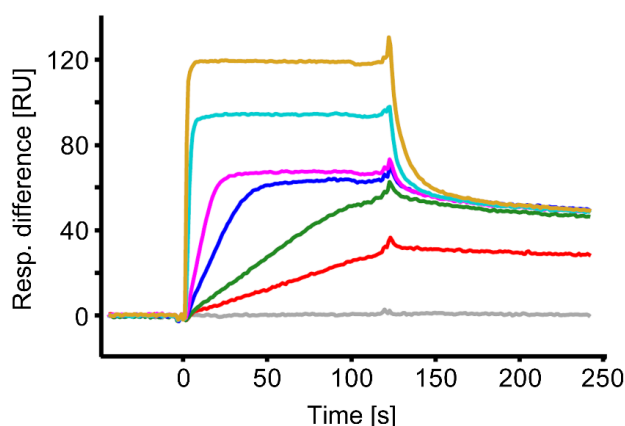

Figure 16 Response difference sensorgram of SPR measurements of the AmtR$_T$-amtB$_{wt}$ interaction. 25 RU of unspecific DNA and amtB$_{wt}$ were immobilized in fc 1 and fc 2 at the SA sensor chip, respectively. The AmtR$_T$-amtB$_{wt}$ interactions was investigated at a flow rate of 50 µl min^{-1} and at concentrations of 1 nM (red), 2 nM (green), 5 nM (blue), 10 nM (pink), 100 nM (turquoise) and 1000 nM (brown) AmtR$_T$. The baseline was obtained by injecting only HBS-EP buffer (grey).

The response difference sensorgram showed diverse graphs for the different AmtR$_T$ concentrations. During association, the graphs of the analyses of 100 nM and 1000 nM

$AmtR_T$ revealed high slopes, almost no curvature and an immediately reached steady-state, while SPR investigations at concentrations of 1 nM to 10 nM $AmtR_T$ showed higher curved graphs and shorter steady-state phases. Furthermore, the graphs obtained from SPR measurements of 100 nM and 1000 nM $AmtR_T$ revealed a biphasic dissociation, due to the two different slopes during dissociation. On the other hand, analyses of 1 nM to 10 nM $AmtR_T$ showed a monophasic dissociation, because of the constant slope during this phase. These results indicated that a 1:1 ($AmtR_T$: operator DNA) binding did only occur at concentrations of 1 nM to 10 nM, while additional binding events or non-specific binding were suggested at $AmtR_T$ concentrations of 100 nM to 1000 nM. This corresponded well to the observations of the EMSAs of this study, which showed additional binding at $AmtR_T$ concentrations of 1000 nM and above.

Due to the suggested non-specific binding, the AmtR interaction to regulated ($amtB_{wt}$ in fc 2) and non-regulated (unspecific DNA in fc 1) sequences was analyzed by SPR measurements. For this purpose, single flow cell sensorgrams of the $AmtR_T$-$amtB_{wt}$ and $AmtR_T$-unspecific DNA binding at different $AmtR_T$ concentrations (see figure 16) were individually monitored as dashed (fc 1) and solid (fc 2) lines of the same color. Additionally, $AmtR_T$ concentrations above 1000 nM (2000 nM, 5000 nM and 10000 nM) were analyzed to assess, if specific or non-specific $AmtR_T$-DNA interaction could be saturated. The obtained sensorgrams of the $AmtR_T$-DNA binding were separately depicted for 100 nM to 10000 nM $AmtR_T$ and for 1 nM to 10 nM $AmtR_T$, respectively (figure 17A and B).

The single flow cell sensorgram of the analysis of 100 nM $AmtR_T$ already showed response signals in flow cell 1, which indicated a distinct recognition of the unspecific DNA by $AmtR_T$ at this concentration. At the $AmtR_T$ concentration of 1000 nM, a response signal in flow cell 1 of about 25 RU were determined corresponding to 18 % of the response difference signal. At the highest investigated $AmtR_T$ concentration of 10000 nM, a response signal of about 175 RU in flow cell 1 and 275 RU in flow cell 2 were measured. This observation suggested an unspecific signal of over 63 % of the response difference signal. Thus, no saturation of specific and non-specific $AmtR_T$-DNA binding was shown, since there was a persistent response signal increase in both flow cells with increasing $AmtR_T$ concentrations, respectively. Vice versa, SPR measurements of 1 nM to 10 nM $AmtR_T$ revealed increasing response signals in flow cell 2 but no response signals in flow cell 1 with increasing $AmtR_T$ concentrations. Therefore, specific $AmtR_T$-DNA binding can be monitored at $AmtR_T$ concentrations up to 10 nM, while non-specific interaction cannot be observed. For subsequent analyses, $AmtR_T$ concentrations below 10 nM were applied to produce valid kinetic data with the least binding of $AmtR_T$ to unspecific DNA.
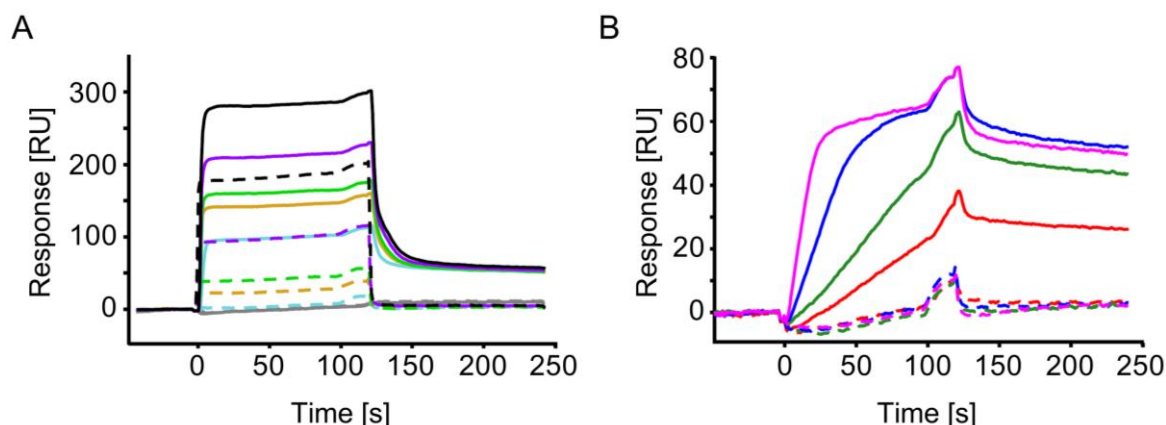
Figure 17 Single flow cell sensorgrams of SPR measurements of the AmtR$_T$-amtB$_{wt}$ interaction. To examine specific and non-specific DNA-binding of AmtR$_T$, single flow cell sensorgrams of the binding studies at different AmtR$_T$ concentrations (see figure 16) were depicted. The sensorgrams showed response signals of flow cell 1 (dashed lines) and flow cell 2 (solid lines), respectively. (A) For analysis of high AmtR$_T$ concentrations, 100 nM (turquoise), 1000 nM (brown), 2000 nM (light green), 5000 nM (purple) and 10000 nM (black) of AmtR$_T$ were applied. (B) Interaction assays of low AmtR$_T$ concentrations were performed with 1 nM (red), 2 nM (green), 5 nM (blue) and 10 nM (pink) of AmtR$_T$.

5.6.2 Alternative quantification method for SPR analysis of the AmtR$_T$-DNA interaction

For initial kinetic analysis, 25 RU of immobilized amtB$_{wt}$ and unspecific DNA were used and AmtR$_T$ was titrated from 0.5 nM to 10 nM. The AmtR$_T$-amtB$_{wt}$ interaction was quantified by single-step kinetics (SSK) analyses (figure 18A). For this purpose, the sensor chip was regenerated with 1.5 M NaCl (diluted in HBS-EP buffer) after the dissociation phase of each concentration step. Nevertheless, the regeneration of the sensor surface obviously led to a strong and persistent decline of the baseline in the measurement of the next AmtR$_T$ concentration step (see figure 18A, -50 s to 0 s, red line). At low response signals as observed for the AmtR$_T$ titration from 0.5 nM to 10 nM, this baseline drift was suggested to overlap too much the measured response signals for kinetic analyses. Therefore, the alternative determination method multi-step kinetics (MSK) analysis was investigated for SPR measurements, based on previous studies (Trutnau 2006; Karlsson *et al.* 2006). For this purpose, the next higher concentration was directly injected after every dissociation phase and finally the sensor surface was regenerated with 1.5 M NaCl after the dissociation of the last concentration step (figure 18B). Consequently, the MSK analysis of the AmtR$_T$-DNA interaction was independent of the regeneration of the sensor surface and allowed the investigation of decreased AmtR$_T$ concentrations of 0.5 nM to 2.5 nM AmtR$_T$.
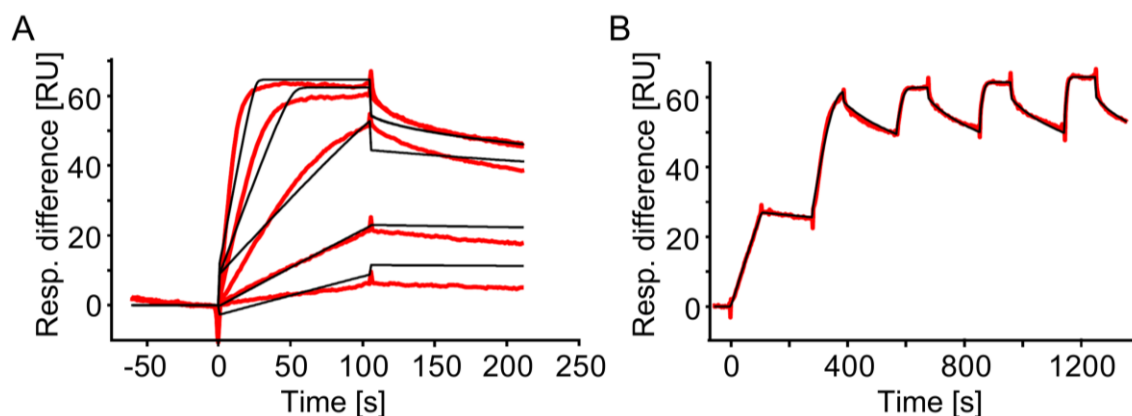
Figure 18 SPR measurements of the AmtR$_T$-DNA interaction using single-step kinetics (SSK) and multi-step kinetics (MSK) analyses. 25 RU of amtB$_{wt}$ (fc 2) and unspecific DNA (fc 1) were immobilized at the SA sensor chip surface. The flow rate was 50 µl min^{-1}. Measured data (red lines) were fitted (black lines) to determine kinetic rates and equilibrium constants. (A) SSK analysis was carried out by regenerating the sensor chip with 1.5 M NaCl after the dissociation phase of each concentration step. For this purpose, AmtR$_T$ at concentrations of 0.5 nM, 1 nM, 2 nM, 5 nM and 10 nM were applied, respectively. (B) MSK analysis was performed by directly injecting the next higher concentration after every dissociation phase. After the dissociation of the last concentration step, the sensor chip was regenerated. 0.5 nM, 0.75 nM, 1 nM, 1.5 nM and 2.5 nM AmtR$_T$ were used.

To determine kinetic rates, a line (black) was fitted through the measured data set (red). For this purpose, the best-fitted values of variables such as rate constants and affinities were identified by the BiaEvaluation software to approximate a perfect overlap. Fits of the measured data of the SSK analysis did not match the association and dissociation of every concentration step. Vice versa, the MSK analysis showed a better superposition of the fitted graphs, since only marginal deviations between measured data and fits were observed. This suggested that kinetic rates and binding affinities, determined by MSK analysis, corresponded more to the real dynamic properties of the AmtR$_T$-DNA interaction. Furthermore, the equilibrium constants of the AmtR$_T$-amtB$_{wt}$ binding were determined by SSK (4.29 x 10^{-11} M) and MSK analysis (2.05 x 10^{-11} M). The equilibrium constants, obtained from MSK analysis, showed an approx. 2-fold increase of the binding affinity between AmtR$_T$ and amtB$_{wt}$ DNA. Consequently, the subsequent SPR measurements were carried out by using only the MSK analysis variant.

5.6.3 Determination of kinetic rates and equilibrium constants of AmtR$_T$ binding to the different operator variants

For SPR analyses, AmtR$_T$ was titrated from 0.5 nM to 2.5 nM (figure 19). Furthermore, 25 RU of unspecific DNA were immobilized in flow cell 1 and 25 RU of the operator variants

amtB$_{wt}$, amtB$_{ri}$ and amtB$_{de}$ were coupled in the flow cell 2 of SA sensor chips, respectively. Each operator variant was individually immobilized on a new sensor chip.
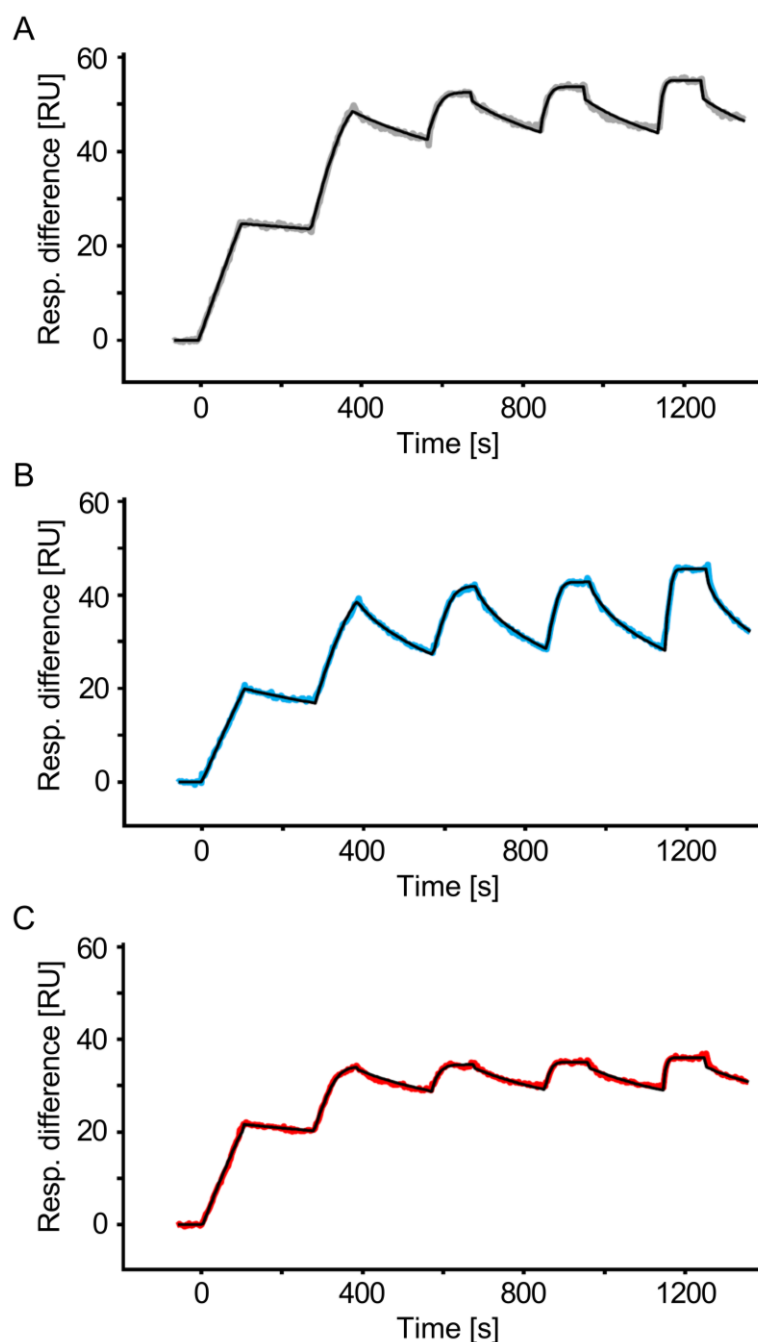
Figure 19 SPR measurements of AmtR$_T$ binding to the different *amtB* operator variants. 25 RU of unspecific DNA in fc 1 and 25 RU of amtB$_{wt}$ (A), amtB$_{ri}$ (B) and amtB$_{de}$ (C) in fc 2 were immobilized at SA sensor chips, respectively. SPR measurements were carried out at 50 µl min^{-1} by analyzing a titration of different AmtR$_T$ concentrations in one cycle (MSK). AmtR$_T$ concentrations of 0.5 nM, 0.75 nM, 1 nM, 1.5 nM and 2.5 nM were applied for analyses. Measured data were depicted for amtB$_{wt}$ (dark grey line), amtB$_{ri}$ (blue line) and amtB$_{de}$ (red line). For the determination of kinetic rates and equilibrium constants, measurements were superposed by an overlay (black line).

The obtained differences in the maximum response signals were attributed to different amounts of immobilized DNA at each sensor chip. These differences did not affect the determination of kinetic rates and binding affinities of the $AmtR_T$-DNA interaction and, therefore, were neglected. During association, all three sensorgrams revealed similar graphs with high slopes and sufficient curvature for the determination of kinetic rates. Vice versa, the SPR analyses showed different graph slopes during dissociation. Investigations of $AmtR_T$ binding to $amtB_{wt}$ and $amtB_{de}$ showed similar graphs, while analysis of the $AmtR_T$-$amtB_{ri}$ interaction revealed a faster decrease of the response difference signal. These observations suggested similar dissociation kinetic rates for the $AmtR_T$-$amtB_{wt}$ and $AmtR_T$-$amtB_{de}$ interaction and increased kinetic rates for the $AmtR_T$ dissociation off $amtB_{ri}$. For quantitative analyses, the kinetic rates of association (k_a) and dissociation (k_d) as well as the dissociation equilibrium constant (K_D) of all three $AmtR_T$-DNA interactions were determined (figure 20).
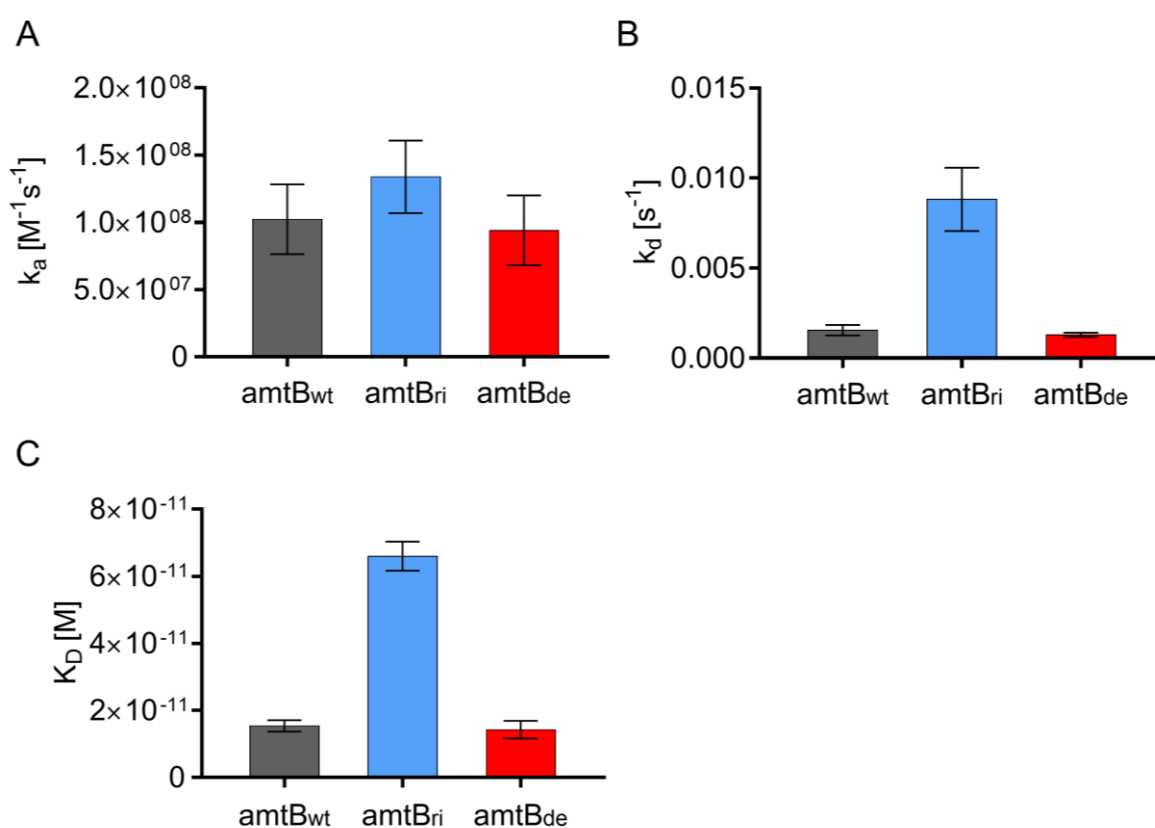
Figure 20 Kinetic rates and equilibrium constants of interactions between $AmtR_T$ and the different operator variants. The kinetic rates of association k_a (A) and dissociation k_d (B) as well as the dissociation equilibrium constant K_D (C) were determined for $AmtR_T$ binding to $amtB_{wt}$, $amtB_{de}$ and $amtB_{ri}$, respectively. Depicted parameters with standard deviations were determined in triplicates.

The association kinetic rates of the $AmtR_T$-$amtB_{wt}$, $AmtR_T$-$amtB_{de}$ and $AmtR_T$-$amtB_{ri}$ complexes were determined at $1.0 \pm 0.25 \times 10^8$ $M^{-1}s^{-1}$, $0.9 \pm 0.26 \times 10^8$ $M^{-1}s^{-1}$ and $1.3 \pm 0.27 \times 10^8$ $M^{-1}s^{-1}$, respectively. This corresponded to a similar $AmtR_T$ association to all three operator variants with a 1.3-fold faster association to the rigid DNA. In contrast, the dissociation rates between $AmtR_T$ and the DNA fragments differed significantly. Similar dissociation kinetic rates of 0.0015 ± 0.00029 s^{-1} and 0.0013 ± 0.00012 s^{-1} were determined for the $AmtR_T$-$amtB_{wt}$ and $AmtR_T$-$amtB_{de}$ complexes, while the analysis of $AmtR_T$-$amtB_{ri}$ interaction revealed an increased dissociation rate of 0.0088 ± 0.0018 s^{-1}. Therefore, a similar $AmtR_T$ dissociation off the wild type and deformable operators and an approx. 6-fold faster $AmtR_T$ diffusion off rigid DNA was determined.

Furthermore, corresponding differences in the equilibrium constants were obtained for the $AmtR_T$-DNA interactions. Similar K_D values of $15 \pm 1.7 \times 10^{-12}$ M and $14 \pm 2.6 \times 10^{-12}$ M for the $AmtR_T$-$amtB_{wt}$ and $AmtR_T$-$amtB_{de}$ complexes were quantified by SPR measurements, respectively. In contrast, the dissociation equilibrium constant of $66 \pm 4.3 \times 10^{-12}$ M between $AmtR_T$ and the rigid DNA was 4.4-fold higher. These observations indicated a stronger $AmtR_T$ binding to flexible than rigid DNA.

Finally, the obtained results allowed to establish a detailed model of the binding process between AmtR and the *amtB* operator DNAs, which should elucidate the correlation between the binding affinity of the AmtR-DNA interaction and structural properties of the DNA targets. This may also be a basis to distinguish binding sites of the AmtR regulon into high and low affinity operators.

6   Discussion

6.1 Principles of the protein-DNA interaction

Protein-DNA interactions play a crucial role in many biochemical processes such as DNA replication, DNA repair or DNA modification (O'Donnell *et al.* 2013; Lamers *et al.* 2000; Casadesus and Low 2006). Besides, transcription regulators also bind to their cognate binding sites and, thereby, activate or repress the production of RNA. This substantially influences the physiological processes, which depend on the products of regulated genes. Due to this key position of transcription regulation, understanding the principles of protein-DNA interaction and protein-DNA recognition is of considerable importance.

Since the phosphate groups of the DNA backbone are negatively charged and the DNA-binding domains of proteins mainly consist of positively charged amino acids (Harteis and Schneider 2014; Cherstvy 2009), an initial non-specific protein-DNA complex is formed by electrostatic interactions (Coulocheri *et al.* 2007). For specific interaction, Janin and coworkers suggested a binding interface with an average of 24 amino acids and 12 base pairs to form protein-DNA complexes (Janin *et al.* 2007). However, a simple recognition code or a 1 to 1 correlation between base pair and amino acid sequences does not exist so far. Since a sequence-based readout seemed not to be enough for specific protein-DNA binding, previous studies postulated and later demonstrated that additional properties like the 3D structure or flexibility of operators additionally influence the affinity of the protein-DNA interaction (Kim *et al.* 2000; Lindemose *et al.* 2014). Therefore, both the readout of the base pair sequence and the DNA shape must be considered to fully understand specific protein-DNA recognition (figure 21).

For the readout of the base pair sequence, functional groups of the four DNA bases are recognized as a unique chemical signature. Specific base readout mainly occurs in the major groove, because all four bases can be recognized (Seeman *et al.* 1976; Harteis and Schneider 2014). Vice versa, some sequences are not differentiated in the minor groove, since not all functional groups of the bases are accessible. The interactions between amino acid residues and functional groups of the bases are formed by hydrophobic bonding, hydrogen bonds (H-bonds) and water mediated H-bonds (Seeman *et al.* 1976; Härd and Lundbäck 1996). Moreover, the number of such contacts and their bonding geometries affect the specificity and affinity of protein-DNA binding (Coulocheri *et al.* 2007). Therefore, an appropriate DNA conformation is essential for the protein-DNA interaction to form a binding interface with the most specific contacts between the protein and the DNA.

The structure and flexibility of the DNA are affected by sequential properties such as base pair composition and base pair stacking (Nelson *et al.* 1987; Travers 2004). Hence, A-T-rich sequences show a higher flexibility than G-C-rich sequences, due to the lower number of H-bonds between adenine and thymine bases compared to guanine and cytosine bases. Moreover, DNA deformability is influenced by the stacking interactions of base pairs, since higher stacking areas resulted in higher thermodynamic stabilities and vice versa (Yakovchuk *et al.* 2006; Harteis and Schneider 2014). Thus, a pyrimidine-purine step is the most deformable step followed by purine-purine or pyrimidine-pyrimidine steps with the purine-pyrimidine step being the least deformable one. The resulting sequence-depending deformation of the DNA can be classified as global and local shape of the DNA (Rohs *et al.* 2009; Rohs *et al.* 2010). While global DNA shape is based on an overall DNA bending or an A/Z-DNA conformation, DNA kinks or minor groove narrowing rather correspond to the local shape of DNA. These kinds of DNA deformation change the accessibility of functional groups of the bases and, therefore, the base readout in the major and minor groove (Harteis and Schneider 2014). As a consequence, both the base pair sequence and the DNA shape must be taken into account to characterize the protein-DNA interaction with respect to the binding affinity and specificity.
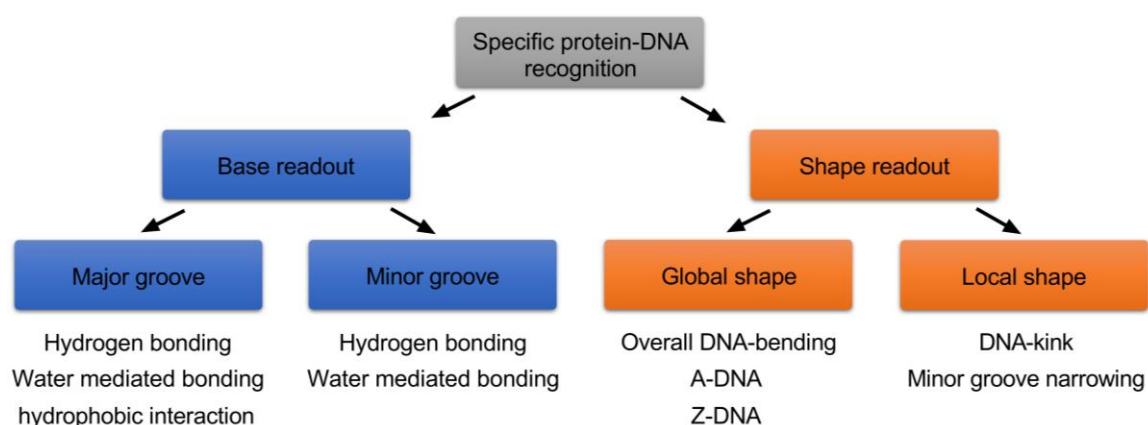
Figure 21 Different mechanisms of the specific protein-DNA recognition. The specific protein-DNA interaction is classified into the readout of the base pair sequence and the intrinsic DNA shape. For base readout, the recognition of functional groups of the bases in the major and minor groove is crucial, while global and local structural properties of the DNA additionally affect the specific protein-DNA recognition (Rohs *et al.* 2010).

Apparently, the DNA recognition by AmtR also depends on DNA properties additional to the operator sequence: the consensus sequence of AmtR operators contains a 6 bp long unspecific sequence in the center (Muhl *et al.* 2009; Hasselt *et al.* 2011) and transcriptome analyses of the *C. glutamicum* genome showed many different sequences that match this

consensus sequence but are not regulated by AmtR (Beckers *et al.* 2005; Silberbach and Burkovski 2006). As a consequence, it was suggested that many of those identified DNA targets were presumably not bound by AmtR because of their shape. To address this idea, AmtR binding to artificial operator DNAs with different structural properties were analyzed in this study. The results of these analyses allowed to derive a dynamic model for AmtR binding to the investigated operator variants and to further elucidate the DNA binding mechanism of AmtR.

6.2 Protein characteristics of AmtR

AmtR preparations were investigated for homogeneity and properly folded protein. SDS-PAGEs showed only one AmtR band in all samples, while native PAGEs revealed stable AmtR preparations with only one distinct band over a period of 144 h and instable AmtR preparations with additional AmtR conformations already after 24 h. Sequencing analysis of the plasmids, isolated from the corresponding cell extracts, showed a deletion of 15 bp in the linker region between the coding sequence of the factor Xa cleavage site and the *amtR* gene of the plasmid of the stable AmtR preparation. The remaining 3 bp of this truncated linker coded for only one additional threonine residue in front of the first N-terminal amino acid of AmtR. The reason for this spontaneous linker mutation is still unknown. Nevertheless, this $AmtR_T$ variant was used for analyses in this study, because of its high protein stability and its high sequence identity to wild type AmtR.

To demonstrate binding of $AmtR_T$ to native operators, the stable AmtR variant was qualitatively tested in EMSAs with six different operators. At high protein concentrations of 1 µM and above, distinct bands additional to the unbound operators and the apparent 1:1 protein-DNA complexes were detected in all samples with the lowest mobilities in the gels. Cooperative binding events, as seen for promoter fragments with multiple binding sites (Bendt *et al.* 2004; Jakoby *et al.* 2000), could be ruled out for these $AmtR_T$-DNA interactions, since DNA sequences with only one single operator were applied. Based on recent crystal structure analyses, an oligomerization of $AmtR_T$ was rather suggested for these binding events (Palanca and Rubio 2016). Below the high protein concentration of 1 µM, the formation of 1:1 $AmtR_T$-DNA complex bands differed slightly but significantly in these EMSAs, because of the obviously high binding affinity of $AmtR_T$ to all these DNA operators. These observations contradicted to previous investigations, that suggested an AmtR binding to the chosen operator sequences with different affinities (Beckers *et al.* 2005). In that study, the RNA hybridization experiments showed a recognizable background expression for the gene *glnA* during AmtR binding, a moderate regulation of *codA* and a full

gene repression of *amtB*, *crnT*, *gltB* and *urtA*. Furthermore, Beckers and coworkers demonstrated in gel retardation experiments that one of the strongest bindings of all analyzed interactions occurred between AmtR and the *amtB* operator. This corresponded well with the results of the EMSAs of the present work, since the best binding was observed between $AmtR_T$ and the wild type *amtB* operator $amtB_{wt}$. Therefore, $amtB_{wt}$ was used as basis to generate operator mutants with distinct conformational properties.

6.3 Structural properties of the *amtB* operator variants

In recent crystal structure analysis of the AmtR-DNA complex, no direct interaction between residues of the DNA binding domain of AmtR and the central six bases of the operator were shown (personal communication, F. Grau and Y.A. Muller; Palanca and Rubio 2016). Thus, differently shaped operator variants were generated by exchanging only the base pair composition and number of flexible pyrimidine-purine steps in the sequence of the spacer but not the respective binding half sites of $amtB_{wt}$. This ensured a specific AmtR-DNA recognition and elucidated the influence of different levels of DNA deformation on the AmtR-DNA binding. The spacer sequence of the wild type operator $amtB_{wt}$ comprised about 83 % adenine or thymine bases and one flexible pyrimidine-purine step. For the deformable variant, the A-T-rich spacer sequence of the wild type operator was exchanged by a G-C-rich (100 % guanine or cytosine) spacer sequence with an increased number of three pyrimidine-purine steps. On the other hand, the rigid operator variant comprised a G-C-rich spacer sequence without any flexible steps. This allowed to investigate the role of both sequence features, the base pair composition and number of flexible steps, in deforming the operator, respectively. For this purpose, the intrinsic shape of these operator variants in unbound state and the effect of AmtR-binding on the DNA conformation of these operators were studied.

In unbound state, each operator variant was deformed. Furthermore, the analyses revealed similar DNA conformations for the wild type and deformable operator variants and a reduced DNA deformation for the rigid operator. This indicated that the identical conformations of $amtB_{wt}$ and $amtB_{de}$ were caused by an A-T-rich sequence with less pyrimidine-purine steps or a G-C-rich sequence with many pyrimidine-purine steps. Nevertheless, neither an A-T-rich sequence nor pyrimidine-purine steps were present in the spacer sequence of $amtB_{ri}$, while a reduced but recognizable DNA distortion was shown for this variant in the unbound state. This reduced DNA deformation can be attributed to the rather rigid purine-purine steps in the spacer region and the single pyrimidine-purine step (T-G) between the binding half site "CTGT" and the spacer sequence "GGGGGG". Moreover, the binding half sites

and flanks, originating from amtB$_{wt}$, comprised approx. 79 % adenine or thymine bases and five pyrimidine-purine steps. This can be additionally responsible for the DNA deformation of all three operator variants. Therefore, the complete base pair sequence seemed to be involved in DNA deformation, while the different levels of DNA deformation of the respective operator variants were caused by variations in the spacer sequences.

In complexed state, each operator variant was deformed, as well. However, the analyses of AmtR$_T$-bound operators showed no differences in the DNA conformation of the wild type, deformable and rigid variant. Therefore, a distinct conformational change of the DNA during AmtR$_T$-binding was suggested, which resulted in uniform macroscopic states of the complex with each operator variant. This seemed to be essential to form a specific and strong interaction between the functional groups of the amino acids of AmtR and the base pairs of the operators. Such protein-induced DNA deformation was frequently observed for many protein-DNA interactions. The corresponding level of DNA distortion ranges from a relatively low deformation as observed in complexes with the tryptophan repressor TrpR or the tetracycline repressor TetR (Otwinowski *et al.* 1988; Orth *et al.* 2000) to strong DNA kinks in complexes with, for example, the integration host factor IHF or the TATA-binding protein TBP (Kim *et al.* 1993; Swinger and Rice 2007). Similar to investigations of the TetR-DNA complex, crystal structure analysis of the TetR-type regulator AmtR bound to DNA suggested a low deformation of only 5° (Palanca and Rubio 2016). Nevertheless, the question that arose here is, how the binding affinity of the AmtR-DNA interaction is affected by such a DNA deformation of the respective operators.

6.4 Characterization of the AmtR-DNA interaction

AmtR binding to differently shaped operator variants were characterized by EMSAs and SPR measurements to analyze thermodynamic as well as dynamic influences on the AmtR-operator interaction.

6.4.1 Approaches to study AmtR-DNA interaction - EMSA vs. SPR analysis

Based on previous studies, the AmtR-DNA interaction was initially investigated by EMSAs (Beckers *et al.* 2005; Muhl *et al.* 2009). This approach was a fast and simple way to estimate the AmtR binding to DNA with different structural properties. Due to digoxigenin-labeled DNA fragments and antibody detection, AmtR$_T$-DNA interaction could be analyzed even at low nanomolar DNA concentrations. Already at 1.5 nM AmtR$_T$, operator DNA was shifted to a complex band, whereas a full shift was obtained at a concentration of 500 nM AmtR$_T$. The reason for the full shift only at that high AmtR$_T$ concentration may be the influence of the

electric field on the complex stability in polyacrylamide gels or the missing chemical equilibrium during electrophoreses (Hellman and Fried 2007). Furthermore, at the same AmtR$_T$ concentration range, additional binding events or non-specific binding was observed in the EMSAs with native operators as well as SPR analyses of 500 nM to 1000 nM AmtR$_T$. Therefore, an appropriate quantification of the binding affinities and kinetic rates between AmtR$_T$ and the operator variants was not achieved by EMSAs in this study.

As a consequence, EMSAs were extended by SPR measurements, which allowed to quantify the interaction between AmtR and operator DNAs at physiological conditions and without interfering labeling molecules, gel matrices or electric repulsion. However, SPR measurements needed to be adjusted to properly analyze the dynamics of the AmtR-DNA interaction. The SA sensor chip was identified as the appropriate sensor chip for the SPR analyses in this work, since no unspecific interaction between AmtR$_T$ and the SA sensor chip matrix was shown. Conditions for mass transport-free SPR measurements were given at a flow rate of 50 µl min^{-1} and 25 RU of immobilized DNA, as described in previous studies (Majka and Speck 2007; Schuck and Zhao 2010). And finally, the best curve progression in sensorgrams was obtained by multi-step kinetics (MSK) analyses, since these approaches allowed to study interactions independent of the regeneration of the sensor surface (Trutnau 2006; Karlsson *et al.* 2006). Based on this, SPR analysis seemed to be the method of choice for characterizing dynamic properties of the AmtR-DNA interaction.

6.4.2   DNA-binding properties of AmtR at different protein concentrations

The optimal AmtR$_T$ concentration range for dynamic analyses was deduced by EMSAs and SPR measurements at different AmtR$_T$ concentrations. However, the quantification of the AmtR$_T$-DNA interaction by EMSAs was limited in this study. Therefore, SPR analyses were mainly used for this purpose. The response difference sensorgram of concentrations of 1 nM to 10 nM AmtR$_T$ revealed highly curved graphs and a short steady-state during association as well as a monophasic dissociation. Furthermore, the analyses at these low nanomolar AmtR$_T$ concentrations showed no additional binding events or non-specific binding and, therefore, allowed to determine ideal 1 to 1 binding kinetics. Vice versa, investigations of 100 nM and 1000 nM AmtR$_T$ showed graphs with high slopes and no curvature during association, and a biphasic dissociation. This corresponded well with analyses of previous studies analyzing the AmtR-DNA interaction in a similar concentration range of 100 nM to 750 nM AmtR (Hasselt *et al.* 2011). Nevertheless, these results indicated a drastic reduction of the data quality for SPR analyses of 100 nM AmtR and above. Moreover, in the present work, the response signals obtained for the AmtR$_T$-amtB$_{wt}$

interaction at 100 nM and 1000 nM $AmtR_T$ suggested additional binding events or non-specific binding. These results matched the observations of the EMSAs of this study.

To analyze these additional binding events and non-specific interaction in more detail, the binding of $AmtR_T$ to $amtB_{wt}$ and unspecific DNA were separately evaluated at the different $AmtR_T$ concentrations, as well. Single flow cell sensorgrams in the range of 1 nM to 10 nM $AmtR_T$ revealed a strong response signal only in the flow cell 2 with the specific operator $amtB_{wt}$ attached. Vice versa, analyses at $AmtR_T$ concentrations of 100 nM and above additionally showed response signals in the flow cell 1, which contained the unspecific DNA sequence. These findings suggested a distinct recognition of unspecific DNA by $AmtR_T$, which was attributed to still unknown effects. Nevertheless, the corresponding binding affinity of this non-specific interaction seemed to be very low, since this complex formation could be observed only at $AmtR_T$ concentrations of 100 nM and above. At $AmtR_T$ concentrations below 10 nM, such non-specific binding was not detected.

6.4.3 Establishment of the binding model of $AmtR_T$ and *amtB* operator variants

The dynamic SPR analyses revealed a dissociation equilibrium constant of 15×10^{-12} M for the interaction between $AmtR_T$ and the wild type operator variant. This corresponded to an approximately 1000-fold higher binding affinity of AmtR to DNA compared to previous investigations (Hasselt 2010; Hasselt *et al.* 2011). Apparently, the reason for this seemed to be that the amount of immobilized ligand and the flow rate was not appropriately adjusted by Hasselt and coworkers to prevent mass transport. Therefore, obtained curves could not be fitted properly in those studies. Furthermore, the obtained K_D of 15×10^{-12} M of the present work also showed that AmtR has one of the highest affinities for its cognate operator among the TetR family regulators. Analyses of local TetR-type regulators like DesT, TetR, as the paradigm of this family, and QacR revealed an approx. 7-fold to 3300-fold weaker DNA-binding (Zhang *et al.* 2007; Kamionka *et al.* 2004; Schumacher *et al.* 2002), while interaction studies of global TetR-type regulators such as KstR and SmcR demonstrated 660-fold to 183,000-fold lower binding affinities than the $AmtR_T$-DNA interaction, respectively (Ho *et al.* 2016; Kim *et al.* 2010). Moreover, the investigations of $AmtR_T$ binding to $amtB_{wt}$ showed a similar binding affinity as other non TetR-type global regulators such as CRP and IHF (Gunasekera *et al.* 1992; Sugimura and Crothers 2006).

In addition, the binding properties of $AmtR_T$ to differently shaped DNA variants were studied. The binding analyses of $AmtR_T$ and deformable DNA ($amtB_{de}$) showed an almost identical equilibrium constant like $AmtR_T$ binding to the wild type DNA. In contrast, the dissociation

equilibrium constant of the $AmtR_T$-$amtB_{ri}$ interaction was 4.4-fold higher and corresponded with the 4.1-fold weaker $AmtR_T$-$amtB_{ri}$ binding obtained from the EMSA quantification. The decreased binding affinity may be attributed to the reduced DNA deformation of the rigid operator, since a higher deformation energy seemed to be necessary for a matching operator conformation. Based on these results, a distinct correlation between the intrinsic structure and deformability of the operator DNA and the DNA-binding affinity of $AmtR_T$ was suggested. This corresponded well to the previous studies of the E2-DNA and CRP-DNA complexes, which proposed high binding affinities for sites with a suitable DNA deformation and low binding affinities for sites that require protein induced bending (Kim *et al.* 2000; Hegde 2002; Lindemose *et al.* 2014).

Additionally, the kinetic rates of the different $AmtR_T$-DNA interactions were determined to assess the influence of the operator conformation on the dynamics of association and dissociation, respectively. The obtained association kinetic rates between $AmtR_T$ and the three tested operator variants were in the same order of magnitude. Only the association rate of $AmtR_T$ to rigid DNA was slightly increased by a factor of 1.3. Apparently, the association of $AmtR_T$ to different DNA targets was not significantly affected by the intrinsic DNA deformation. In contrast, $AmtR_T$ dissociated from $amtB_{wt}$ and $amtB_{de}$ with similar kinetics, while the dissociation of $AmtR_T$ from $amtB_{ri}$ was approx. 6-fold higher. Apparently, AmtR cannot keep the contact to rigid operator DNA as good as to deformable DNA.

Based on the determined ON- and OFF-rates of the $AmtR_T$-DNA interaction studies, a detailed binding model for the $AmtR_T$ association and dissociation was generated with respect to the deformation of $amtB_{wt}$, $amtB_{ri}$ and $amtB_{de}$ (figure 22). Furthermore, this binding model of $AmtR_T$ and the *amtB* operator variants may help to distinguish other operator sequences of the AmtR-regulon into high and low affinity sites.
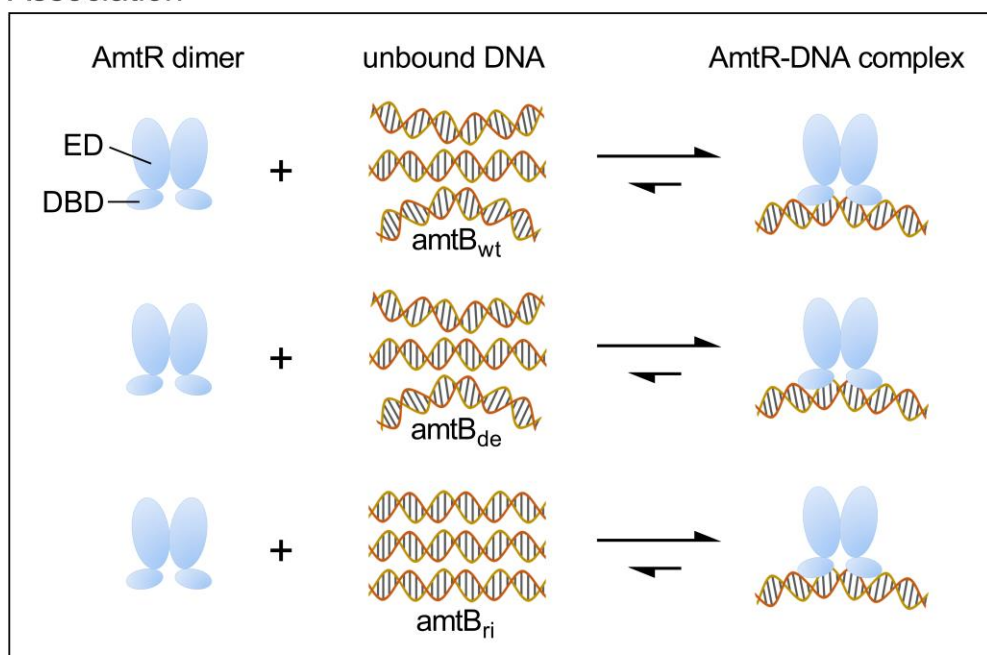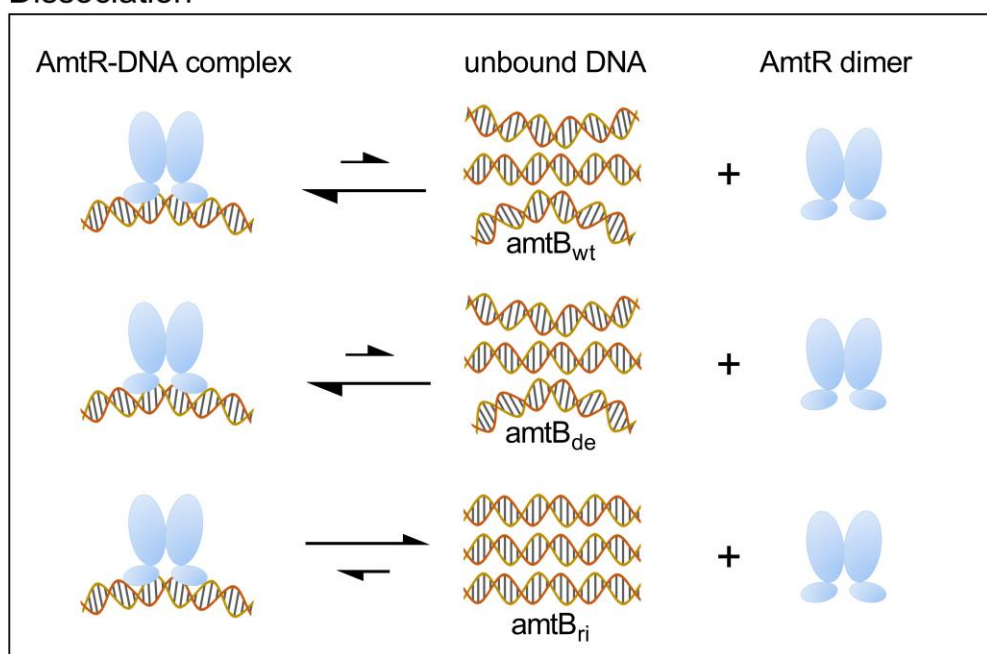
Figure 22 Binding model of AmtR$_T$ and the *amtB* operator variants. The binding process was individually shown for the association and dissociation of AmtR$_T$ and the respective operator variants amtB$_{wt}$, amtB$_{de}$ and amtB$_{ri}$. AmtR$_T$ was depicted as dimer with its corresponding effector (ED) and DNA-binding domain (DBD). Operator sequences were shown as DNA double helices with their respective structural DNA properties (amtB$_{wt}$ and amtB$_{de}$: rather deformable features; amtB$_{ri}$: rather straight features). Differently sized arrows represent the directions of the equilibria between unbound and complexed state of AmtR and the operator variants, respectively.

6.4.4 Classification of high and low affinity operators of the AmtR regulon

Previous studies revealed that the binding half sites "CTAT" and "ATAG" play a crucial role for specific base pair recognition and, therefore, for specific AmtR-DNA interaction (Muhl *et al.* 2009; Hasselt *et al.* 2011). Nevertheless, strong complex formation was also observed between AmtR and operators with only one or none of the conserved half sites (Beckers *et al.* 2005). Therefore, additional properties like the sequence-dependent DNA structure and flexibility of the operator DNA were suggested to modulate the binding affinity of the AmtR-DNA interaction, as well. This was qualitatively and quantitatively confirmed in the present work for AmtR$_T$ binding to the *amtB* operator. The structural characterization of DNA variants of this operator revealed that the DNA conformation was dependent on the base pair composition (A-T-rich vs. G-C-rich sequences) and the total number of flexible pyrimidine-purine steps. Based on this, the operator sequences of the whole AmtR regulon were investigated. The obtained results showed a significant variance in the base pair composition of spacers, while the number of four pyrimidine-purine steps was strongly conserved in the operators. These flexible base pair steps were found in almost every AmtR binding site, either at both ends of the spacer, in the binding half sites or in between. Therefore, DNA deformations at these distinct positions were suggested to be crucial for AmtR-DNA binding. This corresponded well to analyses of the CRP-DNA complex (Lindemose *et al.* 2014), which revealed two DNA kinks at the closest base pair steps to the spacer sequence. Lindemose and coworkers additionally proposed that the deformability of the spacer plays an important role in the respective CRP-DNA binding. Similar correlations were demonstrated for the AmtR-DNA interaction in this study, since strong AmtR binding to the operator variants with rather deformable spacers and a significantly weaker AmtR binding to an operator with reduced deformability in the spacer were shown.

Based on these data, an initial distinction of the binding sites of the AmtR regulon into high- and low-affinity operators was performed with respect to the "CTAT"-"ATAG" binding half sites, an A-T-rich base pair composition and four pyrimidine-purine steps. Thus, the strongest AmtR binding was suggested for the operators of the genes *crnT*, Ncgl1099/1100 and Ncgl1915-1918, because these AmtR binding sites meet all criteria for an optimal target sequence. On the other hand, weaker AmtR binding was predicted for operators of, for example, *amtB*, *ureA* and *codA*, which do not have all appropriate sequence requirements of a high-affinity operator. However, the obtained ranking did not match the results of previous interaction analyses (Beckers *et al.* 2005), since the strongest binding was suggested between AmtR and the operator of *amtB* followed by *ureA* and *codA*, while only moderate binding was assumed for the *crnT* operator. This discrepancy indicated that additional still unknown aspects of AmtR and the DNA may influence the AmtR-DNA

interaction. Moreover, it seemed that the characterization of AmtR binding to operator DNA was presumably limited, due to the small number of only the three investigated sequences of this work.

Therefore, the analyses carried out so far have been supplemented by sequence alignments of AmtR with other TetR-type regulators and by structure comparisons of these regulators in complex with DNA. Eventually, this may provide further insight into the transcription regulation by AmtR.

6.5 AmtR and its DNA binding mechanism

The TetR family contains many different local regulators which control the transcription of one or several genes and global regulators that regulate at least 20 different genes (Rodionov 2007). Due to the large number of 42 directly and indirectly regulated genes in the AmtR regulon and the different binding affinities of AmtR to these DNA targets (Beckers *et al.* 2005; Buchinger *et al.* 2009), AmtR is classified as a global regulator. In order to get information about the difference in operator recognition between local and global regulators, the amino acid sequence of AmtR was compared with the sequences of different local and global TetR-type regulators (Ramos *et al.* 2005; Cuthbertson and Nodwell 2013). For this purpose, a sequence alignment of AmtR and the local regulators AcnR, CgmR, RolR and FasR from *C. glutamicum*, TetR from *E. coli*, QacR from *Staphylococcus aureus*, SimR from *Streptomyces antibioticus* and DesT from *Pseudomonas aeruginosa* was carried out (figure 23A). Additionally, for the comparison of AmtR and global regulators, the amino acid sequences of McbR from *C. glutamicum*, SmcR from *Vibrio vulnificus* and KstR from *Mycobacterium tuberculosis* were aligned to the AmtR sequence (figure 23B). In each alignment, the main focus was on differences and similarities in the sequences of characteristic structures of AmtR for DNA-binding like the N-terminal anchor sequence and the first three α-helices (Muhl *et al.* 2009; Palanca and Rubio 2016).

The alignment with local regulators revealed a weak resemblance between the sequences of AmtR and the respective regulators, since no similarities in the anchor sequence and only a few similar residues were detected at the positions of the three α-helices. Furthermore, N-terminal extensions, as observed for AmtR (Palanca and Rubio 2016), were suggested only for SimR and RolR, based on the long sequences in front of the first α-helix. However, crystal structure analyses of RolR revealed that the N-terminal sequence did not correspond to a disordered extension but a slightly larger first α-helix (Li *et al.* 2011). On the other hand, analysis of SimR showed a long N-terminal extension, which was disordered (Le *et al.* 2011). This region seemed to be crucial for unspecific binding to the DNA backbone outside of the operator.
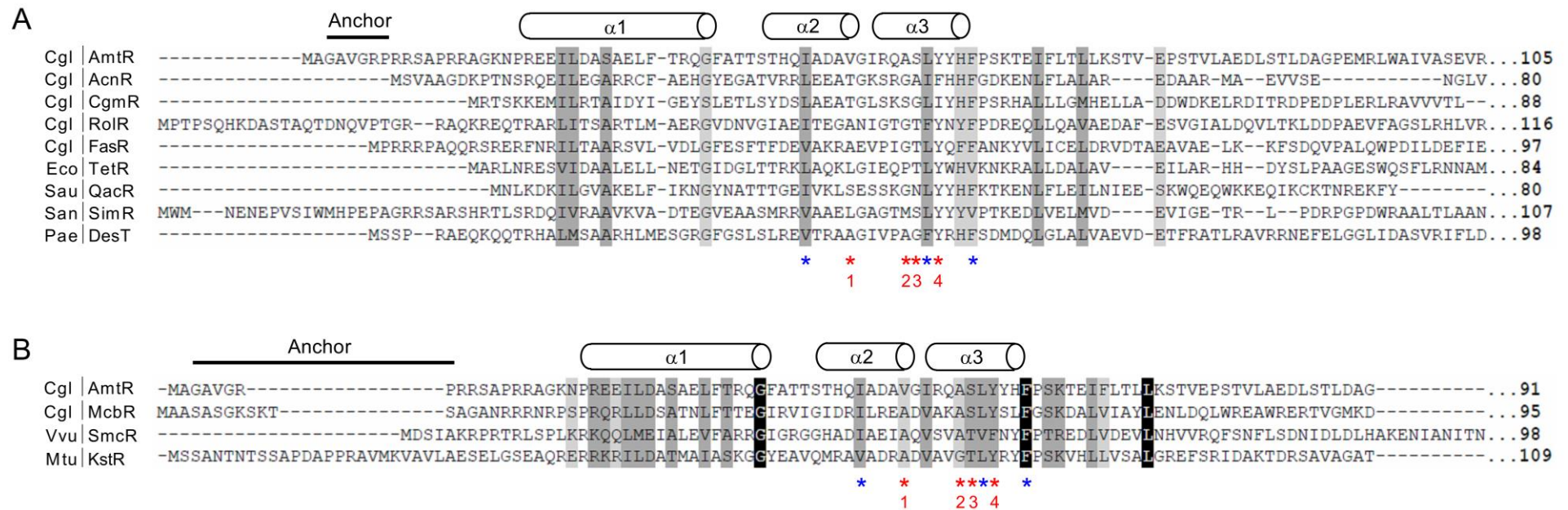
Figure 23 Sequence alignments of the DNA-binding domains of AmtR and different local and global TetR-type regulators. The amino acid sequence of the DNA-binding domain of *C. glutamicum* AmtR was aligned to the sequences of local (A) and global (B) regulatory proteins of the TetR-family. Regulators and species were indicated on the left side (Cgl: *C. glutamicum*; Eco: *E. coli*; Sau: *S. aureus*; San: *S. antibioticus*; Pae: *P. aeruginosa*; Vvu: *V. vulnificus*; Mtu: *M. tuberculosis*) and the number of amino acids on the right side. Amino acids were shown in single letter code and respectively colored (black: fully conserved residue; dark grey: residue with strongly similar properties; bright grey: residue with weakly similar properties). At the top, the positions of the N-terminal anchor and the first three α-helices of *C. glutamicum* AmtR were depicted. Furthermore, distinct positions in the two DNA recognition helices α2 and α3 have been respectively labeled, whereas amino acids at these positions significantly differ (red asterisk) or resemble (blue asterisk) between local and global regulators.

Vice versa, the alignment of AmtR and global regulators showed an increased number of similar residues and fully conserved amino acids at the respective positions of the three α-helices. In addition, a long sequence in front of the first α-helix was identified for each regulator, with the longest extensions observed for KstR and McbR. However, the real conformation of the N-terminal region of McbR could not be determined, because the corresponding crystal structure is still missing. Moreover, respective crystal structure analysis of KstR did not identify an N-terminal disordered region but a larger fist α-helix (Ho *et al.* 2016), similar to RolR. In case of SmcR, structural data did only exist for the unbound state but not for the SmcR-DNA complex. Nevertheless, the published structural data of SmcR predicted an N-terminal disordered region with the arginine residues 9 and 11 of this N-terminal extension as putative recognition residues for unspecific DNA interaction (Kim *et al.* 2010).

Based on these alignments, it was shown that the sequence of AmtR resembles more to those of global TetR-type regulators than to those of local regulators. Furthermore, an N-terminal disordered region, as described for the AmtR-DNA complex (Palanca and Rubio 2016), was observed for several global as well as local regulators of the TetR family and seemed to be involved in the unspecific DNA interaction outside of the operator. The alignments also revealed amino acids at distinct positions in the two recognition helices α2 and α3, which showed strong similarities in both, local and global regulators. On the other hand, distinct amino acids at other positions were found to be conserved only in global but not local regulators. To elucidate the similarities and differences at these specific amino acid positions in more detail, the crystal structure of the binding interface of AmtR was compared with those of chosen local and global regulators in complex with their cognate DNA.

In both alignments, only the hydrophobic amino acids valine, leucine, isoleucine or phenylalanine were identified at the positions with similar residues for local and global regulators (blue asterisk). Additionally, crystal structure analyses showed that each of these residues were oriented towards the center of the respective HTH-motif (Palanca and Rubio 2016; Itou *et al.* 2010; Orth *et al.* 2000; Schumacher *et al.* 2002; Le *et al.* 2011; Kim *et al.* 2010; Ho *et al.* 2016). Apparently, the residues at these positions are involved in the stabilization of the tertiary structure of the HTH-motif and, therefore, must be conserved in both, global and local regulators. For the other investigated positions (red asterisk, position 1 to 4), differences between local and global regulators were shown with respect to the corresponding side chains and orientation. At position 1, the small residues alanine and valine were identified for global regulators and larger residues like leucine, threonine and serine for local regulators. According to crystal structure analyses, these residues were located at the end of the second helix and oriented to the center of the HTH-motif (PDB

entry: 5DY0 (AmtR); 1QPI (TetR); 3ZQL (SimR); 1JT0 (QacR); 5UA2 (KstR); 2YVH (CgmR)). Thus, a larger residue at this position such as Leu34 of TetR (Orth *et al.* 2000) may be the reason that the corresponding α-helix 2 was oriented more towards the major groove of the DNA, compared to the α-helix 2 of AmtR (Palanca and Rubio 2016). The reduced distance between this helix and the DNA could be responsible for the high number of interactions in the binding interface of TetR. Furthermore, at position 2, only small residues like alanine and glycine were found in global regulators, while larger residues like proline, methionine and serine were additionally identified for local regulators. Residues at this position are located at the beginning of α-helix 3 and oriented directly towards the major groove. However, despite the obviously optimal location and orientation of these residues for DNA binding, only one hydrophobic bonding was formed between Ala54 of AmtR and the thymine base of the "ATAG" half site (personal communication, Y.A. Muller and F. Grau). On the other hand, multiple interactions to more than one DNA base were observed for the residues Pro39 of TetR and Met62 of SimR at this position, respectively (Orth *et al.* 2000; Le *et al.* 2011). This additionally seems to contribute to the gene specificity of several local TetR-type regulators. Moreover, the residues serine and threonine were identified for global regulators at the third amino acid position, while the smaller residues alanine and glycine as well as the larger residue asparagine were also found in local regulators at this position. In global regulators, only the DNA backbone was bound by residues at this position. Similar observations were made for the local regulators CgmR, QacR and SimR, whereas hydrogen and hydrophobic bonding was observed between the residue Thr40 of TetR at this position and two cytosine bases of the operator (Orth *et al.* 2000). This extended bonding profile of TetR towards DNA bases may be the result of the α-helix 2 of this regulator, which is oriented more towards the major groove of the DNA than the respective helix of AmtR. Finally, at the last investigated position (amino acid position 4), large aromatic residues were identified for global regulators and aromatic as well as hydrophobic amino acids for local regulatory proteins. These residues are located in α-helix 3 and oriented such that hydrogen bonding towards the DNA backbone is form in both, local and global regulators. Nevertheless, the residues Tyr42 of TetR and Tyr40 of QacR are also involved in the direct interaction towards functional groups of the DNA bases by hydrophobic bonding, respectively (Orth *et al.* 2000; Schumacher *et al.* 2002).

Based on these results, amino acids at distinct positions and with appropriate side chains and orientations were found that allowed to distinguish between local regulators such as TetR and global regulators like AmtR. Furthermore, these findings indicated that significantly less interactions to distinct DNA bases of the operator are formed by residues of AmtR at these positions. This could be one reason for the lower sequence specificity and, therefore, the higher number of operators recognized by AmtR, compared to TetR and other

local regulators. Nevertheless, to achieve high specificity and also high affinity for the DNA binding by AmtR, the highest number of specific contacts between the regulator and the DNA seemed to be achieved by an appropriate DNA deformation.

6.6 Conclusions and outlook

The data obtained in this study showed that a combination of base and shape readout is involved in the specific DNA recognition of the regulator AmtR. Furthermore, a distinct DNA deformation was essential for strong AmtR-DNA binding, while deviations in the DNA conformation resulted in decreasing binding affinities. This may be one reason for the variable but specific repression patterns within the AmtR regulon. Moreover, amino acids at distinct positions and with appropriate side chains and orientations were found, that seemed to be important for the specificity and affinity of the AmtR-DNA interaction.

Nevertheless, the current number of three investigated sequences is too small for the deduction of general binding site patterns that would allow a genome-wide classification of high and low affinity AmtR operators. Suggestions of such patterns will require interaction studies of a larger set of AmtR-DNA complexes. For this purpose, regulated as well as non-regulated operator sequences, identified by the transcriptome analyses, must be investigated in future experiments. This may help to identify the complete and coherent regulatory mechanism of AmtR.

Finally, such studies will provide a basis to encode the DNA recognition by proteins in more detail and elucidate the dynamic relationship between the DNA structure and function in protein-DNA interactions.

7   Appendix
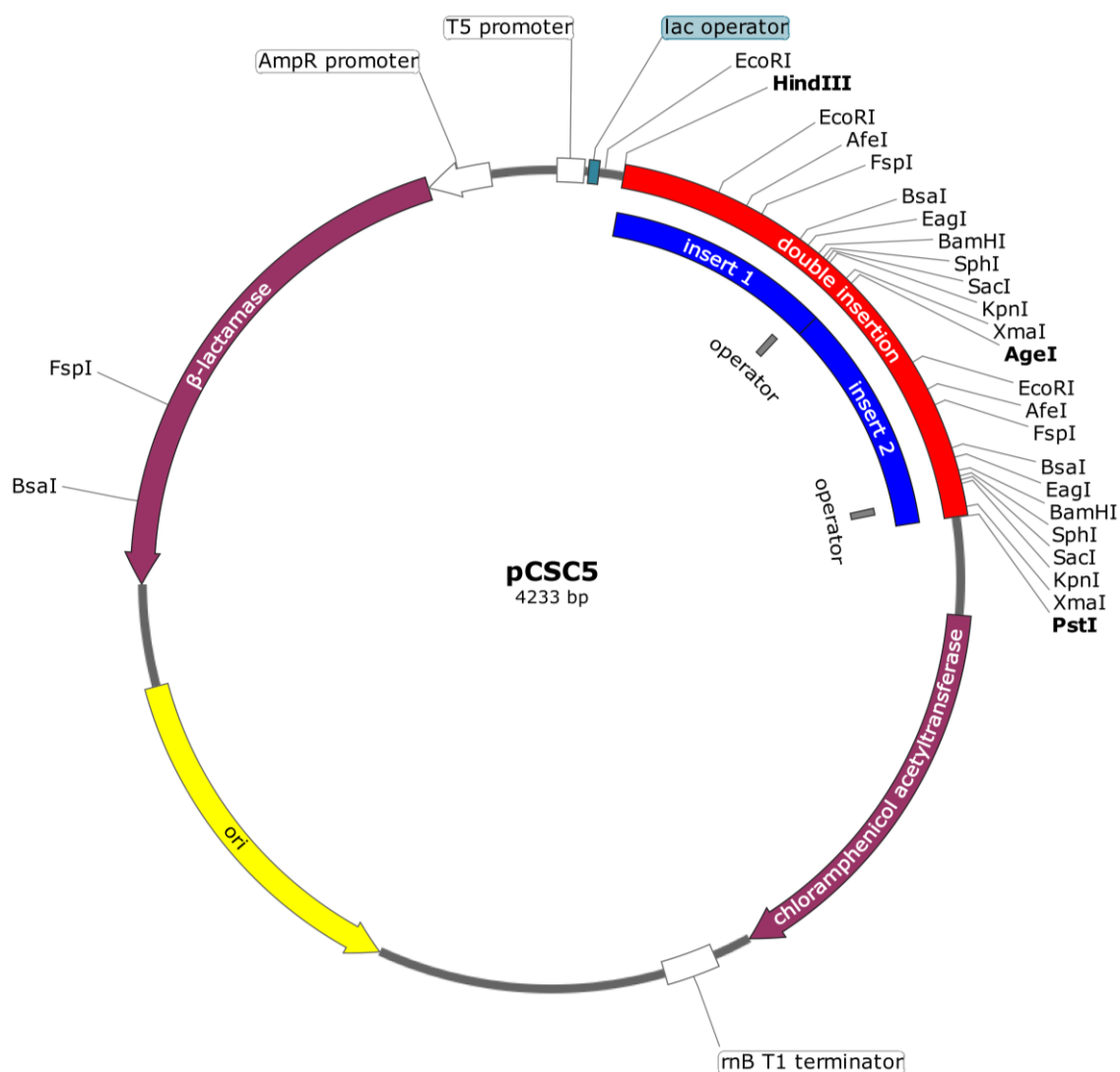
Figure 24 Plasmid map of pCSC5 with the respective operators. Plasmid is shown with the antibiotic resistance cassettes for ampicillin and chloramphenicol, T5 promoter, *lac* operator and rnB T1 terminator. Double insertion is depicted in red containing the two single inserts 1 and 2 with the respective operators for amtB$_{wt}$, amtB$_{ri}$ and amtB$_{de}$.

References

Amon, J., Titgemeyer, F., and Burkovski, A. 2010. "Common patterns - unique features: Nitrogen metabolism and regulation in Gram-positive bacteria." *FEMS Microbiology Reviews* 34 (4): 588-605.

Barksdale, L. 1970. "*Corynebacterium diphtheriae* and its relatives." *Bacteriological Reviews* 34 (4): 378-422.

Beckers, G., Nolden, L., and Burkovski, A. 2001. "Glutamate synthase of *Corynebacterium glutamicum* is not essential for glutamate synthesis and is regulated by the nitrogen status." *Microbiology* 147 (11): 2961-2970.

Beckers, G., Bendt, A. K., Krämer, R., and Burkovski, A. 2004. "Molecular identification of the urea uptake system and transcriptional analysis of urea transporter- and urease-encoding genes in *Corynebacterium glutamicum.*" *Journal of Bacteriology* 186 (22): 7645-7652.

Beckers, G., Strösser, J., Hildebrandt, U., Kalinowski, J., Farwick, M., Krämer, R., and Burkovski, A. 2005. "Regulation of AmtR-controlled gene expression in *Corynebacterium glutamicum*: Mechanism and characterization of the AmtR regulon." *Molecular Microbiology* 58 (2): 580-595.

Bendt, A. K., Beckers, G., Silberbach, M., Wittmann, A., and Burkovski, A. 2004. "Utilization of creatinine as an alternative nitrogen source in *Corynebacterium glutamicum.*" *Archives of Microbiology* 181 (6): 443-450.

Bolivar, F., Rodriguez, R. L., Greene, P. J., Betlach, M. C., Heyneker, H. L., Boyer, H. W., Crosa, J. H., and Falkow, S. 1977. "Construction and characterization of new cloning vehicles. II. A multipurpose cloning system." *Gene* 2 (2): 95-113.

Brinkrolf, K., Brune, I., and Tauch, A. 2007. "The transcriptional regulatory network of the amino acid producer *Corynebacterium glutamicum.*" *Journal of Biotechnology* 129 (2): 191-211.

Browning, D. F., and Busby, S. J. W. 2004. "The regulation of bacterial transcription initiation." *Nature Reviews Microbiology* 2 (1): 57-65.

Brune, I., Brinkrolf, K., Kalinowski, J., Pühler, A., and Tauch, A. 2005. "The individual and common repertoire of DNA-binding transcriptional regulators of *Corynebacterium glutamicum*, *Corynebacterium efficiens*, *Corynebacterium diphtheriae* and *Corynebacterium jeikeium* deduced from the complete genome sequences." *BMC Genomics* 6 (86).

Buchinger, S., Strösser, J., Rehm, N., Hänßler, E., Hans, S., Bathe, B., Schomburg, D., Krämer, R., and Burkovski, A. 2009. "A combination of metabolome and transcriptome analyses reveals new targets of the *Corynebacterium glutamicum* nitrogen regulator AmtR." *Journal of Biotechnology* 140 (1-2): 68-74.

Burgess, R. R. 1969. "Separation and characterization of the subunits of ribonucleic acid polymerase." *The Journal of Biological Chemistry* 244 (22): 6168-6176.

Burkovski, A. 2003a. "Ammonium assimilation and nitrogen control in *Corynebacterium glutamicum* and its relatives: An example for new regulatory mechanisms in actinomycetes." *FEMS Microbiology Reviews* 27 (5): 617-628.

Burkovski, A. 2003b. "I do it my way: Regulation of ammonium uptake and ammonium assimilation in *Corynebacterium glutamicum*." *Archives of Microbiology* 179 (2): 83-88.

Burkovski, A. 2007. "Nitrogen control in *Corynebacterium glutamicum*: Proteins, mechanisms, signals." *Journal of Microbiology and Biotechnology* 17 (2): 187-194.

Burkovski, A. 2013. "Cell envelope of corynebacteria: Structure and influence on pathogenicity." *ISRN Microbiology* 2013: 1-11.

Burkovski, A. 2014. "Diphtheria and its etiological agents. In *Corynebacterium diphtheriae* and related toxigenic species." pp. 1-14. Edited by A. Burkovski. Dordrecht: *Springer Netherlands*.

Burkovski, A. 2018. "The role of corynomycolic acids in *Corynebacterium*-host interaction." *Antonie van Leeuwenhoek, International Journal of General and Molecular Microbiology*, 1-9.

Casadesús, J., and Low, D. 2006. "Epigenetic gene regulation in the bacterial world." *Microbiology and Molecular Biology Reviews* 70 (3): 830-856.

Cherstvy, A. G. 2009. "Positively charged residues in DNA-binding domains of structural proteins follow sequence-specific positions of DNA phosphate groups." *Journal of Physical Chemistry B* 113 (13): 4242-4247.

Constantinides, A. 1980. "Steroid transformation at high substrate concentrations using immobilized *Corynebacterium simplex* cells." *Biotechnology and Bioengineering* 22 (1): 119-136.

Coulocheri, S. A., Pigis, D. G., Papavassiliou, K. A., and Papavassiliou, A. G. 2007. "Hydrogen bonds in protein-DNA complexes: Where geometry meets plasticity." *Biochimie* 89 (11): 1291-1303.

Cuthbertson, L., and Nodwell, J. R. 2013. "The TetR family of regulators." *Microbiology and Molecular Biology Reviews* 77 (3): 440-475.

DeHaseth, P. L., Zupancic, M. L., and Record Jr., M. T. 1998. "RNA polymerase-promoter interactions: The comings and goings of RNA polymerase." *Journal of Bacteriology* 180 (12): 3019-3025.

Dian, C., Baráth, P., Knaust, R., Mcsweeney, S., Moss, E., Hristova, M., Ambros, V., and Birse, D. 2002. "Overcoming protein instability problems during fusion protein cleavage." *Life Science News 10 Amersham Biosciences*, no. 4: 1-5.

Diekmann, S. 1989. "The migration anomaly of DNA fragments in polyacrylamide gels allows the detection of small sequence-specific DNA structure variations." *Electrophoresis* 10: 354-359.

Evans, G. A. 2017. "Molecular cloning: A laboratory manual. Second edition. Volumes 1, 2, and 3. Current protocols in molecular biology. Volumes 1 and 2." *Cell* 61 (1): 17-18.

Fisher, S. H. 1999. "Regulation of nitrogen metabolism in *Bacillus subtilis*: Vive la différence!" *Molecular Microbiology* 32 (2): 223-232.

Giller, K. E., Witter, E., and Mcgrath, S. P. 1998. "Toxicity of heavy metals to microorganisms and microbial processes in agricultural soils: A review." *Soil Biology and Biochemistry* 30 (10-11): 1389-1414.

Grant, S. G., Jessee, J., Bloom, F. R., and Hanahan, D. 1990. "Differential plasmid rescue from transgenic mouse DNAs into *Escherichia coli* methylation-restriction mutants." *Proceedings of the National Academy of Sciences USA* 87 (12): 4645-4649.

di Guan, C., Li, P., Riggs, P. D., and Inouye, H. 1988. "Vectors that facilitate the expression and purification of foreign peptides in *Escherichia coli* by fusion to maltose-binding protein." *Gene* 67 (1): 21-30.

Gunasekera, A., Ebright, Y. W., and Ebright, R. H. 1992. "DNA sequence determinants for binding of the *Escherichia coli* catabolite gene activator protein." *Journal of Biological Chemistry* 267 (21): 14713-14720.

Hanahan, D. 1983. "Studies on transformation of *Escherichia coli* with plasmids." *Journal of Molecular Biology* 166 (4): 557-580.

Härd, T., and Lundbäck, T. 1996. "Thermodynamics of sequence-specific protein-DNA interactions." *Biophysical Chemistry* 62 (1-3): 121-139.

Harteis, S., and Schneider, S. 2014. "Making the bend: DNA tertiary structure and protein-DNA interactions." *International Journal of Molecular Sciences* 15 (7): 12335-12363.

Hasselt, K. 2010. "Biochemische und molekularbiologische Untersuchungen zu AmtR, dem Stickstoffregulator in *Corynebacterium glutamicum*."

Hasselt, K., Rankl, S., Worsch, S., and Burkovski, A. 2011. "Adaptation of AmtR-controlled gene expression by modulation of AmtR binding activity in *Corynebacterium glutamicum*." *Journal of Biotechnology* 154 (2-3): 156-162.

Hasselt, K., Sevvana, M., Burkovski, A., and Muller, Y. A. 2009. "Crystallization and preliminary crystallographic analysis of the global nitrogen regulator AmtR from *Corynebacterium glutamicum*." *Acta Crystallographica Section F: Structural Biology and Crystallization Communications* 65 (11): 1123-1127.

Hegde, R. S. 2002. "The papillomavirus E2 proteins: Structure, function, and biology." *Annual Review of Biophysics and Biomolecular Structure* 31 (1): 343-360.

Hellman, L. M., and Fried, M. G. 2007. "Electrophoretic mobility shift assay (EMSA) for detecting protein-nucleic acid interactions." *Nature Protocols* 2 (8): 1849-1861.

Hermann, T. 2003. "Industrial production of amino acids by coryneform bacteria." *Journal of Biotechnology* 104 (1-3): 155-172.

Ho, N. A. T., Dawes, S. S., Crowe, A. M., Casabon, I., Gao, C., Kendall, S. L., Baker, E. N., Eltis, L. D., and Lott, J. S. 2016. "The structure of the transcriptional repressor KstR in complex with CoA thioester cholesterol metabolites sheds light on the regulation of cholesterol catabolism in *Mycobacterium tuberculosis*." *Journal of Biological Chemistry* 291 (14): 7256-7266.

Hoischen, C., and Krämer, R. 1989. "Evidence for an efflux carrier system involved in the secretion of glutamate by *Corynebacterium glutamicum*." *Archives of Microbiology* 151 (4): 342-347.

Hsu, L. M. 2010. "Monitoring abortive initiation." *Methods* 47 (1): 25-36.

Ikeda, M., and Nakagawa, S. 2003. "The *Corynebacterium glutamicum* genome: Features and impacts on biotechnological processes." *Applied Microbiology and Biotechnology* 62 (2-3): 99-109.

Inoue, H., Nojima, H., and Okayama, H. 1990. "High efficiency transformation of *Escherichia coli* with plasmids." *Gene* 96 (1): 23-28.

Itou, H., Watanabe, N, Yao, M., Shirakihara, Y., and Tanaka, I. 2010. "Crystal structures of the multidrug binding repressor *Corynebacterium glutamicum* CgmR in complex with inducers and with an operator." *Journal of Molecular Biology* 403 (2): 174-184.

Jakoby, M., Krämer, R., and Burkovski A. 1999. "Nitrogen regulation in *Corynebacterium glutamicum*: Isolation of genes involved and biochemical characterization of corresponding proteins." *FEMS Microbiology Letters* 173 (2): 303-310.

Jakoby, M., Nolden, L., Meier-Wagner, J., Krämer, R., and Burkovski, A. 2000. "AmtR, a global repressor in the nitrogen regulation system of *Corynebacterium glutamicum.*" *Molecular Microbiology* 37 (4): 964-977.

Janin, J., Rodier, F., Chakrabarti, P., and Bahadur, R. P. 2007. "Macromolecular recognition in the protein data bank." *Acta Crystallographica Section D: Biological Crystallography* 63 (1): 1-8.

Jenny, R. J., Mann, K. G., and Lundblad, R. L. 2003. "A critical review of the methods for cleavage of fusion proteins with thrombin and factor Xa." *Protein Expression and Purification* 31 (1): 1-11.

Kalinowski, J., Bathe, B., Bartels, D., Bischoff, N., Bott, M., Burkovski, A., Dusch, N., Eggeling, L., Eikmanns, B. J., Gaigalat, L., Goesmann, A., Hartmann M., Huthmacher, K., Krämer, R., Linke, B., McHardy, A. C., Meyer, F., Möckel, B., Pfefferle, W., Pühler, A., Rey, D. A., Rückert, C., Rupp, O., Sahm, H., Wendisch, V. F., Wiegräbe, I., and Tauch, A. 2003. "The complete *Corynebacterium glutamicum* ATCC 13032 genome sequence and its impact on the production of L-aspartate-derived amino acids and vitamins." *Journal of Biotechnology* 104 (1-3): 5-25

Kamionka, A., Bogdanska-Urbaniak, J., Scholz, O., and Hillen, W. 2004. "Two mutations in the tetracycline repressor change the inducer anhydrotetracycline to a corepressor." *Nucleic Acids Research* 32 (2): 842-847.

Kane, J. F., Wakim, J., and Fischer, R. S. 1981. "Regulation of glutamate dehydrogenase in *Bacillus subtilis.*" *Journal of Bacteriology* 148 (3): 1002-1005.

Karlsson, R., Katsamba, P. S., Nordin, H., Pol, E., and Myszka, D. G. 2006. "Analyzing a kinetic titration series using affinity biosensors." *Analytical Biochemistry* 349 (1): 136-147.

Kim, S. S., Tam, J. K., Wang, A. F., and Hegde, R. S. 2000. "The structural basis of DNA target discrimination by papillomavirus E2 proteins." *Journal of Biological Chemistry* 275 (40): 31245-31254.

Kim, Y., Kim, B. S., Park, Y. J., Choi, W. C., Hwang, J., Kang, B. S., Oh, T. K., Choi, S. H., and Kim, M. H. 2010. "Crystal structure of SmcR, a quorum-sensing master regulator of *Vibrio vulnificus*, provides insight into its regulation of transcription." *Journal of Biological Chemistry* 285 (18): 14020-14030.

Kim, Y., Geiger, J. H., Hahn, S., and Sigler, P. B. 1993. "Crystal structure of a yeast TBP/TATA-box complex." *Nature* 365 (6446): 512-520.

Kinoshita, S., Udaka, S., and Shimono, M. 1957. "Studies on the amino acid fermentation. Part 1. Production of L-glutamic acid by various microorganisms." *The Journal of General and Applied Microbiology* 3 (3): 193-205.

Kolb, A., Busby, S., Buc, H., Garges, S., and Adhya, S. 1993. "Transcriptional regulation by cAMP and its receptor protein." *Annual Review of Biochemistry* 62 (1): 749-797.

Krause, J. P., Polen, T., Youn, J. W., Emer, D., Eikmanns, B. J., and Wendisch, V. F. 2012. "Regulation of the malic enzyme gene MalE by the transcriptional regulator MalR in *Corynebacterium glutamicum.*" *Journal of Biotechnology* 159 (3): 204-215.

Kronemeyer, W., Peekhaus, N., Krämer, R., Sahm, H., and Eggeling, L. 1995. "Structure of the *gluABCD* cluster encoding the glutamate uptake system of *Corynebacterium glutamicum.*" *Journal of Bacteriology* 177 (5): 1152-1158.

Lamers, M. H., Perrakis, A., Enzlin, J. H., Winterwerp, H. H. K., de Wind, N., and Sixma, T. K. 2000. "The crystal structure of DNA mismatch repair protein MutS binding to a G·T mismatch." *Nature* 407 (6805): 711-717.

Le, T. B. K., Schumacher, M. A., Lawson, D. M., Brennan, R. G., and Buttner, M. J. 2011. "The crystal structure of the TetR family transcriptional repressor SimR bound to DNA and the role of a flexible N-terminal extension in minor groove binding." *Nucleic Acids Research* 39 (21): 9433-9447.

Lehmann, K. B., and Neumann, R. 1896. *Atlas und Grundriss der Bakteriologie und Lehrbuch der speziellen bakteriologischen Diagnostik.*

Lewis, M. 2005. "The *lac* repressor." *Comptes Rendus - Biologies* 328 (2005): 521-548.

Li, D. F., Zhang, N., Hou, Y. J., Huang, Y., Hu, Y., Zhang, Y., Liu, S. J., and Wang, D. C. 2011. "Crystal structures of the transcriptional repressor RolR reveals a novel recognition mechanism between inducer and regulator." *PLoS ONE* 6 (5): e19529.

Liebl, W., Ehrmann, M., Ludwig, W., and Schleifer, K. H. 1991. "Transfer of *Brevibacterium divaricatum* DSM 20297T, '*Brevibacterium flavum*' DSM 20411, '*Brevibacterium lactofermentum*' DSM 20412 and DSM 1412, and *Corynebacterium glutamicum* and their distinction by rRNA gene restriction patterns." *International Journal of Systematic Bacteriology* 41 (2): 255-260.

Lindemose, S., Nielsen, P. E., Valentin-Hansen, P., and Møllegaard, N. E. 2014. "A novel indirect sequence readout component in the *E. coli* cyclic AMP receptor protein operator." *ACS Chemical Biology* 9 (3): 752-760.

Maina, C. V., Riggs, P. D., Grandea, A. G., Slatko, B. E., Moran, L. S., Tagliamonte, J. A., McReynolds, L. A., and di Guan, C. 1988. "An *Escherichia coli* vector to express and purify foreign proteins by fusion to and separation from maltose-binding protein." *Gene* 74 (2): 365-373.

Majka, J., and Speck, C. 2007. "Analysis of protein–DNA interactions using surface plasmon resonance." *Advances in Biochemical Engineering / Biotechnology* 104: 13-36.

Marrakchi, H., Lanéelle, M. A., and Daffé, M. 2014. "Mycolic acids: Structures, biosynthesis, and beyond." *Chemistry and Biology* 21 (1): 67-85.

Merkens, H., Beckers, G., Wirtz, A., and Burkovski, A. 2005. "Vanillate metabolism in *Corynebacterium glutamicum*." *Current Microbiology* 51 (1): 59-65.

Merrick, M. J., and Edwards, R. A. 1995. "Nitrogen control in bacteria." *Microbiological Reviews* 59 (4): 604-622.

Muhl, D., Jessberger, N., Hasselt, K., Jardin, C., Sticht, H., and Burkovski, A. 2009. "DNA binding by *Corynebacterium glutamicum* TetR-type transcription regulator AmtR." *BMC Molecular Biology* 10: 73.

Mullis, K., Faloona, F., Scharf, S., Saiki, R., Horn, G., and Erlich, H. 1986. "Specific enzymatic amplification of DNA *in vitro*: The polymerase chain reaction." *Cold Spring Harbor Symposia on Quantitative Biology* 51 (1): 263-273.

Nelson, H. C., Finch, J. T., Luisi, B. F., Klug, A. 1987. "The structure of an oligo(dA).oligo(dT) tract and its biological implications." *Nature* 330, 221-226.

Niederweis, M., and Hillen, W. 1993. "Electrophoretic analysis of protein-induced DNA bending and twist changes." *Electrophoresis* 14: 693-698.

Ninfa, A. J., and Atkinson, M. R. 2000. "PII signal transduction proteins." *Trends in Microbiology* 8 (4): 172-179.

Nolden, L., Beckers, G., Möckel, B., Pfefferle, W., Nampoothiri, K. M., Krämer, R., and Burkovski, A. 2000. "Urease of *Corynebacterium glutamicum*: Organization of corresponding genes and investigation of activity." *FEMS Microbiology Letters* 189 (2): 305-310.

Nolden, L., Farwick, M., Krämer, R., and Burkovski, A. 2001a. "Glutamine synthetases of *Corynebacterium glutamicum*: Transcriptional control and regulation of activity." *FEMS Microbiology Letters* 201 (1): 91-98.

Nolden, L., Ngouoto-Nkili, C. E., Bendt, A. K., Krämer, R., and Burkovski, A. 2001b. "Sensing nitrogen limitation in *Corynebacterium glutamicum*: The role of GlnK and GlnD." *Molecular Microbiology* 42 (5): 1281-1295.

O'Donnell, M., Langston, L., and Stillman, B. 2013. "Principles and concepts of DNA replication in bacteria, archaea, and eukarya." *Cold Spring Harbor Perspectives in Biology* 5: a010108.

Ohnishi, J., Mitsuhashi, S., Hayashi, M., Ando, S., Yokoi, H., Ochiai, K., and Ikeda, M. 2002. "A novel methodology employing *Corynebacterium glutamicum* genome information to generate a new L-lysine-producing mutant." *Applied Microbiology and Biotechnology* 58 (2): 217-223.

Orth, P., Schnappinger, D., Hillen, W., Saenger, W., and Hinrichs, W. 2000. "Structural basis of gene regulation by the tetracycline inducible Tet repressor-operator system." *Nature Structural Biology* 7 (3): 215-219.

Otwinowski, Z., Schevitz, R. W., Zhang, R. G., Lawson, C. L., Joachimiak, A., Marmorstein, R. Q., Luisi, B. F., and Sigler, P. B. 1988. "Crystal structure of *trp* repressor/operator complex at atomic resolution." *Nature* 335 (6188): 321-329.

Palanca, C., and Rubio, V. 2016. "Structure of AmtR, the global nitrogen regulator of *Corynebacterium glutamicum*, in free and DNA-bound forms." *FEBS Journal* 283 (6): 1039-1059.

Perez-Rueda, E., and Collado-Vides, J. 2000. "The repertoire of DNA-binding transcriptional regulators in *Escherichia coli* K-12." *Nucleic Acids Research* 28 (8): 1838-1847.

Perez-Rueda, E., and Collado-Vides, J. 2001. "Common history at the origin of the position - function correlation in transcriptional regulators in archaea and bacteria." *Journal of Molecular Evolution* 53 (3): 172-179.

Ramos, J. L., Martínez-Bueno, M., Molina-Henares, A. J., Terán, W., Watanabe, K., Zhang, X., Gallegos, M. T., Brennan, R., and Tobes, R. 2005. "The TetR family of transcriptional repressors." *Microbiology and Molecular Biology Reviews* 69 (2): 326-356.

Rehm, N., Georgi, T., Hiery, E., Degner, U., Schmiedl, A., Burkovski, A., and Bott, M. 2010. "L-glutamine as a nitrogen source for *Corynebacterium glutamicum*: Derepression of the AmtR regulon and implications for nitrogen sensing." *Microbiology* 156 (10): 3180-3193.

Rodionov, D. A. 2007. "Comparative genomic reconstruction of transcription regulatory networks in bacteria." *Chemical Reviews* 107 (8): 3467-3497.

Rohs, R., West, S. M., Sosinsky, A., Liu, P., Mann, R. S., and Honig, B. 2009. "The role of DNA shape in protein - DNA recognition." *Nature* 461 (7268): 1248-1253.

Rohs, R., Jin, X., West, S. M., Joshi, R., Honig, B., and Mann, R. S. 2010. "Origins of specificity in protein-DNA recognition." *Annual Review of Biochemistry* 79: 233-269.

Rückert, C., Eimer, J., Winkler, A., and Tauch, A. 2015. "Complete genome sequence of the type strain *Corynebacterium epidermidicanis* DSM 45586, isolated from the skin of a dog suffering from pruritus." *Genome Announcements* 3 (4): e00959-15.

Sahm, H., Eggeling, L., Eikmanns, B. J., and Krämer, R. 1996. "Construction of L-lysine-, L-threonine-, or L-isoleucine-overproducing strains of *Corynebacterium glutamicum*." *Annals of the New York Academy of Sciences* 782: 25-39.

Sambrook, J., Fritsch, E. F., and Maniatis, T. 1989. *Molecular Cloning: A Laboratory Manual. New York*.

Sanchez, S., Rodríguez-Sanoja, R., Ramos, A., and Demain, A. L. 2018. "Our microbes not only produce antibiotics, they also overproduce amino acids." *Journal of Antibiotics* 71 (1): 26-36.

Schröder, J., Maus, I., Trost, E., and Tauch, A. 2011. "Complete genome sequence of *Corynebacterium variabile* DSM 44702 isolated from the surface of smear-ripened cheeses and insights into cheese ripening and flavor generation." *BMC Genomics* 12 (1): 545.

Schuck P., and Zhao, H. 2010. "The role of mass transport limitation and surface heterogeneity in the biophysical characterization of macromolecular binding processes by SPR biosensing." *Methods in Molecular Biology* 627: 15-54.

Schulz, A. A., Collett, H. J., and Reid, S. J. 2001. "Nitrogen and carbon regulation of glutamine synthetase and glutamate synthase in *Corynebacterium glutamicum* ATCC 13032." *FEMS Microbiology Letters* 205 (2): 361-367.

Schumacher, M. A., Miller, M. C., Grkovic, S., Brown, M. H., Skurray, R. A., and Brennan, R. 2002. "Structural basis for cooperative DNA binding by two dimers of the multidrug-binding protein QacR." *EMBO Journal* 21 (5): 1210-1218.

Seeman, N. C., Rosenberg, J. M., and Rich, A. 1976. "Sequence-specific recognition of double helical nucleic acids by proteins." *Proceedings of the National Academy of Sciences USA* 73 (3): 804-808.

Sevvana, M., Hasselt, K., Grau F. C., Burkovski, A., and Muller Y. A. 2017. "Similarities in the structure of the transcriptional repressor AmtR in two different space groups suggest a model for the interaction with GlnK." *Acta Crystallographica Section:F Structural Biology Communications* 73: 146-151.

Shin, W., Islam, R., Benson, A., Joe, M. M., Kim, K., Gopal, S., Samaddar, S., Banerjee, S., and Sa, T. 2016. "Role of diazotrophic bacteria in biological nitrogen fixation and plant growth improvement." *Korean Journal of Soil Science and Fertilizer* 49 (1): 17-29.

Silberbach, M. 2004. "Biotechnologische und molekularbiologische Analyse eines Signaltransduktionsweges in *Corynebacterium glutamicum.*"

Silberbach, M., and Burkovski, A. 2006. "Application of global analysis techniques to *Corynebacterium glutamicum*: New insights into nitrogen regulation." *Journal of Biotechnology* 126 (1): 101-110.

Stackebrandt, E., Rainey, F. A., and Ward-Rainey, N. L. 1997. "Proposal for a new hierarchic classification system, *Actinobacteria* classis nov." *International Journal of Systematic Bacteriology*, 47 (2): 479-491.

Strösser, J., Lüdke, A., Schaffer, S., Krämer, R., and Burkovski, A. 2004. "Regulation of GlnK activity: Modification, membrane sequestration and proteolysis as regulatory principles in the network of nitrogen control in *Corynebacterium glutamicum.*" *Molecular Microbiology* 54 (1): 132-147.

Studier, F. W., Rosenberg, A. H., Dunn, J. J., and Dubendorff, J. W. 1990. "Use of T7 RNA polymerase to direct expression of cloned genes." *Methods in Enzymology* 185 (C): 60-89.

Sugimura, S., and Crothers, D. M. 2006. "Stepwise binding and bending of DNA by *Escherichia coli* integration host factor." *Proceedings of the National Academy of Sciences USA* 103 (49): 18510-18514.

Swinger, K. K., and Rice, P. A. 2007. "Structure-based analysis of HU-DNA binding." *Journal of Molecular Biology* 365 (4): 1005-1016.

Tauch, A., and Burkovski, A. 2015. "Molecular armory or niche factors: Virulence determinants of *Corynebacterium* species." *FEMS Microbiology Letters* 362 (23): 1-6.

Tauch, A., and Sandbote, J. 2014. "The family *Corynebacteriaceae.*" *The Prokaryotes: Actinobacteria*.

Tesch, M., de Graaf, A. A., and Sahm, H. 1999. "*In vivo* fluxes in the ammonium-assimilatory pathways in *Corynebacterium glutamicum* studied by 15N nuclear magnetic resonance." *Applied and Environmental Microbiology* 65 (3): 1099-1109.

Thompson, J. F., and Landy, A. 1988. "Empirical estimation of protein-induced DNA bending angles: Applications to λ site-specific recombination complexes." *Nucleic Acids Research* 16 (20): 9687-9705.

Tovar, K., and Hillen, W. 1989. "Tet repressor binding induced curvature of *tet* operator DNA." *Nucleic Acids Research* 17 (16): 6515-6522.

Travers, A. A. 2004. "The structural basis of DNA flexibility." *Philosophical Transactions of the Royal Society A: Mathematical, Physical and Engineering Sciences* 362: 1423-1438.

Trutnau, H. H. 2006. "New multi-step kinetics using common affinity biosensors saves time and sample at full access to kinetics and concentration." *Journal of Biotechnology* 124 (1): 191-195.

Ventura, M., Canchaya, C., Tauch, A., Chandra, G., Fitzgerald, G. F., Chater, K. F., and van Sinderen, D. 2007. "Genomics of actinobacteria: Tracing the evolutionary history of an ancient phylum." *Microbiology and Molecular Biology Reviews* 71 (3): 495-548.

Walter, B., Küspert, M., Ansorge, D., Krämer, R., and Burkovski, A. 2008. "Dissection of ammonium uptake systems in *Corynebacterium glutamicum*: Mechanism of action and energetics of AmtA and AmtB." *Journal of Bacteriology* 190 (7): 2611-2614.

Wehrmann, A., Phillipp, B., Sahm, H., and Eggeling, L. 1998. "Different modes of diaminopimelate synthesis and their role in cell wall integrity: A study with *Corynebacterium glutamicum*." *Journal of Bacteriology* 180 (12): 3159-3165.

WHO/IVB database 2017. Diphteria global annual reported cases and DTP3 coverage, 1980-2016

Wu, H. M., and Crothers, D. M. 1984. "The locus of sequence-directed and protein-induced DNA bending." *Nature* 308 (5959): 509-513.

Yakovchuk, P., Protozanova, E., and Frank-Kamenetskii, M. D. 2006. "Base-stacking and base-pairing contributions into thermal stability of the DNA double helix." *Nucleic Acids Research* 34 (2): 564-574.

Yokota, T., Omori, T., and Kodama, T. 1987. "Purification and properties of haloalkane dehalogenase from *Corynebacterium sp.* strain M15-3." *Journal of Bacteriology* 169 (9): 4049-4054.

Zhang, Y.-M., Zhu, K., Frank, M. W., and Rock, C. O. 2007. "A *Pseudomonas aeruginosa* transcription factor that senses fatty acid structure." *Molecular Microbiology* 66 (3): 622-632.

Table of abbreviations

A	Adenine
ADP	Adenosine diphosphate
AMP	Adenosine monophosphate
APS	Ammonium persulfate
ATP	Adenosine triphosphate
C	Cytosine
CSPD	[3-(1-chloro-3'-methoxyspiro [adamantane-4,4'-dioxetane]-3'-yl) phenyl] dihydrogen phosphate
DIG	Digoxigenin
DMSO	Dimethyl sulfoxide
DNA	Deoxyribonucleic acid
NTP	Nucleoside triphosphate
EDTA	Ethylenediaminetetraacetic acid
EMSA	Electrophorese mobility shift assay
fc	Flow cell
G	Guanine
GDH	Glutamate dehydrogenase
GOGAT	Glutamate synthase
GS	Glutamine synthetase
HEPES	4-(2-hydroxyethyl)-1-piperazineethanesulfonic acid
IPTG	Isopropyl β-D-1-thiogalactopyranoside
MBP	Maltose-binding protein
MOPS	3-(N-morpholino) propane sulfonic acid
MSK	Multi-step kinetics
NADPH	Nicotinamide adenine dinucleotide phosphate
oD_{600}	Optical density at 600 nm
PAGE	Polyacrylamide gel electrophorese
PCR	Polymerase chain reaction
RNA	Ribonucleic acid
SDS	Sodium dodecyl sulfate

SPR	Surface plasmon resonance
SSK	Single-step kinetics
T	Thymine
TAE	Tris base, acetic acid and EDTA
TBE	Tris base, boric acid and EDTA
TEMED	Tetramethyl ethylenediamine
Tris	tris(hydroxymethyl)aminomethane
v v^{-1}	Volume per volume
w v^{-1}	Weight per volume

Units

°C	Degree Celsius
bp	Base pair
Da	Dalton
h	Hour
g	Gram
k	Kilo
l	Liter
m	Meter
M	Molar or mol l^{-1}
min	Minute
n	Nano
p	Pico
rpm	Revolution per minute
RU	Resonance units
s	Second
V	Volt
xg	Gravitational force
µ	Micro

Table of figures

Danksagung

Christian Schwab

Zell- und Molekularbiologe, M.Sc.

Fachbereich Mikrobiologie

Akademische Ausbildung

10/2014 - 10/2018	**Promotion** Friedrich-Alexander-Universität Erlangen-Nürnberg Lehrstuhl für Mikrobiologie Betreuer: Prof. Dr. Andreas Burkovski „Characterization of transcription factor AmtR-DNA interaction"/ „Charakterisierung der Transkriptionsfaktor AmtR-DNA Interaktion"
10/2012 – 10/2014	**Masterstudium Zell- und Molekularbiologie** Friedrich-Alexander-Universität Erlangen-Nürnberg Schwerpunkte: Biochemie, Biotechnik, Mikrobiologie und Entwicklungsbiologie **Masterarbeit** Lehrstuhl für Mikrobiologie Betreuer: Prof. Dr. Andreas Burkovski „Untersuchungen zur Interaktion von *Corynebacterium glutamicum* AmtR mit seiner Ziel-DNA"
13.10.2014	Abschluss: **Master of Science**
10/2009 – 09/2012	**Bachelorstudium Biologie** Friedrich-Alexander-Universität Erlangen-Nürnberg Schwerpunkte: Mikrobiologie, Virologie und Biochemie **Bachelorarbeit** Lehrstuhl für Biochemie Betreuer: Prof. Dr. Uwe Sonnewald
17.10.2012	Abschluss: **Bachelor of Science**
09/2008 – 08/2009	**Bachelorstudium Regenerative Energietechnik** Fachhochschule Flensburg
08/2007 – 04/2008	**Zivildienst**
06/2007	**Abitur** Gymnasium Berchtesgaden

Persönliches

Geboren am 06.01.1987 in Berchtesgaden
Staatsangehörigkeit: deutsch
Familienstand: ledig

SPR Spektroskopie

Säulenchromatographie

Protein Charakterisierung

Electro mobility shift assays

Western Blot Quantifizierung

Workshops/Fortbildungen

05/2015	Bioinformatik Workshop
02/2016	Chromatographie und Life Sciences Seminar
12/2014	CS Photoshop Kurs

Sprachkenntnisse

Deutsch (Muttersprache)
Englisch (fließend in Wort und Schrift)
Italienisch (Grundlagen)
Französisch (Grundlagen)

Qualifikationen

Methoden	Arbeiten im S2 Labor mit biotechnologisch relevanten Mikroorganismen
	Interaktionsanalysen durch Gel-Retardationsassays und Oberflächen-Plasmonen-Resonanz (SPR) Spektroskopie
	Protein Aufreinigung (Affinitäts- und Gel-Permeations-Chromatographie)
	Quantifikationsassays (Western Blot und ELISA)
	RNA-/DNA-Techniken
Verantwortlichkeiten	Planung und Betreuung von Bachelorpraktika
	Betreuung, Wartung und Durchführung von SPR-Analysen, Säulenchromatographie und Ultra-/Zentrifugation
	Einweisung von Personal in die Handhabung von Laborgeräten
EDV-Kenntnisse	MS Office
	Endnote, Mendeley
	Clone Manager, SnapGene, Genome Compiler
	ImageLab, BiaEvaluation, PrimeView
	Photoshop, ImageJ, Prism

Publikation (in Bearbeitung)

Christian Schwab, Madhumati Sevvana, Gerald Seidel, Achim Sandmann, Florian Grau, Yves A. Muller, Heinrich Sticht and Andreas Burkovski (2018). The role of DNA flexibility in transcription regulator AmtR-DNA interaction.

Christian Schwab